2006

Damping controller design for FACTS devices in power systems using novel control techniques

Qian Liu
Iowa State University

Damping controller design for FACTS devices in power systems using novel control techniques

by

Qian Liu

A dissertation submitted to the graduate faculty

in partial fulfillment of the requirements for the degree of

DOCTOR OF PHILOSOPHY

Major: Electrical Engineering

Program of Study Committee:
Vijay Vittal, Co-major Professor
Nicola Elia, Co-major Professor
James D. McCalley
Venkataramana Ajjarapu
Wolfgang Kliemann

Iowa State University

Ames, Iowa

2006

Graduate College
Iowa State University

This is to certify that the doctoral dissertation of

Qian Liu

has met the dissertation requirements of Iowa State University

Signature was redacted for privacy.

Co-major Professor

Signature was redacted for privacy.

Co-major Professor

Signature was redacted for privacy.

For the Major Program

This dissertation is dedicated to my beloved parents, Guifang Sun and Zhenghong Liu, my boyfriend Ran Cao, and my best friend Xiaofan Yang and Benhong Zhang.

They are always there to encourage and support me.

TABLE OF CONTENTS

LIST OF FIGURES

LIST OF TABLES

ACKNOWLEDGMENTS

I am deeply indebted to my co-major professor, Dr. Vijay Vittal, for his constant support. Without his guidance, this work would not be even possible. I also appreciate all the help provided by my other co-major professor Dr. Niocal Elia. I would also like to thank the members of my committee Dr. James D. McCalley, Dr. Venkataramana Ajjarapu, and Dr. Kliemann Wolfgang (Mathematics). Their advice and patience is highly appreciated.

I would like to acknowledge my comrades in the power group at Iowa State University who provided me with outstanding advice throughout the years. Discussions with Dr. Wenzheng Qiu paved the way for the first part of my research. Additionally, I would be amiss without particularly acknowledging the support of Dr. Xiaoming Wang who provided invaluable suggestions at the beginning of the second part of my research. I would also like to thank one of my best friends, Xiaofan Yang, for her constant encouragement and support.

I am also indebted to the fellow graduate students before me: Dr. Haibo You, Dr. Qiming Chen, Dr. Jiang Huang, and Dr. Zhong Zhang.

Finally, I would like to thank Wei Shao, Shu Liu, Haifeng Liu, Yong Jiang, Ramanathan Badri, Ana Margarida Quelhas, Bo Yang, Weiqing Jiang and many others. Their great friendship accompanied me throughout my school years and made my life in Ames so meaningful. These memories will never be forgotten.

ABSTRACT

Power systems are under increasing stress as deregulation introduces several new economic objectives for operation. Since power systems are being operated close to their limits, weak connections, unexpected events, hidden failures in protection system, human errors, and a host of other factors may cause a system to lose stability and even lead to catastrophic failure. Therefore, the need for improved system damping in a wider operating range is gaining more attention. Among the available damping control methods, each approach has advantages and disadvantages in different systems. The effectiveness of damping control depends on the devices chosen, the system modal feature, and the applied controller design method.

In the literature, many approaches have been proposed to undertake this task. However, some of these approaches only take a fixed operating point into consideration without describing the changing uncertainty in varying system conditions; others require a great deal of computational effort. Furthermore, no systematic comparison of controller design methods has been conducted with regard to different system profiles. Attention has been drawn to the enhanced susceptibility to inter-area oscillations between groups of machines under large variation of system operating conditions. The linear parameter varying (LPV) approach, which has been widely studied in the literature, provides a potential method for capturing the varying system condition precisely without formulation of system uncertainty. However, in some cases no solution can be achieved if the system variation is too large using the traditional LPV approach. Also, sometimes the system structure imposes limitations in the achievable damping performance. In general, there is a critical need for a cost-effective control strategy applicable to different systems from an economic point of view.

In this dissertation, a comprehensive comparison among controller design methods has been conducted to study the damping effectiveness of different FACTS devices. Based on these, a robust regional pole-placement method is applied in a TCSC damping controller design in a 4-machine system; an interpolated LPV approach is proposed and applied to designing a SVC damping controller in the IEEE 50-machine system; finally with the advantage of an additional feedback signal, limitations in achieving satisfactory damping performance can be relieved using a two-input single-output (TISO) damping controller for a TCSC in the IEEE 50-machine system.

1 INTRODUCTION

The electric power system in North America has undergone unprecedented changes with the advent of a competitive market place and deregulation. These changes in the system have resulted in higher levels of loading on the system, resulting in increased stress. At the same time, the transmission grid has seen very little expansion due to prevailing economic conditions and lack of incentives in the market. As a result, available transmission and generation facilities are highly utilized with large power interchanges among companies and geographical regions. It is envisioned that this trend will continue to grow and result in more stringent requirements for maintenance of reliability and adequate system dynamic performance. Among several problems that have arisen in the heavily stressed network, enhancement of the damping ratio for low-frequency oscillations remains an important concern. It is well known that low frequency oscillations occur due to inadequate damping torque in some generators, causing both local-mode oscillations (1.0HZ-2.0HZ) and some inter-area oscillations (0.2-1.0HZ). The traditional approach to damp inter-area oscillations is through the installation of power system stabilizers (PSS's) [1] to provide supplementary control action through the excitation control of generators.

In recent times, the use of flexible AC transmission system (FACTS) devices has become a common practice in order to fully utilze existing transmission capacities instead of adding new lines which may be restricted due to economic and environmental reasons. Some examples of FACTS devices include thyristor-switched series capacitors (TSSC), unified power-flow controllers (UPFC), and high-voltage direct-current (HVDC) controls capable of modulating large blocks of power. Apart from faster power flow and voltage control in the network, appropriate supplementary control can be

added to these FACTS devices to damp out inter-area oscillations. As the PSS design has matured and become widely-used, there are many remaining problems in FACTS controller design with respect to the damping improvement issue. It is important to investigate these difficulties in FACTS controller design in order to fully utilize the promise of FACTS devices in future power grids, where such economic factors as the high cost of long lines and the revenue obtainable from the delivery of additional power give strong incentives to explore all the economically and technically feasible means of increasing the stability limit.

1.1 FACTS Devices

FACTS devices are mostly used to regulate voltage and schedule power flows through some lines. There are both series devices and shunt devices. The static VAR compensator (SVC) is one of the shunt devices. The primary application of the SVC is to maintain the bus-bar voltage at or near a constant value. The SVC is equipped with a voltage regulator that provides synchronizing torque while damping torque contributions are small [2]. An additional damping controller is necessary for extra damping. On the other hand, the common use of the thyristor controlled series capacitor (TCSC) devices is to regulate the power flow through the transmission line in which it is installed. By tuning the parameters in the main controller, the system damping can be improved slightly [3]. Since the tuning process is complicated and heavily dependent on system operating condition, a secondary controller will most likely be better for damping the system oscillations under varying operating condition. In general, a FACTS device is usually comprised of three major control components: the main controller for the power scheduling or the voltage control, the secondary damping controller for damping improvement, and the reference value which sets the compensation level of the device.

The outputs of the three control components are added together at a summing point as shown in Fig. 1.1, and the combined signal will then go through a single lag block representing the thyristor firing and other delays. Finally there is a limiter before final signal output.

Conventionally, the supplementary damping controller for FACTS devices is designed at a particular operating point. This could lead to non-optimal damping over the entire operating range. When used in a multi-machine power system, it may even decrease the damping in some cases. Therefore, a robust controller for FACTS devices is greatly needed to account for possible changes in the system operating point. Also, an increasing transfer demand in the system may require the expansion of the stability limit by using some appropriately designed FACTS controllers.

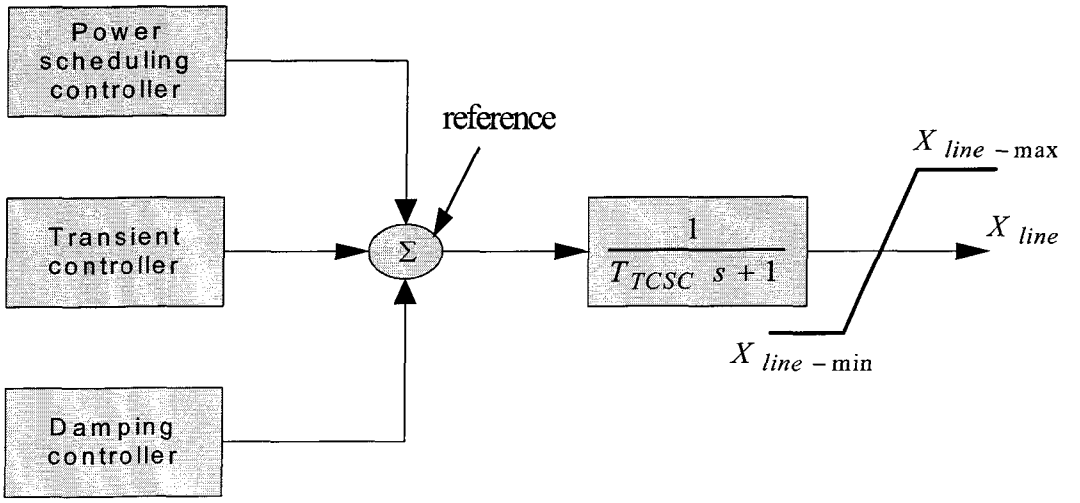

Figure 1.1 Block diagram for the TCSC model for typical stability studies

1.2 Challenges in FACTS damping control in power systems

1.2.1 Damping influence of different FACTS devices with change of operating conditions

The effectiveness of FACTS controllers on damping has been investigated in [4,5]. However, the unified Phillips-Heffron model derived was based on a single-machine infinite-bus power system, which is not a practical model for real power systems. It may help in understanding the basic concepts of the damping contribution of the FACTS controller, but it does not provide a detailed analytical explanation of how the different FACTS will affect a real system under variation of system operating conditions. In this dissertation the intention is to obtain a clear understanding of how the effectiveness of a FACTS controller's changes with the variation of system operating conditions in realistic systems.

1.2.2 Extension of the existent operating range

The power transfer capability of long, inter-regional transmission lines is usually limited by both large- and small-signal stability. In the current power grid the small-signal stability limit for the system has not been extended enough to keep up with the increasing transferring limit. The difficulties include the heavy design-method dependence of the obtained controller, and achievement of a reasonable formulation of large uncertainty when the operating range of the system is expanded.

1.2.3 Uncertainty representation in a wider operating range

Proper design of these controllers to produce robust system-wide stability and performance is essential. The need for robust operation arises as a consequence of large variation in system parameters and operating conditions. Under such conditions, a conventional fixed structure controller will not guarantee the desired performance and

robustness. Yet guaranteed system-wide robustness is needed to provide for reliable operation of the interconnected power system. Some modern robust stability tools have been successfully applied to analyze and design controls for realistic power systems. Most of these approaches are primarily based on mixed-sensitivity synthesis to represent uncertainty as some weighting function block. However, a larger variation of power system operating scenarios may challenge the uncertainty formulation based on a nominal case in the mixed-sensitivity synthesis. Also, in some large stressed systems, when the extension of the current operating range is absolutely necessary, conventional controller design can neither manage to represent the increasing uncertainty nor obtain a feasible solution.

1.2.4 Power system model reduction before controller design

To obtain an accurate model, power system state-space equations and network algebraic equations should be developed before the controller is designed. Then linearization can be performed at each operating point to cast the problem into a linear controller design framework. Large systems consist of hundreds of generators and several devices, and consequently a linearized model may have a very high order, which will definitely add more complexity to the computation and solvability of the controller design problem. Also, the controller obtained will have the same high order as the original open loop system, which is probably not feasible for practical use. Therefore, it is necessary to find a better way to reduce the system order. Reference [6] suggests an approach of retaining lightly damped modes and unstable modes while reducing other modes. However, in a large system like the IEEE 50-machine system [7], there are more than 20 pairs of lightly damped modes that should be retained; this method would not be practical because the reduced system will still have a very high order. New approaches must be developed corresponding to the mode profiles in different systems.

1.2.5 Performance limitations due to system structures

Usually most modern control theory-based controller design is based on a mixed sensitivity setup, in which the damping performance is translated into the minimization of the norm of some specific transfer function. However, it is well-known that a plant's RHP poles and zeros and its relative degree, as well as bandwidth limitations, impose constraints on sensitivity minimization [8]. Research dealing with the theory of inherent design limitation in [9]-[11] provides the background and the results for the field of linear feedback control. . In addition, due to such physical attributes as plant/controller structure in power system applications, one single-input single-output (SISO) controller for FACTS devices may not be sufficient to achieve desired damping effects in large complex systems even after a careful selection of locations and feedback signals is conducted. Thus combining a secondary controller in a different location to enhance the overall damping for the critical mode is studied in [12]. However, a large computational effort is required to carefully develop the coordination scheme between the two controllers due to their possible interactions. An alternative is to add a secondary feedback signal. Thus, using the same simple controller design method, by which no solution can be obtained with a single measurement, a two-input single-output controller can be achieved to improve system performance as well as provide a simple structure for realization.

1.3 Controller design methods used in this dissertation

1.3.1 LMI-based robust pole-placement controller design

There are several approaches that mainly use a linear time-invariant (LTI) controller to guarantee robust stability and robust performance after describing the changes of operating condition as uncertainties [13].

Normally the problem is formulated as a weighted mixed-sensitivity design. References [14,15] deal with controller design intended to guarantee robust stability and

performance. The standard Riccati solution to this problem will usually cause some pole-zero cancellation problems and also requires careful weighting function selection. It is clearly known that the design objective of a conventional controller is to minimize the infinity norm from some output signals to some input signals, but the obtained controller with the minimal infinity norm does not guarantee a closed loop system with the largest damping ratio at some critical modes because the norm index is not directly related to the damping issue. Although the weighting functions can be selected to get a better controller, the conventional controller design still has its intrinsic limit in achieving this specific goal.

Recently the Linear Matrix Inequality (LMI) approach has been successfully applied in the control area [16]. The stability problem can be formulated as LMI's. Also, other specific objectives from the time domain performance can be easily expressed in terms of some LMI's. Previously these would have been translated into some weighting function selection. This LMI based pole placement SDC is easier to develop compared to using a conventional controller design in the way that the performance requirement is explicitly formed in terms of LMIs instead of being included in a complex weighting function selection. The approach is practical and provides a fixed structure controller. The controller obtained is robust and can improve the system damping over a wide operating range. In Chapter 5, a supplementary controller for a TCSC device in power systems is designed with this LMI pole placement technique in a 4-machine test system.

1.3.2 LPV method

With the advent of restructuring, power transfer levels between regions around the North American interconnection have increased significantly and the interconnection is operating close to its operating limit. This has led to a larger variation of power system operating scenarios which cannot easily be represented as uncertainties based on a nominal operating point. An easier approach to circumvent the difficulty of uncertainty

representation is by using a gain-scheduling approach in which a different linear controller is obtained for each linearized plant; then an overall nonlinear controller that covers the entire operating range is obtained using a suitable scheduling scheme. The gain-scheduling approach is perhaps one of the most popular nonlinear control design techniques, and has been widely used in fields ranging from aerospace to process control. Although these controllers work well in practice, stability and performance guarantees cannot be provided except for slow-varying parameters [17, 18]. Furthermore, since the operating points are usually indexed by some combination of state or reference state trajectories, complex parameter-identification blocks are needed to perform scheduling and to deal with delicate stability questions in the switching zone.

Recently, a systematic gain-scheduling design technique has been developed in the form of linear parameter varying (LPV) control theory [19, 20]. This class of systems is different from the standard linear time-varying counterparts due to the causal dependence of its controller gains on the variations of plant dynamics. With real measurable scheduling variables, LPV can achieve a larger system operating range while guaranteeing stability and performance not only for slowly changing parameters but also for arbitrarily fast-changing parameters. Compared with classical gain-scheduling design, not only does it eliminate the strict limitations on the changing rates of scheduling variables, but it also provides theoretical guarantees for stability and performance instead of just rules of thumb. In addition, LPV control theory has been proven useful in simplifying the interpolation and realization problems associated with conventional gain-scheduling. Specifically, it allows us to treat a series of scheduled controllers as a single entity, with the gain scheduling achieved entirely by the parameter dependent controller.

In Chapter 6 a LPV model for a power system is proposed and then an LPV-based TCSC SDC is designed in a 50-machine system using a single quadratic Lyapunov function (SQLF). The sufficient conditions that guarantee the exponentially stability and the induced-norm performance objective of an LPV system are given. The SQLF method

exploits the realness of the varying parameters, but is still conservative in the sense that the parameters are allowed to vary arbitrarily fast. To reduce the conservatism, the known bounds on the parameters' rates of variation can be introduced in the LPV controller design based on a parameter-dependent Lyapunov function.

1.3.3 Interpolated LPV using multiple Lyapunov functions

For a given LPV system, it is clear that the achievable performance relies on the choice of the Lyapunov function. In [21] an interpolated LPV technique with multiple parameter-dependent Lyapunov functions is proposed and applied in a detailed AMB (Active Magnetic Bearing) controller design. The interpolated LPV has the advantage of improving the obtained performance by finding the most appropriate Lyapunov functions in a local sense. Then a globally constructed Lyapunov can be found to extend the local stability property to the entire parameter range. Since a power system is more complex and requires adequate damping under larger variation of system operating conditions, the interpolated LPV controller design using multiple Lyapunov functions (MLPV) is promising in the damping controller design for a large power system. In Chapter 6, an MLPV SDC is designed for a SVC in an IEEE 50-machine test system with the interpolated LPV approach. The results from both small-signal analysis and transient stability analysis show that, with the improved MLPV SDC, the system can achieve more consistent damping in a much wider operating range than a system with an LPV controller based on a single parameter-dependent Lyapunov function (SLPV SDC) or a conventional controller designed by the root locus method (RL SDC).

1.4 Controller design method comparison and selection

Three controller design methods have been discussed, each having its advantages and disadvantages. For example, with regional pole placement, a controller with fixed structure and fixed parameters can be obtained, which is certainly easy for a real-life field

application. But, when a system is large and consequently has a massive number of poles that cannot be all placed within acertain type of region, some difficulties may arise and a solution may not be obtained. Also, this method is still based on the premise that it is hard to deal with the formulation of the uncertainty block when the system is undergoing a large operating-point change. Therefore, in a large system where the extension of the system operating range is more important and the formulation of the traditional uncertainty is challenged, the LPV method is a good option. When a LPV controller cannot be achieved in a larger range, the interpolated LPV technique can be considered. However, the associated computational effort will increase when the LPV technique is applied as compared to the regional pole placement method. In addition, a realization scheme for the LPV approach should also be developed to facilitate the application of the LPV controller.

For a specific system, different methods might produce different effectiveness. There is a tradeoff between the obtained performance and the complexity of the controller structure. It is necessary to compare efficacy and feasibility of controller design methods in a specific power network in order to obtain a suitable controller design. The oscillatory modes and their shapes will be different in different power networks, which will consequently cause various problems in some controller design approaches. For example, the regional pole placement method works well in a four–machine [22] system, in which there is only one pair of poorly damped modes. By restricting all the poles into some appropriate region, the minimum damping for the system is guaranteed and achieved. However, for a large system like the IEEE 50-machine system, there are several poorly damped local modes very close to the imaginary axis and almost unobservable and uncontrollable, as shown in Figure 1.2,. Thus in such a case, the regional pole placement method is no longer feasible because of the existence of these uncontrollable modes. Other schemes such as the LPV technique must be developed to target this complex situation.

In considering controller design in the 50-machine system for a TCSC device, problems in achieving desired damping performance due to the system structure occur. An additional feedback signal may be used to relax the constraints set by the system. Then a two-input single-output (TISO) controller has the advantage of achieving desired performance and also simple structural realization.

In all, there is a need to find an efficient controller design method based on each different and unique power network.

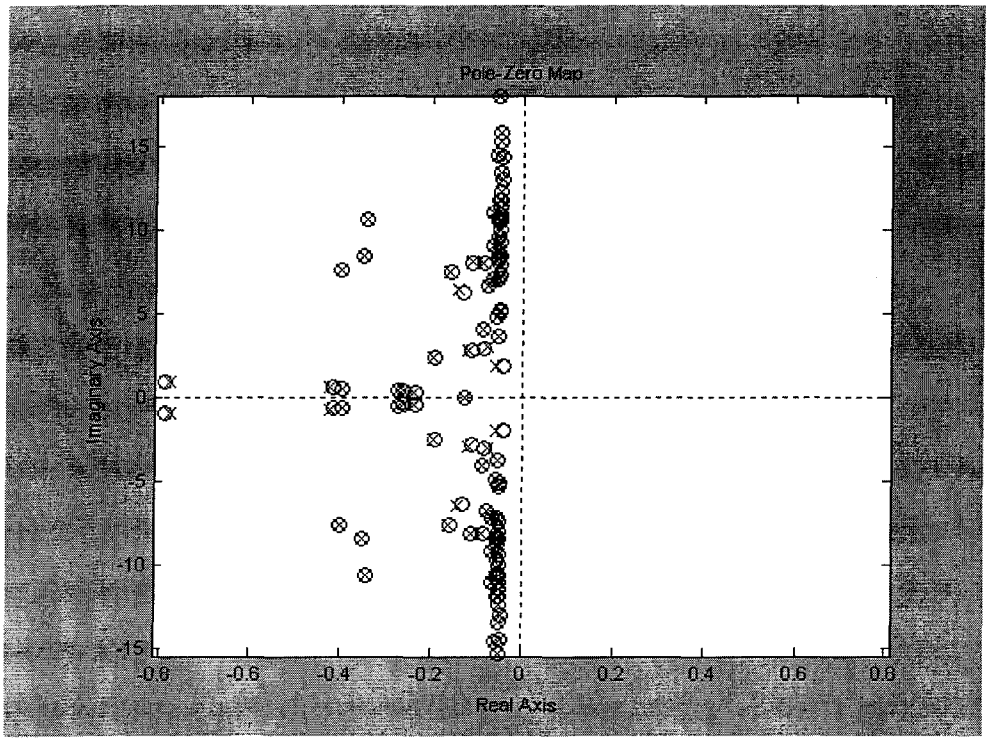

Figure 1.2 Pole-zero map for 50-machine system at P93,110=1300MW

1.5 Problem Objectives

The main objective of this research work is to overcome the difficulties in existing controller designs by carefully choosing an effective controller design method based on different system structures and by improving the controller design method with advanced technologies such as LMI and LPV. This requires developing a good understanding of differences in effectiveness of different FACTS damping controllers, and then choosing an

effective FACTS device based on detailed analysis of modal oscillations and dynamics for a particular system. This analysis also includes a detailed consideration of the tradeoffs in different controller design methods in different systems, a careful selection and development of appropriate improved controller design methods, along with their controller applications in two typical test systems. Consequently, the resulting advanced controller not only guarantee system robust stability and achieve desired damping performance, but also extend the system's operating range with relatively moderate complexity in field realizations.

The scope of this research work includes the following.

Compare effectiveness of PSS's, SVC controllers, and TCSC controllers on damping inter-area oscillations under various system operating conditions, and select an appropriate FACTS device to achieve the desired overall damping performance with respect to different power system networks and modal oscillatory analysis.

Investigate effectiveness of different FACTS devices on damping enhancement under changes in system operating conditions. Using network equations and differential equations, equations are derived to show the influence of different FACTS devices. The derivations are well established by two test systems, a 4-machine system and the IEEE 50-machine system. Then a TCSC damping controller will be designed for the four-machine system and a SVC damping controller will be designed for the IEEE 50-machine system.

Describe detailed location selections for the TCSC or the SVC in the 50-machine system using modal shape analysis and modal controllability calculations.

Develop a robust regional pole placement controller design method based on LMIs to directly address the damping improvement problem. A TCSC controller with fixed parameters is obtained and applied in the 4-machine system and its damping effects are compared with that for a traditional controller.

Investigate difficulties in obtaining feasible LPV solutions in a larger operating range

than with the conventional LPV technique. To improve limited performance, an interpolated LPV technique using multiple Lyapunov functions is developed in divided parameter subsets and this result is applied to the same IEEE 50-machine system. The performance achieved by the conventional LPV controller and the interpolated LPV controller are compared and it is found that the operating range is significantly extended with the interpolated LPV technique.

Investigate difficulties due to pole-zero interactions in a TCSC controller design for the IEEE 50-machine system and relieve them by adding a secondary measurement. A two-input one-output controller will be developed and applied with obvious performance improvements.

1.6 Dissertation outline

In this dissertation, the effectiveness of TCSC controllers and SVC controllers in damping oscillatory modes is first analyzed and compared. Then an improved robust regional pole placement method based on LMIs is presented. Furthermore, a LPV controller design method that outperforms the mixed sensitivity controller design with respect to uncertainty representation is introduced and provides improved performance over a wider range of operation. Finally an interpolated LPV method to achieve better performance in a further extended operating range is proposed. In addition, a two-input single-output damping controller for a TCSC device applied to the IEEE 50-machine system is developed, since a single-input single-output controller for the TCSC device has limits in achieving the desired damping performance due to the interaction between zeros and poles. The efficacy and feasibility of applying different modern control techniques to power systems has been clearly demonstrated, and the choice and development of the appropriate advanced control techniques to obtain the desired performance is described.

2 LITERATURE REVIEW

2.1 Damping improvements

With regard to the issue of improving damping of the power system, installing a supplementary damping controller (SDC) for FACTS device is another effective approach in addition to PSS. In current power system networks, more FACTS devices are needed to extend the possible transfer level over several regions. Therefore, adding a supplementary controller to improve damping is an extension of such a unit's economic benefits in power systems.

The use of series-connected controllable components for power flow control in electric power systems is described in [23][24]. In 1966 Kimbark showed that the transient stability could be improved by a switched series capacitor [25]. Later work has explored the benefits of the controllable series capacitor for improving small disturbance stability [26]. Reference [27] gives some concepts about the effectiveness of improving the damping by a FACTS SDC. In [28] some exploratory concepts were presented on the details of the control of TCSC in transmission systems. In [4][5], a unified Phillips-Heffron Model, which has been used for the study of power system oscillation stability for decades, has been extended to a single-machine infinite-bus power system as well as multi-machine power systems with FACTS stabilizers to show the theoretical feasibility of improving system damping by applying suitable FACTS devices at suitable locations. The application of TCSC for damping power oscillations has been demonstrated consistently via time domain simulations in many technical publications [29]. Several references [30] [31] have shown that FACTS controllers can have a significant impact in damping inter-area system oscillations if a such controllers can be designed and applied at a suitable location. The concept of interaction of FACTS SDC

and PSS is introduced and explained in reference [32]. Observations from both field tests and analysis reveal that the damping of inter-area modes from a FACTS SDC tends to be inferior to that expected from the design of multi-machine PSS's based on damping torque concepts.

2.2 Damping controller design methodology

In order to increase the damping in the system, point-wise pole-placement based on a Root locus Plot was used in [1], where the controller design was based only on a nominal operating case. In reality, the power system network cannot be fixed at one operating point as it experiences load variation, generation variation, and some topology changes due to faults etc. To address the robustness issue, several approaches have been developed using a linear time invariant (LTI) controller to guarantee robust stability and robust performance, and describing the changes in operating condition as uncertainties [14, 15]. These methods aim to minimize the induced norm in order to increase damping. These techniques do not address the objective of closed-loop damping in a straightforward manner. The weighting functions required in these methods do not have explicit relationships with the closed-loop damping ratio. However, new techniques such as linear matrix inequalities (LMIs) give more flexibility in dealing with damping control. Researchers have shown that elementary manipulation of Linear Matrix Inequalities (LMI) can be used to formulate damping requirements in terms of an appropriate region for poles in the control problem [33]. Further research has developed LMI-based formulations for multi-objective H2/H, control design [16]. Meanwhile, the availability of fast and efficient tools (such as convex optimization techniques) has made the LMI-based control synthesis practical.

Meanwhile, some large power networks have been undergoing large variations in operating conditions due to the operation of the real-time market, emergencies as well as actions from automatic devices. Under these conditions, describing the changes in

operating conditions as uncertainties is no longer feasible in the robust controller design. In [34] an artificial neural network-based fuzzy-logic excitation control system has been proposed to enhance the damping of electric power systems. Also, extensive research has focused on developing analysis and synthesis techniques for gain-scheduled controllers in linear parameter varying (LPV) systems [35,36,37,38,39,40]. The notation of LPV systems was first introduced in [41]. The technique is commonly referred to as an LPV gain-scheduling approach. The LPV design technique provides guaranteed stability and performance properties, and simplifies the interpolation and realization problems associated with conventional gain-scheduling methods. Usually a single quadratic Lyapunov function (SQLF) is used to obtain a LPV controller [36], [42]. The LPV SQLF method exploits the realness of the varying parameters, but is still conservative in the sense that the parameters are allowed to vary arbitrarily. To reduce the conservatism, the known bounds on the parameters' rates of variation can be introduced in the LPV controller design based on a parameter-dependent Lyapunov function. An LPV gain-scheduling technique has been successfully applied in many engineering applications such as flight and process control [43,44,45,46]. In [47], the LPV technique has been successfully used in the design of PSS's in two typical power systems. In [48], the gain-scheduling controller design method is suggested and successfully used in developing an HVDC control strategy. Although gain-scheduling controllers work well in practice, stability and performance guarantees cannot be provided except for slowly varying parameters [17,18]. A systematic gain-scheduling design technique has been developed in the form of linear parameter varying (LPV) control theory [19,20]. In [7], an LPV-based PSS was designed to achieve better damping than the conventionally designed PSS's, both in the four-machine system and the 50-machine system.

A remaining primary practical difficulty in the LPV approach is solvability under an extended operating range in some power networks, or when the controllability of the device is too small, as is the case for some FACTS devices. Usually to solve the infinite

number of constraints, an ad hoc gridding method is used to divide the parameter space and render the semi-infinite optimization problem finite. However, when the parameter space is too large due to the extended operating range, a controller that satisfies an increasing number of LMIs at more gridding points cannot be obtained. Furthermore, the performance achieved might possibly be sacrificed for a LPV system in order to get a controller based on single parameter-dependent Lyapunov function. For the given LPV system, it is clear that achievable performance relies on the choice of the Lyapunov function. In [21] an interpolated LPV technique with multiple parameter-dependent Lyapunov functions is proposed and successfully applied to a detailed AMB (Active Magnetic Bearing) controller design. The promising results obtained in process control strongly suggest the significant potential of this improved LPV technique when applied to large power systems to increase and extend the operating range.

3 POWER SYSTEM MODEL AND TEST SYSTEMS

3.1 Generator Model

The complete mathematical description of the synchronous machines is too complicated to be used directly for system anlysis and synthesis. Different degrees of approximations are adopted to simplify the generator model. Two kinds of generator models are used in the dissertation, which are the two-axis model and the classical model [49]. It is assumed that in a *n*-generator system, the first *m* generators are represented by the two-axis model and equipped with exciters and the remaining *n-m* generators are represented using the classical model.

3.1.1 Classical Model

The classical model represents the simplest model for generators and it assumes the following:

Mechanical power input is constant.

Damping or asynchronous power is negligible.

Constant-voltage-behind-transient-reactance model for the synchronous machines is valid.

The mechanical rotor angle of a machine coincides with the angle of the voltage behind the transient reactance.

The dynamic equations for the classical model are given by (Increase font size of equations)

$$M_i\dot{\omega}_i = P_i - P_{ei} \tag{3.1}$$

$$\dot{\delta}_i = \omega_i - \omega_S \quad i = m+1, m+2, ..., n \tag{3.2}$$

Where,

$$P_i = P_{mi} - E_i^2 G_{ii} \tag{3.3}$$

$$P_{ei} = \sum_{j=1, j\neq i}^{n} [E_i E_j B_{ij} \sin(\delta_i - \delta_j) + E_i E_j G_{ij} \cos(\delta_i - \delta_j)] \tag{3.4}$$

and

E_i : internal bus voltage of generator i

M_i : inertia constant of generator i

P_{mi} : mechanical power input of generator I

G_{ii} : driving point conductance of node i

$G_{ij} + jB_{ij}$: the transfer admittance between node I and node j in the reduced network

ω_i : rotor speed of generator I (with respect to the synchronous frame)

ω_S : synchronous speed

3.1.2 Two-axis Model

In the two-axis model the transient effects are accounted for and the following assumptions are required.

In the stator voltage equations the variation of flux linkages of *d-q* axes are negligible compared to the speed voltage terms.

$$\omega \cong \omega_S = 1 p.u. \tag{3.5}$$

The resultant dynamic equations are given by

$$\tau'_{d0i} \dot{E}'_{qi} = E_{FDi} - E'_{qi} + (x_{di} - x'_{di}) I_{di} \tag{3.6}$$

$$\tau'_{q0i} \dot{E}'_{di} = -E'_{di} + (x_{qi} - x'_{qi}) I_{qi} \tag{3.7}$$

$$M_i \dot{\omega}_i = P_{mi} - (I_{di} E'_{di} + I_{qi} E'_{qi}) + (x'_{qi} - x'_{di}) I_{qi} I_{di} - D_i(\omega_i - \omega_S) \tag{3.8}$$

$$\dot{\delta}_i = \omega_i - \omega_S \qquad i = 1,2,...,m \tag{3.9}$$

where,

E'_d, E'_q : direct and quadrature axes stator EMFs corresponding to rotor transient flux components, respectively

I_d, I_q : the d and q axes stator currents.

τ'_{d0}, τ'_{q0}: open-circuit direct and quadrature axes transient time constants

x_d, x'_d: direct axis synchronous and transient reactances

x_q, x'_q : quadrature axis synchronous and transient reactances

E_{FD}: stator EMF corresponding to the field voltage

D_i: damping coefficient of generator i

Angle Reference

In (3.2) and (3.9), the absolute rotor angles $(\delta_i, i = 1,2,...,n)$ are used as state variables. Since these n-state variables are not independent, the relative rotor angles are introduced as new state variables which are independent. Without loss of generality, δ_1 is chosen as reference, then the relative rotor angles are defined as:

$$\delta_{i1} = \delta_i - \delta_1, \quad i = 2,3,...,n \tag{3.10}$$

The dynamic equations (3.3)-(3.8) remain unchanged with each δ_i replaced by δ_{i1} and ω_S replaced by ω_1. Therefore (3.2) and (3.9) becomes

$$\dot{\delta}_{i1} = \omega_i - \omega_1, \quad i = 2,3,...,n \tag{3.11}$$

3.2 Excitation System Model

The type of excitation system used in ETMSP Type-30 [50](same as IEEE AC-4, see [51]). The state variables are E_{FD}, X_{E1}, and X_{E2}, and the dynamic equations are given by

$$\dot{E}_{FDi} = \frac{K_{Ai}}{T_{Ai}} X_{E2i} - \frac{1}{T_{Ai}} E_{FDi} + \frac{aK_{Ai}}{T_{Ai}} (V_{REFi} - X_{E1i}) \tag{3.12}$$

$$\dot{X}_{E1i} = -\frac{1}{T_{Ri}} X_{E1i} + \frac{1}{T_{Ri}} V_{Ti} \tag{3.13}$$

$$\dot{X}_{E2i} = -\frac{1}{T_{Bi}} X_{E2i} + \frac{1-a}{T_{Bi}} (V_{REFi} - X_{E1i}) \tag{3.14}$$

$$V_T = V_{Tq} + jV_{Td}$$

$$= (E'_q + x'_d I_d) + j(E'_d - x'_q I_q) \qquad i = 1,2,...,m \tag{3.15}$$

Where,

V_T : generator terminal voltage

V_{REF} : exciter reference voltage

$a = T_{Ci} / T_{Bi}$, T_{Bi} and T_{Ci} are time constants

3.3 FACTS model

3.3.1 SVC model

The standard ETMSP Type-1 model is used for the SVC [50]. Its block diagram is shown in Figure 3-1. The state variables are X_{S1}, X_{S2}, and B_{SVC}, and the dynamic equations are given by:

$$\dot{X}_{S1} = -\frac{1}{T_3} X_{S1} + \frac{(1-a_1)K}{T_3} (V_{SVC} - V_{REF}) \tag{3.16}$$

$$\dot{X}_{S2} = \frac{1-a_2}{T_4} X_{S1} - \frac{1}{T_4} X_{S2} + \frac{(1-a_2)a_1 K}{T_4} (V_{SVC} - V_{REF}) \tag{3.17}$$

$$\dot{B}_{SVC} = \frac{a_2}{T_5} X_{S1} + \frac{1}{T_5} (X_{S2} - B_{SVC}) + \frac{a_1 a_2 K}{T_5} (V_{SVC} - V_{REF}) \tag{3.18}$$

where,

B_{SVC} : equivalent admittance of the SVC

V_{SVC} :voltage magnitude of the SVC bus ($=V_{n+1}$)

V_{REF} : SVC reference voltage

$$a_1 = \frac{T_1}{T_3} \tag{3.19}$$

$$a_2 = \frac{T_2}{T_4} \tag{3.20}$$

Later in Chapter 6 of this dissertation, a supplementary damping controller (SDC) will be designed and added to the SVC's voltage control loop to damp the interarea oscillations, as shown in Fig. 3.1.

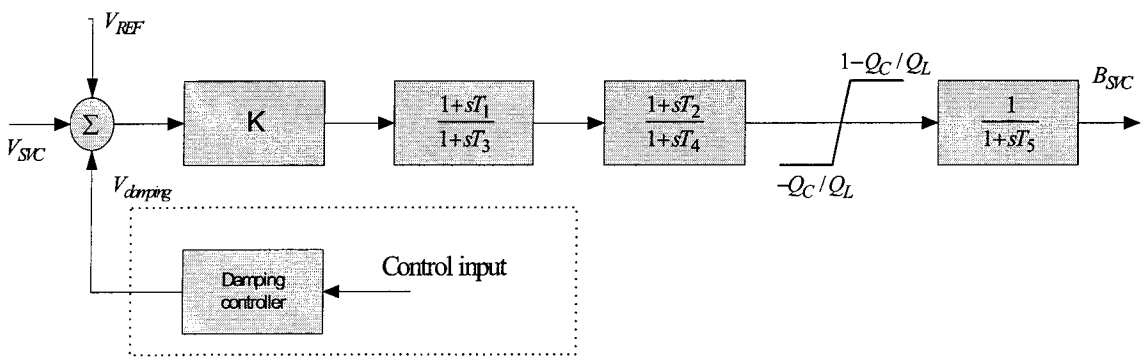

Figure 3.1 . ETMSP standard SVC type-1 with SDC added.

3.3.2 TCSC model

Its block diagram is shown in Figure 3-2. The state variables are $X_{S1}, X_{S2}, X_{S3}, X_{S4}$ and X_{TCSC}, and the dynamic equations are given by:

$$\dot{X}_{s1} = -\frac{1}{T_W} X_{s1} - \frac{K_1}{T_W} P_{n+1,n+2} \tag{3.21}$$

$$\dot{X}_{s2} = -\frac{1}{T_W} X_{s2} - \frac{K_2}{T_W} V_{n+1} \tag{3.22}$$

$$\dot{X}_{s3} = \frac{1}{T} X_{s3} - \frac{1}{T} X_{s1} + \frac{K_1}{T} P_{n+1,n+2} \tag{3.23}$$

$$\dot{X}_{s4} = \frac{1}{T} X_{s4} - \frac{1}{T} X_{s2} + \frac{K_2}{T} V_{n+1} \tag{3.24}$$

$$\dot{X}_{TCSC} = \frac{1}{T_{TCSC}} X_{s3} + \frac{1}{T_{TCSC}} X_{s4} - \frac{1}{T_{TCSC}} X_{TCSC} - \frac{1}{T_{TCSC}} V_{REF} \tag{3.25}$$

where,

X_{TCSC} : equivalent reactance of the TCSC

V_{SVC} :voltage magnitude of the SVC bus ($= V_{n+1}$)

V_{REF} : TCSC reference voltage

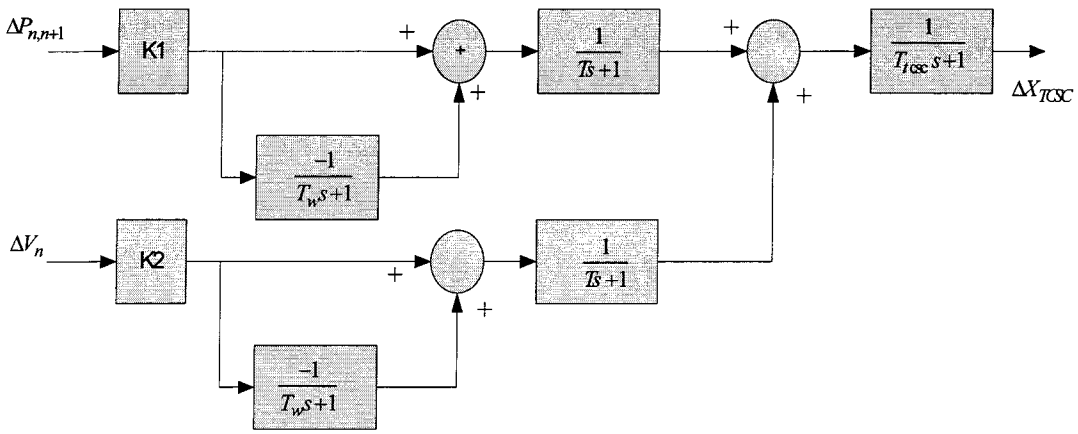

Figure 3.2 TCSC Controller Model

Later in Chapter 7 of this dissertation, a supplementary damping controller (SDC) will be designed and added to the TCSC's voltage control loop to damp the interarea oscillations, as shown in Fig. 3.2.

3.3.3 General FACTS model used for damping controller design

Fig. 3.3 shows a block diagram for the FACTS model for typical transient and oscillatory stability studies [52]. In engineering applications, conventional FACTS

controls consist of, in general, three control loops: power flow control loop, damping loop to suppress the subsequent power oscillation, and transient control loop for improving the first swing stability. The device thyristor firing and other delays are usually represented by a single lag of about 15ms. In this dissertation, the focus is on the damping controller design while neglecting the power flow control and the transient control. Thus, only one dynamic equation is used to represent the delay block in the FACTS device,

$$\dot{X}_{FACTS} = -\frac{1}{T_{FACTS}} X_{FACTS} - \frac{1}{T_{FACTS}} V_{REF} \tag{3.26}$$

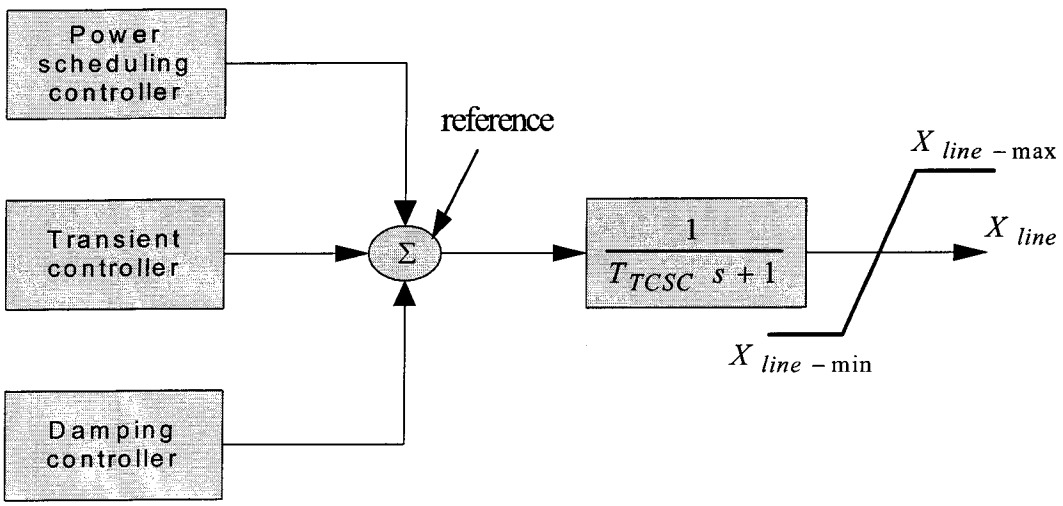

Figure 3.3 Block diagram for the FACTS model for typical stability studies

3.4 Load model

All of the loads are represented by constant impedance in this research. The load nodes and the terminal voltage nodes of the generators are eliminated except for the bus nodes where the FACTS devices are installed. Therefore, the resulting network contains only the internal generator nodes (numbered from 1 to n) and the FACTS nodes (numbered from n+1 to n+2). The generator reactance and the constant impedance loads are included

in the bus admittance matrix.

3.5 Network Modeling

The reduced network contains only the generator internal buses. The bus admittance (the equations are not in line with the text) matrix Y_{bus} consists of $Y_{ij}\angle\gamma_{ij} = G_{ij} + jB_{ij}$.

Since generators are reduced to their internal buses, the associated currents and voltages are usually in the $d-q$ axis reference frame, as shown in (3.5)-(3.9).

The generator currents can be given in the following form:

$$I_{qi} = \sum_{j=1}^{m}[F_{G+B}(\delta_{ij})E'_{qj} - F_{B-G}(\delta_{ij})E'_{dj}] + \sum_{k=m+1}^{n} F_{G+B}(\delta_{ik})E_k \tag{3.27}$$

$$I_{di} = \sum_{j=1}^{m}[F_{B-G}(\delta_{ij})E'_{qj} + F_{G+B}(\delta_{ij})E'_{dj}] + \sum_{k=m+1}^{n} F_{B-G}(\delta_{ik})E_k \tag{3.28}$$

$i = 1,2,...,n$

where

$$F_{G+B}(\delta_{ij}) = G_{ij}\cos(\delta_{ij}) + B_{ij}\sin(\delta_{ij}) \tag{3.29}$$

$$F_{B-G}(\delta_{ij}) = B_{ij}\cos(\delta_{ij}) - G_{ij}\sin(\delta_{ij}) \tag{3.30}$$

$$\delta_{ij} = \delta_i - \delta_j \tag{3.31}$$

For the buses where FACTS are installed, based on $I_{qn+1} = I_{qn+2} = I_{dn+1} = I_{dn+2} = 0$,

$$0 = \sum_{j=1}^{m}\left[F_{G+B}\left(\delta_{n+1,j}\right)E'_{qj} - F_{B-G}\left(\delta_{n+1,j}\right)E'_{dj}\right] + F_{G+B}\left(\delta_{n+1,n+1}\right)V_{n+1} + F_{G+B}\left(\delta_{n+1,n+2}\right)V_{n+2} = g_1 \tag{3.32}$$

$$0 = \sum_{j=1}^{m}\left[F_{B-G}\left(\delta_{n+1,j}\right)E'_{qj} + F_{G+B}\left(\delta_{n+1,j}\right)E'_{dj}\right] + F_{B-G}\left(\delta_{n+1,n+1}\right)V_{n+1} + F_{B-G}\left(\delta_{n+1,n+2}\right)V_{n+2} = g_2 \tag{3.33}$$

$$0 = \sum_{j=1}^{m}\left[F_{G+B}\left(\delta_{n+2,j}\right)E'_{qj} - F_{B-G}\left(\delta_{n+2,j}\right)E'_{dj}\right] + F_{G+B}\left(\delta_{n+2,n+1}\right)V_{n+1} + F_{G+B}\left(\delta_{n+2,n+2}\right)V_{n+2} = g_3 \tag{3.34}$$

$$0 = \sum_{j=1}^{m}\left[F_{B-G}\left(\delta_{n+2,j}\right)E'_{qj} + F_{G+B}\left(\delta_{n+2,j}\right)E'_{dj}\right] + F_{B-G}\left(\delta_{n+2,n+1}\right)V_{n+1} + F_{B-G}\left(\delta_{n+2,n+2}\right)V_{n+2} = g_4 \tag{3.35}$$

$$\begin{bmatrix} \Delta V_{n+1} \\ \Delta\theta_{n+1} \\ \Delta V_{n+2} \\ \Delta\theta_{n+2} \end{bmatrix} = -\begin{bmatrix} \frac{\partial f_{10}}{\partial V_{n+1}} & \frac{\partial f_{10}}{\partial \theta_{n+1}} & \frac{\partial f_{10}}{\partial V_{n+2}} & \frac{\partial f_{10}}{\partial \theta_{n+2}} \\ \frac{\partial f_{11}}{\partial V_{n+1}} & \frac{\partial f_{11}}{\partial \theta_{n+1}} & \frac{\partial f_{11}}{\partial V_{n+2}} & \frac{\partial f_{11}}{\partial \theta_{n+2}} \\ \frac{\partial f_{12}}{\partial V_{n+1}} & \frac{\partial f_{12}}{\partial \theta_{n+1}} & \frac{\partial f_{12}}{\partial V_{n+2}} & \frac{\partial f_{12}}{\partial \theta_{n+2}} \\ \frac{\partial f_{13}}{\partial V_{n+1}} & \frac{\partial f_{13}}{\partial \theta_{n+1}} & \frac{\partial f_{13}}{\partial V_{n+2}} & \frac{\partial f_{13}}{\partial \theta_{n+2}} \end{bmatrix}^{-1}$$

$$\begin{bmatrix} \frac{\partial f_{10}}{\partial E'_{qj}} & \frac{\partial f_{10}}{\partial E'_{dj}} & 0 & \frac{\partial f_{10}}{\partial \delta_{k1}} & 0 & 0 & 0 & 0 & 0 & 0 & 0 & \frac{\partial f_{10}}{\partial X_{TCSC}} \\ \frac{\partial f_{11}}{\partial E'_{qj}} & \frac{\partial f_{11}}{\partial E'_{dj}} & 0 & \frac{\partial f_{11}}{\partial \delta_{k1}} & 0 & 0 & 0 & 0 & 0 & 0 & 0 & \frac{\partial f_{11}}{\partial X_{TCSC}} \\ \frac{\partial f_{12}}{\partial E'_{qj}} & \frac{\partial f_{12}}{\partial E'_{dj}} & 0 & \frac{\partial f_{12}}{\partial \delta_{k1}} & 0 & 0 & 0 & 0 & 0 & 0 & 0 & \frac{\partial f_{12}}{\partial X_{TCSC}} \\ \frac{\partial f_{13}}{\partial E'_{qj}} & \frac{\partial f_{13}}{\partial E'_{dj}} & 0 & \frac{\partial f_{13}}{\partial \delta_{k1}} & 0 & 0 & 0 & 0 & 0 & 0 & 0 & \frac{\partial f_{13}}{\partial X_{TCSC}} \end{bmatrix} \begin{bmatrix} \Delta E'_{qi} \\ \Delta E'_{di} \\ \Delta \omega_i \\ \Delta \delta_{k1} \\ \Delta E_{FDi} \\ \Delta X_{E1i} \\ \Delta X_{E2i} \\ \Delta X_{S1} \\ \Delta X_{S2} \\ \Delta X_{S3} \\ \Delta X_{S4} \\ \Delta X_{TCSC} \end{bmatrix} \tag{3.36}$$

3.6 Overall System Equation

From the above discussions, the dynamic equations governing the generators and exciters could be cast in the following form:

$$\dot{X} = f(X, Y, u) \tag{3.37}$$

where

$X^T = [X_{SM}^T, X_{ES}^T, X_{FACTS}]$, the vector of state variables

$X_{SM} = [E'_{q1}, E'_{d1}, \omega_1, ..., E'_{qm}, E'_{dm}, \omega_m, \delta_{m1}, \omega_{m+1}, \delta_{(m+1)1}, ..., \omega_n, \delta_{n1}]^T$

$X_{ES} = [E_{FD1}, X_{E11}, X_{E21}, ..., E_{FDm}, X_{E1m}, X_{E2m}]^T$

$Y = [V_{n+1}, \theta_{n+1}, V_{n+2}, \theta_{n+2}]^T$

$u = V_{REF}$, the reference input of the FACTS device.

And f is the vector of nonlinear functions summarized below

$$f_{1i} = \dot{E}'_{qi} = \frac{1}{\tau'_{d0i}}\left[E_{FDi} - E_{qi} + (x_{di} - x'_{di})I_{di}\right] \qquad i = 1, ..., m \tag{3.38}$$

$$f_{2i} = \dot{E}'_{di} = \frac{1}{\tau'_{q0i}}\left[-E_{di} + (x_{qi} - x'_{qi})I_{qi}\right] \qquad i = 1, ..., m \tag{3.39}$$

$$f_{3i} = \dot{\omega}_i = \frac{1}{M_i}\left[P_{mi} - (I_{di}E'_{di} + I_{qi}E'_{qi}) + (x'_{qi} - x'_{di})I_{qi}I_{di} - D_i(\omega_i - \omega_s)\right] \qquad i = 1, ..., n \tag{3.40}$$

$$f_{4i} = \dot{\delta}_{i1} = \omega_i - \omega_1 \qquad i = 2, ..., n \tag{3.41}$$

$$f_{5i} = \dot{E}_{FDi} = \frac{K_{Ai}}{T_{Ai}}X_{E2i} - \frac{1}{T_{Ai}}E_{FDi} + \frac{aK_{Ai}}{T_{Ai}}(V_{REFi} - X_{E1i}) \qquad i = 1, ..., m \tag{3.42}$$

$$f_{6i} = \dot{X}_{E1i} = -\frac{1}{T_{Ri}}X_{E1i} + \frac{1}{T_{Ri}}V_{Ti} \qquad i = 1, ..., m \tag{3.43}$$

$$f_{7i} = \dot{X}_{E2i} = -\frac{1}{T_{Bi}} X_{E2i} + \frac{1-a}{T_{Bi}} (V_{REFi} - X_{E1i}) \qquad i = 1,...,m$$

$$f_8 = \dot{X}_{FACTS} = -\frac{1}{T_{FACTS}} X_{FACTS} - \frac{1}{T_{FACTS}} V_{REF} \tag{3.44}$$

Linearization of (3.37) leads to

$$\Delta\dot{X} = \frac{\partial f}{\partial X}\Delta X + \frac{\partial f}{\partial Y}\Delta Y + \frac{\partial f}{\partial u}\Delta u$$

(3.45)

the network algebraic equation are given by

$$g(X,Y) = 0 \tag{3.46}$$

Its linearization results in

$$\frac{\partial g}{\partial X}\Delta X + \frac{\partial g}{\partial Y}\Delta Y = 0 \tag{3.47}$$

$$\Delta Y = -(\frac{\partial g}{\partial Y})^{-1} \frac{\partial g}{\partial X}\Delta X \tag{3.48}$$

the details of the linearization in (3.45) and (3.47) can be found in Appendix A.

Substitute (3.48) into (3.45),to obtain the representation of the whole system in the state space form

$$\Delta\dot{X} = A\Delta X + B\Delta u \tag{3.49}$$

where

$$A = \frac{\partial f}{\partial X} - \frac{\partial f}{\partial Y}(\frac{\partial g}{\partial Y})^{-1} \frac{\partial g}{\partial X} \tag{3.50}$$

$$B = \frac{\partial f}{\partial u} \tag{3.51}$$

The detailed expressions for the elements of A and B matrices are listed in Appendix A.

3.7 Test system

3.7.1 4-machine system

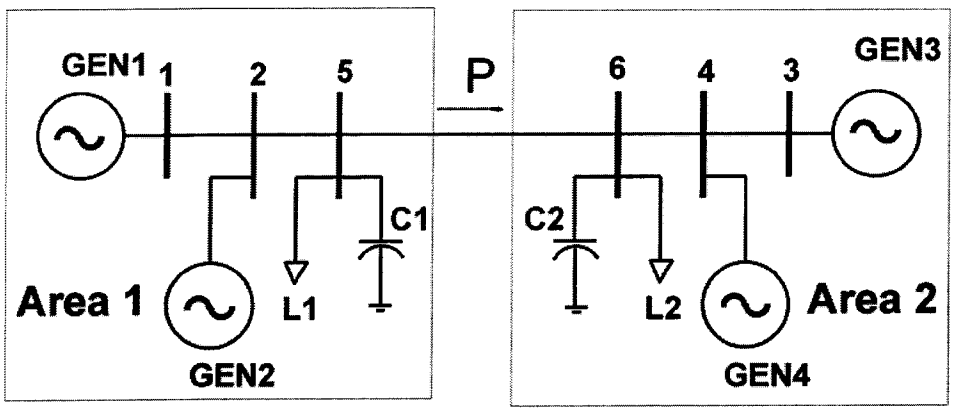

Figure 3.4 4-machine test system

3.7.2 IEEE 50-machine system

A 50-machine [53] is used in this paper. This is a moderate sized system that includes all the modeling features and the complexity of a large-scale power system. A one-line diagram of the area of interest is shown in Fig. 3.5. This test system contains 44 generators represented by the classical model with uniform damping and 6 generators represented by a two-axis model. No PSS is installed in the system. The operating point is characterized by setting the real power generation at Buses #93 and #110. This generation varies in the range of [2× 1200– 2× 1700] MW. Six gridding points are chosen for each generator. They correspond to 2× 1200 MW, 2× 1300 MW, 2× 1400 MW, 2× 1500MW, 2× 1600 MW, and 2× 1700 MW of generation at Buses #93 and #110. For each gridding point, the power flow for the interconnected system is solved and the real and reactive power output of each generator can be determined.

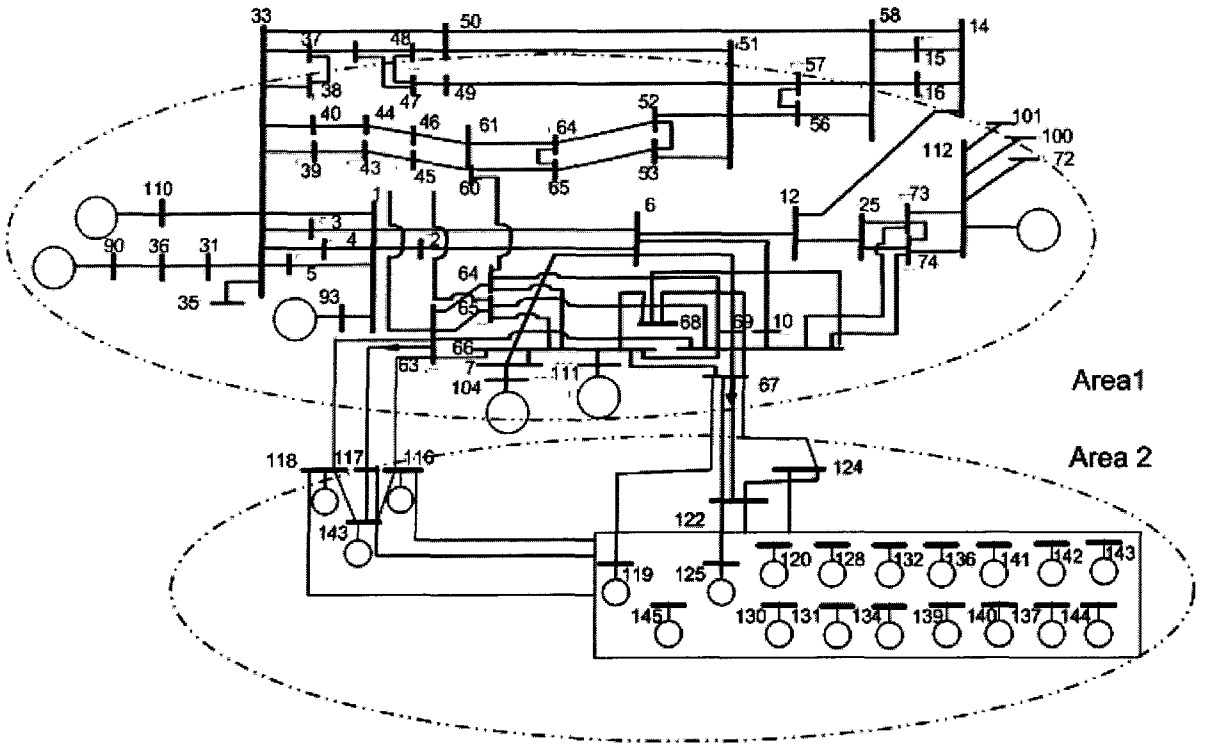

Figure 3.5 IEEE 50-Machine Test System

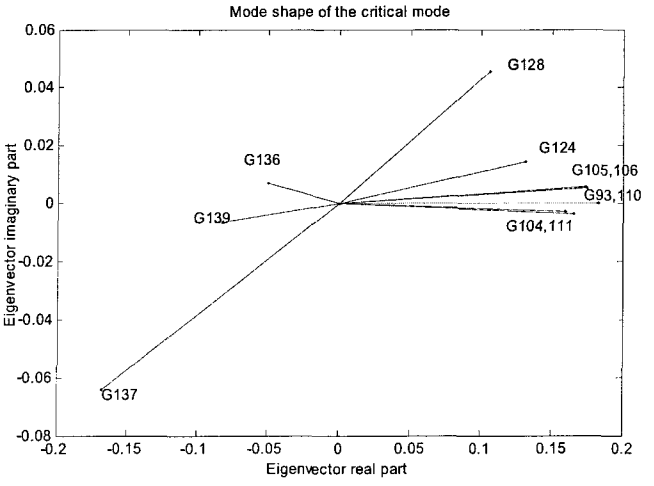

Figure 3.6 Mode shape for the critical mode at 0.28 Hz

There are a several poorly damped modes for this system in the frequency range of 0.1Hz to 2Hz. Since the TCSC is more effective in improving the damping of the inter-area

modes than the damping of the local modes, the inter-area modes are first identified. Among the poorly damped inter-area modes shown in Table 3.1, a pair of modes around 0.28 Hz has an obvious decreasing damping ratio with the increase of the generation at G93 and G110. Therefore, this mode is critical to the system stability with regard to the increase of the system stress level. Hence the focus will primarily be on the damping improvement of this pair of modes. From its mode shape in Fig. 3.6, observe that the mode involves lots of generators in the system. From the participation factor calculated, it is found that the critical inter-area mode is mainly due to the oscillation between area 1, which is formed by G93, G110, G104, G111, G105, G106, and area 2, which is mainly formed by G139, G136 and G137.

Table 3.1 INTER_AREA MODES IN THE OPEN-LOOP SYSTEM

Gen level at G93, G110	Mode 1	Mode 2
1200	8.53%@0.4447Hz	4.74%@0.2968Hz
1300	8.71%@0.4362Hz	3.17%@0.2914Hz
1400	8.94%@0.4298Hz	1.09%@0.2847Hz
1500	9.22%@0.4245Hz	-1.62% @0.2768Hz
1600	9.49%@0.4200Hz	-5.10% @0.2671Hz
1700	9.73%@0.4160Hz	-9.71%@0.2550Hz

4 DAMPING CONTROL EFFECTIVENESS AND LOCATION SELECTION

4.1 Comparison of the effectiveness of different FACTS devices on damping control under system operating condition changes

The effectiveness of a TCSC controller and a SVC controller will now be compared with regard to the damping issue based on controllability calculation.

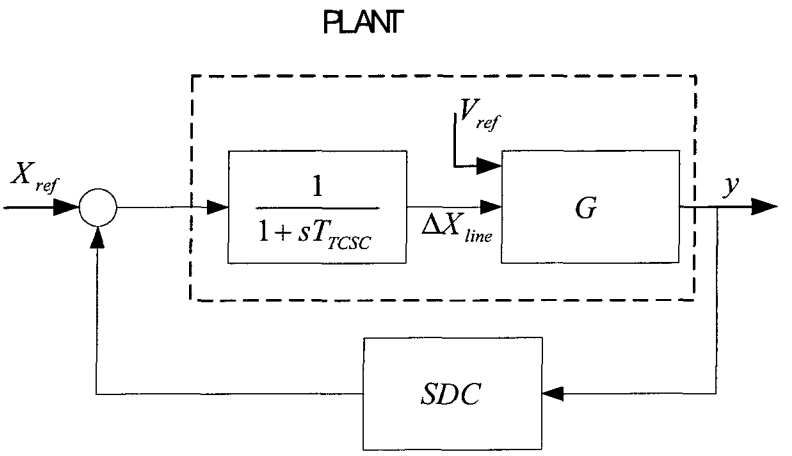

Figure 4.1 system with FACT controllers

In figure 4.1, the FACTS device introduces an adaptive impedance block which is indirectly interrelated with the system G through intermediate variables y.

System G has a state-space representation which captures the differential dynamics of the various components

$$\dot{X} = f(X, Y, V_{ref}) \tag{4.1}$$

At the same time, there is a set of algebraic equations based on the power network

$$g(X, Y, \Delta X_{line}) = 0 \tag{4.2}$$

Linearizing equations (4.2), $\Delta Y = G_1 \Delta X + G_2 \Delta X_{line}$ (4.3)

Linearizing (4.1) and substituting into (4.3), one obtains

$$\Delta \dot{X} = \frac{\partial f}{\partial X}\Delta X + \frac{\partial f}{\partial Y}G_1 \Delta X + \frac{\partial f}{\partial Y}G_2 \Delta X_{line} + \frac{\partial f}{\partial V_{ref}}\Delta V_{ref} \tag{4.4}$$

where V_{ref} represents the reference voltage signal to the AVR or the pre-set mechanical power P_m,etc.

For the FACTS main block, the state space equation is

$$\Delta \dot{X}_{line} = -\frac{1}{T_{FACTS}}\Delta X_{line} + \frac{1}{T_{FACTS}}\Delta X_{ref} + \frac{1}{T_{FACTS}}u \tag{4.5}$$

Here, u is the output of the FACTS controller and the input to the FACTS main block.

Thus, the whole system can be represented by.

$$\begin{cases} \Delta \dot{X} = A_{11}\Delta X + A_{12}\Delta X_{line} + B_{11}\Delta V_{ref} \\ \Delta \dot{X}_{line} = 0 * \Delta X + A_{22}\Delta X_{line} + B_{22}\Delta X_{ref} + B_{23}u \end{cases} \tag{4.6}$$

Since the controllability of the controller needs to be considered, $\Delta V_{ref}, \Delta X_{ref}$ are set to zero and only B_{23} which is related to the controller output is considered.

Therefore $\dot{X} = AX + B_u u$ (4.7)

Where $A = \begin{bmatrix} A_{11} & A_{12} \\ 0 & A_{22} \end{bmatrix}, B_u = \begin{bmatrix} 0 \\ B_{23} \end{bmatrix}$ (4.8)

The nonzero matrix A_{12} links the generator variables and the FACTS variables, enabling the controller on the FACTS's side to affect the generator variables. .

For the PSS in Figure 4.2, the control is located directly at the reference of the AVR, which is exactly located at the generator. Therefore the same state-space representation can be used, except set $A_{12} = 0$.

Then for a system with a PSS and without a FACTS controller

$$\dot{X} = AX + B_{V_{ref}} \Delta V_{ref} + B_{u_{TCSC}} u_{FACTS} \tag{4.9}$$

$$A = \begin{bmatrix} A_{11} & 0 \\ 0 & A_{22} \end{bmatrix}, B_{V_{ref}} = \begin{bmatrix} B_{11} \\ 0 \end{bmatrix}, B_{u_{TCSC}} = \begin{bmatrix} 0 \\ B_{23} \end{bmatrix} \tag{4.10}$$

A_{11} and B_{11} can be decoupled from the above A and $B_{V_{ref}}$. The objective of PSS control is to directly target the control of the generators. Therefore, the PSS control is a direct control on the generator side.

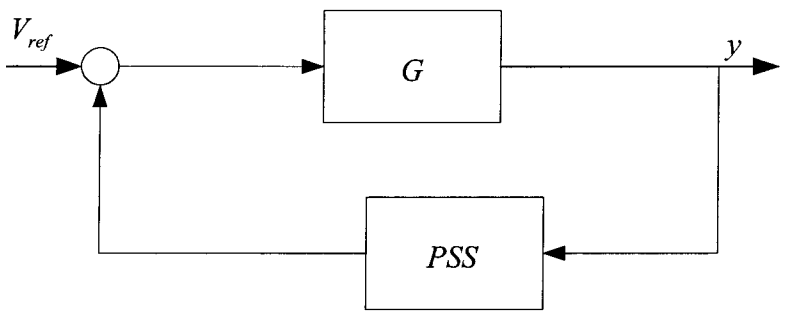

Figure 4.2 System with PSS

4.1.1 Controllability from SVC and TCSC

FACTS devices affect the generator variables through the coupling matrix A_{12}. The larger the elements of A_{12}, the stronger the linkage between the generator side and the FACTS side.

In the following section, the different effects on controllability produced by a SVC controller and a TCSC controller are analyzed through A_{12}.

$$A_{12} = \frac{\partial f}{\partial Y} \frac{\partial g / \partial X_{line}}{\partial g / \partial Y} \tag{4.11}$$

The FACTS devices are commonly installed at tie-lines between two areas which are involved in a low-frequency inter-area oscillation. Thus it is assumed the SVC is installed at Bus n+1 while TCSC is installed between Bus n+1 and Bus n+2.

Thus the intermediate variables become $Y = [V_{n+1}, \theta_{n+1}, V_{n+2}, \theta_{n+2}]$

which are related to the two buses n+1 and n+2.

$$\text{In (4.2)} \quad g = \begin{cases} g_1 = I_{q_{n+1}} = 0 \\ g_2 = I_{d_{n+1}} = 0 \\ g_3 = I_{q_{n+2}} = 0 \\ g_4 = I_{d_{n+2}} = 0 \end{cases} \tag{4.12}$$

The equation (4.2) can be written as

$$g_1 = \sum_{j=1}^{m}\left[F_{G+B}(\delta_{n+1,j})E'_{qj} - F_{B-G}(\delta_{n+1,j})E'_{dj}\right] + G_{n+1,n+1}V_{n+1} + G_{n+1,n+2}\cos(\delta_{n+1,n+2})V_{n+2} + B_{n+1,n+2}\sin(\delta_{n+1,n+2})V_{n+2} \tag{4.13}$$

$$g_2 = \sum_{j=1}^{m}\left[F_{B-G}(\delta_{n+1,j})E'_{qj} + F_{G+B}(\delta_{n+1,j})E'_{dj}\right] + B_{n+1,n+1}V_{n+1} + B_{n+1,n+2}\cos(\delta_{n+1,n+2})V_{n+2} - G_{n+1,n+2}\sin(\delta_{n+1,n+2})V_{n+2} \tag{4.14}$$

$$g_3 = \sum_{j=1}^{m}\left[F_{G+B}(\delta_{n+2,j})E'_{qj} - F_{B-G}(\delta_{n+2,j})E'_{dj}\right] + G_{n+2,n+1}\cos(\delta_{n+2,n+1})V_{n+1} + B_{n+2,n+1}\sin(\delta_{n+2,n+1})V_{n+1} + G_{n+2,n+2}V_{n+2} \tag{4.15}$$

$$g_4 = \sum_{j=1}^{m}\left[F_{B-G}(\delta_{n+2,j})E'_{qj} + F_{G+B}(\delta_{n+2,j})E'_{dj}\right] + B_{n+2,n+1}\cos(\delta_{n+2,n+1})V_{n+1} + G_{n+2,n+1}\sin(\delta_{n+2,n+1})V_{n+1} + B_{n+2,n+2}V_{n+2} \tag{4.16}$$

$$\text{Where} \quad \begin{aligned} F_{G+B}(\delta_{ij}) &= G_{ij}\cos(\delta_{ij}) + B_{ij}\sin(\delta_{ij}) \\ F_{B-G}(\delta_{ij}) &= B_{ij}\cos(\delta_{ij}) - G_{ij}\sin(\delta_{ij}) \\ \delta_{ij} &= \delta_i - \delta_j \end{aligned} \tag{4.17}$$

The linearization of (4.5) for TCSC is

$$\frac{\partial g}{\partial Y}\Delta Y = \frac{\partial g}{\partial X}\Delta X + \frac{\partial g}{\partial X_{TCSC}}\Delta X_{TCSC} \tag{4.18}$$

For SVC the linearization of (4.5) is

$$\frac{\partial g}{\partial Y}\Delta Y = \frac{\partial g}{\partial X}\Delta X + \frac{\partial g}{\partial B_{SVC}}\Delta B_{SVC} \tag{4.19}$$

In (4.5) where X_{line} represents the general state for FACTS device, the only difference between the SVC controller and the TCSC controller results from the different

$\frac{\partial g}{\partial X_{line}}$, which is $\frac{\partial g}{\partial X_{TCSC}}$ for the TCSC and $\frac{\partial g}{\partial B_{SVC}}$ for the SVC.

Because SVC is a shunt device, its change of shunt susceptance will only affect $B_{n+1,n+1}$. In contrast, for the TCSC, the change is the series reactance $X_{n+1,n+2}$, which will affect not only $B_{n+1,n+2}$ but also $B_{n+1,n+1}$ and $B_{n+2,n+2}$. This change is governed by the relationship $B_{n+1,n+2} = -B_{n+1,n+1} = -B_{n+2,n+2}$.

Now by investigating $\frac{\partial g}{\partial X_{TCSC}}$ and $\frac{\partial g}{\partial B_{SVC}}$, the changes and affect on controllability can be analyzed.

TCSC

$$\partial g / \partial X_{line} = \begin{bmatrix} \sin\delta_{n+1.n+2} V_{n+2} \dfrac{\partial B_{n+1,n+2}}{\partial X_{TCSC}} + (\cos\delta_{n+1,n+2} V_{n+2} - V_{n+1}) \dfrac{\partial G_{n+1,n+2}}{\partial X_{TCSC}} \\ (V_{n+2}\cos\delta_{n+1,n+2} - V_{n+1}) \dfrac{\partial B_{n+1,n+2}}{\partial X_{TCSC}} - \sin\delta_{n+1,n+2} V_2 \dfrac{\partial G_{n+1,n+2}}{\partial X_{TCSC}} \\ \sin\delta_{n+2,n+1} V_{n+1} \dfrac{\partial B_{n+1,n+2}}{\partial X_{TCSC}} + (\cos\delta_{n+2,n+1} V_{n+1} - V_{n+2}) \dfrac{\partial G_{n+1,n+2}}{\partial X_{TCSC}} \\ (\cos\delta_{n+2,n+1} V_{n+1} - V_{n+2}) \dfrac{\partial B_{n+1,n+2}}{\partial X_{TCSC}} + \sin\delta_{n+2,n+1} V_{n+1} \dfrac{\partial G_{n+1,n+2}}{\partial X_{TCSC}} \end{bmatrix} \quad (4.20)$$

Where $\frac{\partial B_{n+1,n+2}}{\partial X_{TCSC}} = -\left(\frac{X^2 - R^2}{(R^2 + X^2)^2}\right) \approx -\frac{1}{X^2}$ due to $R/X \approx 0.1$

$$\frac{\partial G_{n+1,n+2}}{\partial X_{TCSC}} = -\left(\frac{-2RX}{(R^2 + X^2)^2}\right) \approx \frac{0.2}{X^2} \quad (4.21)$$

Obviously $\frac{\partial B_{n+1,n+2}}{\partial X_{TCSC}}$ is almost five times as large as $\frac{\partial G_{n+1,n+2}}{\partial X_{TCSC}}$. Thus to simplify the last column, ignore $\frac{\partial G_{n+1,n+2}}{\partial X_{TCSC}}$.

$$\partial g / \partial X_{line} = \begin{bmatrix} \sin\delta_{n+1.n+2} V_{n+2} (-\frac{1}{X^2}) \\ (V_{n+2}\cos\delta_{n+1,n+2} - V_{n+1})(-\frac{1}{X^2}) \\ \sin\delta_{n+2,n+1} V_{n+1} (-\frac{1}{X^2}) \\ (\cos\delta_{n+2,n+1} V_{n+1} - V_{n+2})(-\frac{1}{X^2}) \end{bmatrix}$$

Then, (4.22)

The first element of the above column is close to $-\frac{\sin\delta_{n+1,n+2} V_{n+2} V_{n+1}}{X * X} \approx -\frac{P_{n+1,n+2}}{X}$ since $V_{n+1} \approx 1$ in most power networks.

Furthermore, the angle difference between Bus n+1 and Bus n+2 is very small, therefore the fourth element of the above column can be approximated as:

$$(V_{n+2}\cos\delta_{n+1,n+2} - V_{n+1})(-\frac{1}{X^2}) \approx -\frac{(V_{n+2} - V_{n+1})}{X * X} \approx -\frac{I_{n+1,n+2}}{X} \quad (4.23)$$

Therefore the approximation to (4.9) is

$$\partial g / \partial X_{line} = \begin{bmatrix} -\frac{P_{n+1,n+2}}{X} \\ -\frac{I_{n+2,n+1}}{X} \\ -\frac{P_{n+2,n+1}}{X} \\ -\frac{I_{n+1,n+2}}{X} \end{bmatrix} \quad (4.24)$$

In conclusion, the larger the power transfer through the line where the TCSC is installed, the larger the interaction between ΔX_{TCSC} with the rest of the states in the ODE, and consequently the larger the controllability. Hence the effectiveness of the TCSC SDC on the damping issue is almost proportional to the transfer level between the two oscillating areas. The more stressed the tie-line between these two areas, the more effective the TCSC SDC.

SVC

$$\text{For a SVC } \partial g / \partial X_{line} = \begin{bmatrix} 0 \\ V_{n+1} \dfrac{\partial B_{n+1,n+1}}{\partial B_{SVC}} \\ 0 \\ 0 \end{bmatrix} = \begin{bmatrix} 0 \\ V_{n+1} \\ 0 \\ 0 \end{bmatrix} \tag{4.25}$$

Usually V_{n+1} will decrease with the increase of the transfer level between the two areas. As a result, the decrease of the above column will cause the decrease of the controllability which finally affects its effectiveness on damping.

4.1.2 Test System and results

Modal controllability

In a linear system with state space equations of

$\dot{X} = AX + Bu$,

the right and left eigenvectors of A , corresponding to an eigenvalue λ_i, are defined as follows:

$\lambda_i e_i = Ae_i$

$f_i^T \lambda_i = f_i^T A$

Where e_i is the right eigenvector corresponding to λ_i while f_i is the left eigenvector corresponding to λ_i.

Then modal controllability vector is defined as

$\beta_i = (f_i^T B)^T = B^T f_i$.

In the 4-machine test system in Figure 3-4, the result of modal controllability is shown in Table 4.1.

Table 4.1 MODAL CONTROLLABILITY FOR DIFFERENT CONTROLLER IN THE FOUR-MACHINE TEST SYSTEM

Ptie (MW)	PSS at Gen2	SVC at Bus 7	TCSC between Bus 5 and Bus 7
0	0.178	0.0127	0.003
100	0.176	0.0125	0.088
200	0.172	0.0115	0.160
300	0.162	0.00958	0.203

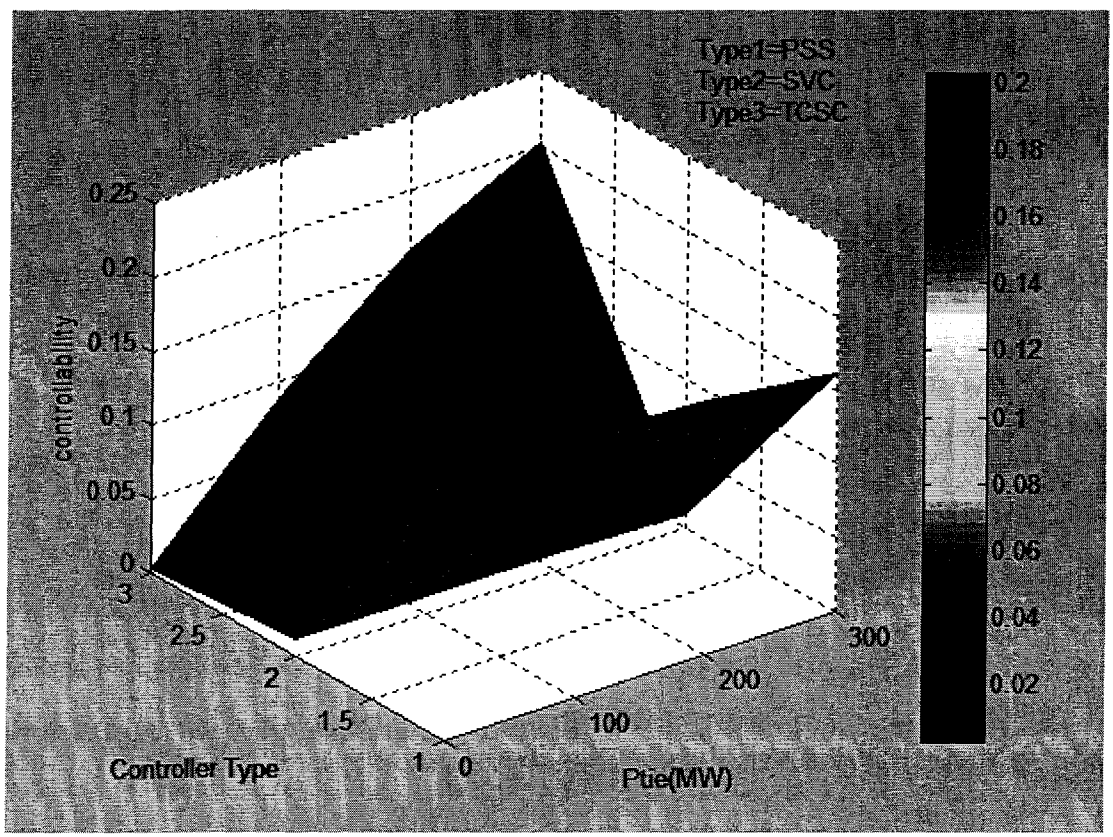

Figure 4.3 Comparison of controllability between PSS's, TCSC controllers and SVC controllers

In Figure 4.3, the controllability of PSS barely changes with the variation of Ptie. The controllability of SVC is decreasing with the increase of Ptie. It is obvious that the effectiveness of the TCSC SDC increases with the active power flowing through the TCSC, being negligible for zero power flow conditions. This is consistent with the theoretical analysis given in the section above. It may be observed that PSS's always have robustly good controllability under various operating conditions, and therefore it is the most commonly used type of controller for damping out low frequency oscillations. The advantage of the TCSC lies in its increasing effectiveness on enhancing the damping ratio when the system is more stressed.

The derivation above is based on the assumption that the SVC is installed at one of the buses between which the TCSC is installed. The conclusion is that if the voltage at the SVC bus is decreasing with the increase of the active power flowing through the TCSC, the TCSC is more effective in affecting the system with Xline. The effectiveness of a TCSC and an SVC on enhancing the system damping for the 50-machine test system is now compared.

The TCSC is installed between Bus 63 and Bus 66 while the SVC is installed at Bus 63. Both of them use the active power flow through Line 63-66 as the input to the damping controller. Modal controllability of the critical mode around 0.29 Hz is calculated (need to say how this is done) for each device at different operating points in Table 4.2 and in Fig. 4.4.

Table 4.2 MODAL CONTROLLABILITY OF THE CRITICAL MODE COMPARISON BETWEEN TCSC AND SVC IN THE IEEE 50-MACHINE SYSTEM

	TCSC63-66	SVC63(63-66)
1300	0.01640	0.0116
1400	0.01660	0.0112
1500	0.01667	0.0100
1600	0.01669	0.0094

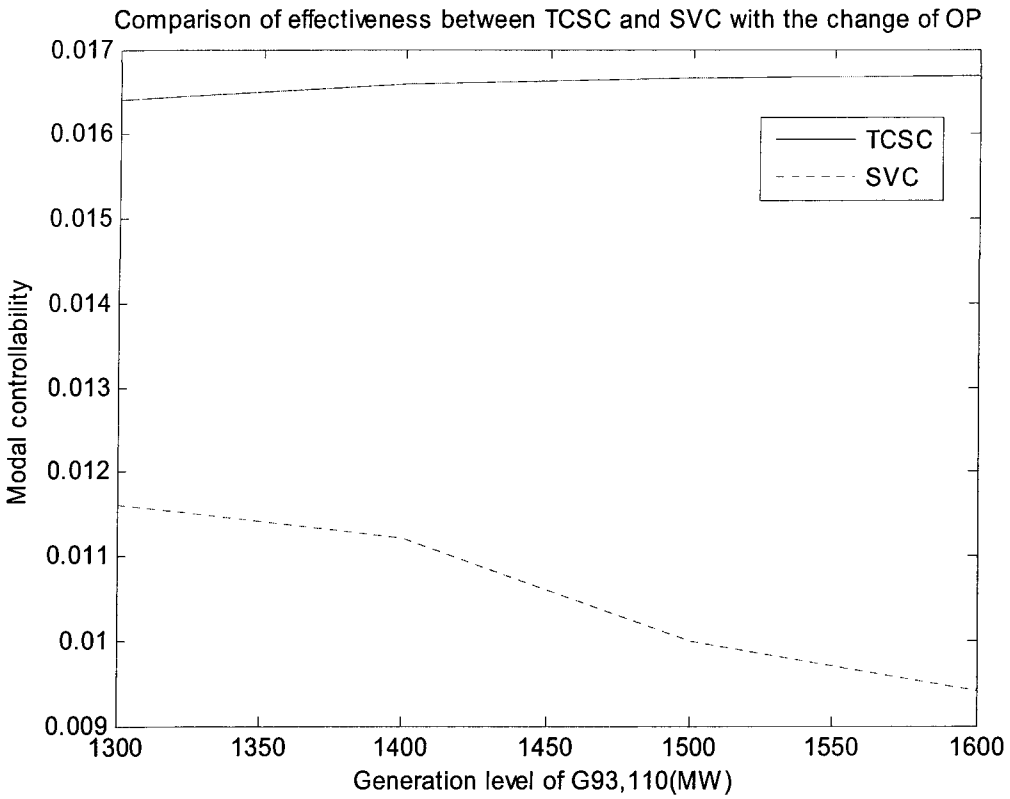

Figure 4.4 Comparison of controllability between TCSC controllers and SVC controllers in the IEEE 50-machine system

It is obvious from Fig. 4.4 that the controllability of a TCSC slightly increases with the increase of the generation level of G93, G110 in this 50-machine system. In comparison, the controllability of an SVC installed at the same position decreases a little with the increase of the generation level of G93, G110. This phenomenon is consistent with the conclusions derived in the previous section. In the 50-machine system, however, the TCSC does not have such a dramatic increase in controllability as the four-machine system exhibits with increasing system stress. This is because in the large 50-machine system, Line 63-66 is not a real tie-line which connects the two oscillating areas. The power flow through the line increases by approximately 20MW every time the generation

level from G93, G110 increases by 100MW. In general, the effectiveness of the TCSC controller on damping the inter-area modal oscillation depends heavily on the increasing amount of power flow through it under varying system conditions. In the four-machine system, the increase of the power flow through the line containing the TCSC coincides with the increase of system stress. Yet, in the 50-machine system, since the Line 63-66 is not the only tie-line connecting the two areas, the increase of power flow through it is not proportional to the increase of the generation level, which makes the application of TCSC less appealing than in the smaller system. Thus the TCSC is not necessarily the first choice for damping control in the case of this 50-machine system, where the tie-line is difficult to identify. Meanwhile, the voltage in the whole network changes slightly with the increase of the generation level of G93 and G110, and therefore an SVC will have satisfactory controllability under changing operating conditions.

4.2 Location selection

4.2.1 In the 4-machine system

It is obvious from section 4.1 that in the small test system with two closely-connected areas the TCSC is a better choice with regard to the damping enhancement of inter-area oscillation. Its best location is in the tie-line connecting the two areas oscillating against each other.

4.2.2 In the 50-machine system

A. TCSC location selection

As discussed in the previous section, the TCSC is not favored in this large test system because there are no easily identified tie-lines connecting two areas oscillating against each other. However, in ordert to find a good location for a TCSC, the mode shape has to

be analyzed to help identify both the oscillating groups and possible tie-lines between the groups.

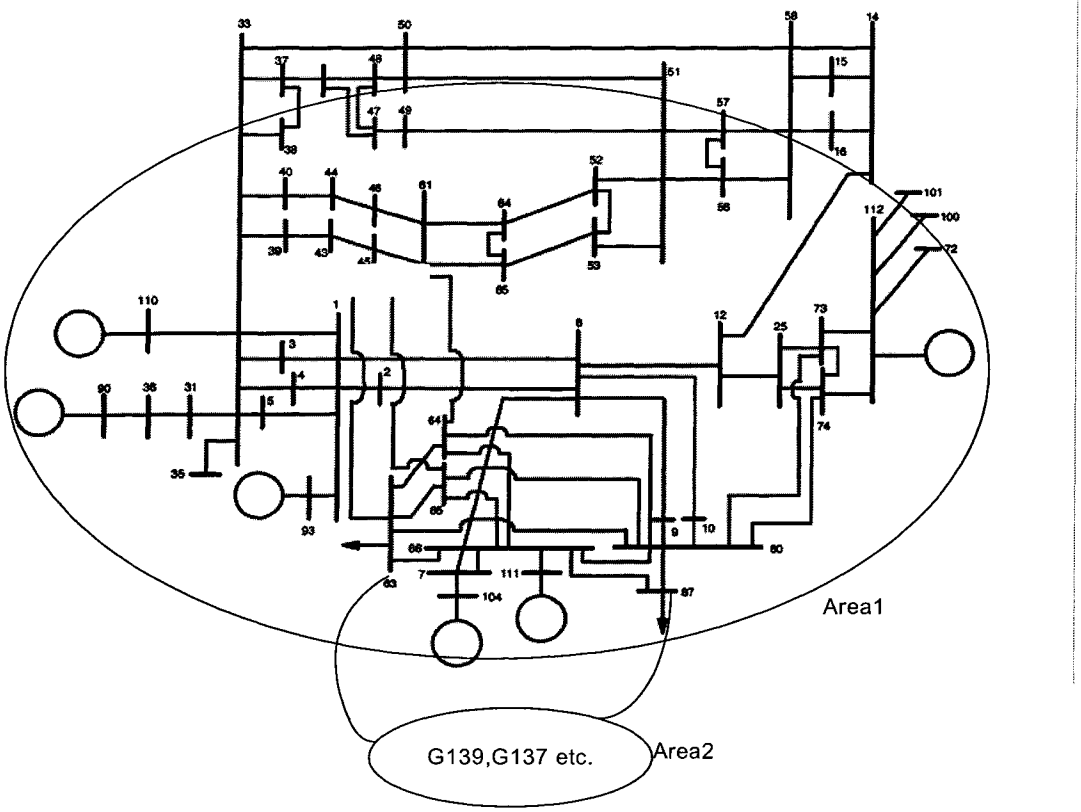

Figure 4.5. 50-Machine Test System

According to the mode shape in Figure 3.6, the system can be demarcated into two areas as shown in Fig. 4.5. Six generators with detailed generator models form one area, while the rest of the generators such as G139,137 etc. form the second area.

Figure 4.4 shows that the more the power flow increase though the line with an increase of generation level, the more effective the TCSC would be. Therefore, the candidates for the installation based on the modal analysis above are first selected, and

then the power flow through these lines under the variation of the system condition calculated, as shown in Table 4.3. Among these candidates, Line 63-66, Line 67-127 are chosen as the possible tie-lines between the two oscillating areas. Meanwhile, oscillations are also occuring among G93, G110 and G104, G111 in area 1. Therefore, Line1-6, Line 6-7 can be selected as potential candidates for the TCSC installation since they do convey a large amount of active power. Line139-145, Line139-141 and Line128-129 are lines in area2 through which large active power is transferred and are thus similarly considered as potential candidates.

Table 4.3 ACTIVE POWER THROUGH THE CANDIDATE LINE UNDER DIFFERENT OPERATING CONDITION

Line	P=1200MW	P=1300MW	P=1400MW
63-66	-498	-518	-539
67-124	-833.71	-773	-720
1-6	689.49	769	839
6-7	-1351.62	-1315.51	-1278.87
139-145	-2373.66	-2278.21	-2173.95
139-141	-393.01	-437.46	-485.95
128-129	2582.60	2584.87	2587.20

Next the modal controllability from each candidate line is calculated and compared as shown in Table 4.4. It may be seen that Line128-129 has the largest modal controllability among all the candidates while Line63-66, Line 67-124 have the second and third largest modal controllability, respectively. Considering that Line63-66 and Line 67-124 are two of the lines between two areas from Fig.4.5, they can be selected as possible locations for a TCSC controller with regard to the damping enhancement for the critical mode.

Table 4.4 MODAL CONTROLLABILITY CALCULATION

TCSC location	Modal controllability
63-66	0.0164
67-124	0.0154
1-6	0.0077
6-7	0.0070
139-145	0.0114
139-141	0.0062
128-129	0.0201

B. SVC location selection

From the analysis conducted, it can be observed from Table 4.5 that Bus 66 has the largest controllability.

Table 4.5 SVC LOCATION SELECTION IN 50-MACHINE SYSTEM

SVC bus	Modal controllability
66	0.0244
63	0.0116
1	0.0139
6	0.0158
67	0.0062
44	0.0139

Controllability alone cannot determine the best location of FACTS devices in a large system. There are interactions among modes in such a system. A location chosen based on its large modal controllability does not guarantee that a good controller can be designed for this location. The controller might deteriorate other modes when it effectively

improves the damping of the critical mode. Hence, there are limitations to the effectiveness of damping enhancement to the critical modes because of the interaction of other modes. For this reason, a simple controller based on root-locus methods is generated to test the effectiveness of the location chosen and to investigate the interaction among modes that could disturb the functionality of the controller which is eventually designed. The investigation will show that Bus66 is the best location for an SVC controller to damp the critical inter-area mode without affecting other modes.

4.3 Summary

In this chapter, the effectiveness of different FACTS devices on the damping enhancement under change of system operating conditions is investigated. Several equations to show the influence of different FACTS devices are derived. The derivations are well established by two test systems, a 4-machine test system and a 50-machine test system. Under the assumption of the same installation location for the TCSC and the SVC, it is shown that the TCSC is more effective when the system has clearly demarcated areas oscillating against each other and the power flow through the tie-line connecting these two areas increases significantly with the increase of system stress level. However, the effectiveness of the SVC relates in some form to the bus voltage variation at the bus where it is installed. Therefore, in the four-machine system, where there are two areas tightly connected by a tie-line, the obvious choice with regard to the damping improvement is the TCSC installed in the tie-line. In contrast, in the 50-machine system, since there are no obvious areas and tie-lines to choose, the TCSC is not the first choice. The SVC, which has a robust modal controllability in this case, in some manner due to the slight change of the voltage under variation of the system conditions, is the better choice. Also, the location selection for the TCSC or the SVC in the 50-machine system is described in detail using modal shape analysis and modal controllability calculations. In

the following chapter, the focus will be on designing a TCSC damping controller for the four-machine system and a SVC damping controller for the 50-machine system.

5 TCSC CONTROLLER SYNTHESIS IN A 4-MACHINE SYSTEM WITH LMI REGIONAL POLE PLACEMENT

5.1 The LMI regional pole placement method

5.1.1 Minimal damping constraints

The objective of the controller design is to place the closed loop poles in some chosen regions while still satisfying some infinity norm constraints. It is well-known that the transient response of a linear system is related to the location of its poles [54]. For example, the step response of a second–order system with poles $\lambda = -\varsigma\omega_n \pm j\omega_d$ is fully characterized in terms of the undamped natural frequency $\omega_n = |\lambda|$, the damping ratio ς, and the damped natural frequency ω_d. Confining the closed-loop poles to some chosen region can ensure a minimum damping ratio $\varsigma = \cos\theta$, which is the objective of this damping problem in the power systems.

5.1.2 LMI regions

Definition 1: An LMI region is any subset D of the complex plane that can be defined as

$$\mathsf{D} = \{z \in C : L + zM + \bar{z}M^T < 0\} \qquad (5.1)$$

where L and M are real matrices such that $L^T = L$.

The matrix-valued function $f_{\mathsf{D}}(z) = L + zM + \bar{z}M^T$ is called the characteristic function of D. Some typical LMI regions are shown in Fig. 5.1:

(1) Half-plane $\mathrm{Re}(z) < -\alpha$: $f_{\mathsf{D}}(z) = z + \bar{z} + 2\alpha < 0$

(2) Disk centered at (-q,0) with radius r:

$$f_{\mathsf{D}}(z) = \begin{bmatrix} -r & q+z \\ q+\bar{z} & -r \end{bmatrix} < 0;$$

(3) Conic sector with apex at the origin and inner angle 2θ ($S(0,0,\theta)$):

$$f_D(z) = \begin{bmatrix} \sin\theta(z+\bar{z}) & \cos\theta(z-\bar{z}) \\ \cos\theta(\bar{z}-z) & \sin\theta(z+\bar{z}) \end{bmatrix} < 0$$

An LMI region is a subset of the complex plane that is representable by an LMI in z and $\bar{z}$.

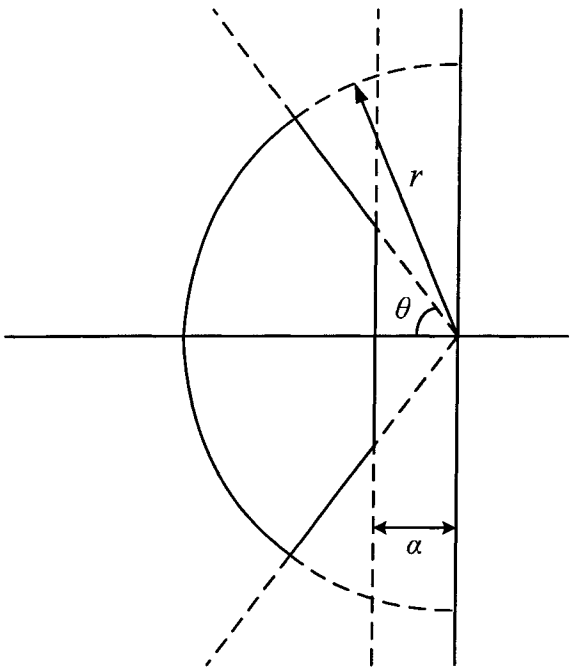

Figure 5.1 LMI region

5.1.3 Quadratic D -stable

Definition 2: The system $\dot{x} = Ax$ is called D-stable if all its poles lie in D.

***Theorem I**: The matrix A is* D *-stable if and only if there exists a symmetric matrix X such that*

$M_{\mathsf{D}}(A,X)<0, \quad X>0$

where

$$M_{\mathsf{D}}(A,X) := L \otimes X + M \otimes (AX) + M^T \otimes (AX)^T \tag{5.2}$$

In the case of confining the poles in a conic sector of $S(0,0,\theta)$,

$$L=0, \quad M=\begin{bmatrix} \sin\theta & \cos\theta \\ -\cos\theta & \sin\theta \end{bmatrix} \tag{5.3}$$

Based on Theorem I, the system matrix has poles in $S(0,0,\theta)$ if and only if

$$\begin{pmatrix} \sin\theta(AX_{\mathsf{D}} + X_{\mathsf{D}}A^T) & \cos\theta(AX_{\mathsf{D}} - X_{\mathsf{D}}A^T) \\ \cos\theta(X_{\mathsf{D}}A^T - AX_{\mathsf{D}}) & \sin\theta(AX_{\mathsf{D}} + X_{\mathsf{D}}A^T) \end{pmatrix} < 0 \tag{5.4}$$

Note that when this D is the entire left–half plane, this notion reduces to asymptotic stability, which is characterized in LMI terms by the Lyapunov theorem [55].

5.1.4 The H_∞ constraint

The classical H_∞ robust controller design in the mixed sensitivity problem [56] is represented as

$$\left\| \begin{matrix} W_1 S \\ W_2 T \\ W_3 KS \end{matrix} \right\| \le \gamma, \tag{5.5}$$

Where γ is the upper bound on the H_∞ norm.

The H_∞ constraint is equivalent to the existence of a solution $X_\infty > 0$ to the LMI

$$\begin{pmatrix} A_{cl}X_\infty + X_\infty A_{cl}^T & B_{cl} & X_\infty C_{cl}^T \\ B_{cl}^T & -I & D_{cl}^T \\ C_{cl}X_\infty & D_{cl} & -\gamma^2 I \end{pmatrix} < 0 \tag{5.6}$$

Where $A_{cl}, B_{cl}, C_{cl}, D_{cl}$ are A, B, C, D matrices of the closed loop system.

By combining the pole-placement constraint in (5.4) with the H_∞ constraint in (5.6), the

goal can be restricted to the following suboptimal formulation of H_∞ synthesis with pole-placement constraints.

The controller design objective is to find $X > 0$ and a controller $K(s)$ that satisfy (5.4) and (5.6) with $X = X_\infty = X_D$ (5.7).

The difficulty is that there are nonlinearities in both (5.4) and (5.6). Appropriate changes of controller variable are made [57] in the following.

Let $A \in R^{n\times n}$ and $D_{22} \in R^{p_2\times m_2}$, and let k be the controller order ($A_k \in R^{k\times k}$). As in the state-feedback case, the change of controller variables is implicitly defined in terms of the (unknown) Lyapunov matrix X. Specifically, with partition X and its inverse defined as

$$X = \begin{pmatrix} R & M \\ M^T & U \end{pmatrix}, \quad X^{-1} = \begin{pmatrix} S & N \\ N^T & V \end{pmatrix}, \tag{5.8}$$

$R \in R^{n\times n}$, $S \in R^{n\times n}$

Define the new controller variables as

$$\begin{cases} \mathrm{B}_K = NB_K + SB_2D_K \\ \mathrm{C}_K := C_KM^T + D_KC_2R \\ \mathrm{A}_K = NA_KM^T + NB_KC_2R + SB_2C_KM^T + S(A + B_2D_KC_2)R \end{cases} \tag{5.9}$$

This change of variable has the following properties:

1) A_K, B_K, C_K have dimensions $n\times n$, $n\times m_2$ and $p_2 \times n$, respectively.

2) If M and N are square invertible, A_K, B_K, C_K can be uniquely determined from the known A_K, B_K, C_K and matrices R, S, M, N, D_K

The identity $XX^{-1} = I$ together with (5.8)

gives $MN^T = I - RS$ (5.10)

After the change of variables tractable necessary and sufficient conditions can be given for the solvability of (5.4) and (5.6) with $X = X_\infty = X_D$.

Theorem II: *Let D be an arbitrary LMI region contained in the open left-half plane and let* $f_D(z) := \alpha + z\beta + \bar{z}\beta^T = \{\alpha_{kl} + \beta_{kl} z + \beta_{lk} \bar{z}\}_{1 \le k \le m}$ *be its characteristic function. The modified problem (5.5) is solvable if and only if the following LMIs are feasible.*

Find $R = R^T \in R^{n \times n}$ $S = S^T \in R^{n \times n}$, *and matrices* A_K, B_K, C_K, D_K *such that*

$$\begin{pmatrix} R & I \\ I & S \end{pmatrix} > 0 \qquad (5.11)$$

$$\left[\alpha_{kl} \begin{pmatrix} R & I \\ I & S \end{pmatrix} + \beta_{kl} \Phi + \beta_{lk} \Phi^T \right]_{k,l} < 0 \qquad (5.12)$$

$$\begin{bmatrix} \Psi_{11} & \Psi_{21}^T \\ \Psi_{21} & \Psi_{22} \end{bmatrix} < 0 \qquad (5.13)$$

with shorthand notation as follows:

$$\Phi = \begin{bmatrix} AR + B_2 C_K & A + B_2 D_K C_2 \\ \mathrm{A}_K & SA + \mathrm{B}_K C_2 \end{bmatrix} \qquad (5.14)$$

$$\Psi_{11} := \begin{bmatrix} AR + RA^T + B_2 \mathrm{C}_K + \mathrm{C}_K^T B_2^T & B_1 + B_2 D_K D_{21} \\ (B_1 + B_2 D_K D_{21})^T & -\gamma I \end{bmatrix} \qquad (5.15)$$

$$\Psi_{21} := \begin{bmatrix} \mathrm{A}_K + (A + B_2 D_K C_2)^T & SB_1 + \mathrm{B}_K D_{21} \\ C_1 R + D_{12} \mathrm{C}_K & D_{11} + D_{12} D_K D_{21} \end{bmatrix} \qquad (5.16)$$

$$\Psi_{22} := \begin{bmatrix} A^T S + SA + \mathrm{B}_K C_2 + C_2^T \mathrm{B}_K^T & (C_1 + D_{12} D_K C_2)^T \\ C_1 + D_{12} D_K C_2 & -\gamma I \end{bmatrix} \qquad (5.17)$$

5.1.5 Basic steps of LMI controller sythesis

Given any solution of this LMI system:

Step1: Compute via SVD a full-rank factorization $MN^T = I - RS$ of the matrix $I - RS$ (M and N are then square invertible).

Step2: Solve the system of linear equations (5.9) for B_K, C_K and A_K (in that order).

Step3: Set $K(s) := D_K + C_K (sI - A_K)^{-1} B_K$

Then $K(s)$ is an nth order controller that places the closed-loop poles in D and such that

$\|T_{wz}\|_\infty < \gamma$

5.2 TCSC SDC synthesis

Based on H_∞ setup to represent the uncertainty block

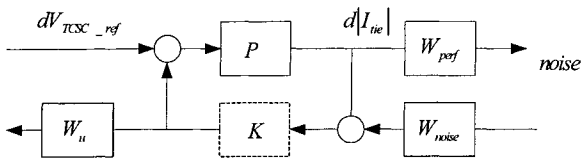

Figure 5.2. Supplementary damping controller (SDC) design setup

1. Set up the problem using the framework shown in Fig. 5.2.
2. Select the appropriate Wperf to represent the multiplicative uncertainty of the open-loop system. Because robust stability calls for $\|W_I T\| < 1$, by setting the W_{perf} equal to W_I, the uncertainty of the open loop system has been taken care of.
3. Select the appropriate pole region to give the minimum damping constraints, and formulate it as an LMI.
4. Obtain the solution.

5.3 Results

The parameters of the obtained controller are shown in the following. A washout filter of $10s/(1+10s)$ is applied in series with the controller to maintain the original steady-state gain of the open loop system.

$$A_K = \begin{bmatrix} -2.043 & 0.069 & 2.568 & 0.108 & 0.062 \\ -2535.121 & -118.863 & -458.565 & -71.423 & -65.507 \\ -10.468 & -0.080 & -5.368 & 0.001 & -0.135 \\ 3033.348 & 143.087 & 547.975 & 83.040 & 83.570 \\ -1322.438 & -63.945 & -241.625 & -37.649 & -38.524 \end{bmatrix}$$

$$B_K = \begin{bmatrix} 0.0026 \\ 14.19 \\ 0.0121 \\ -17.0251 \\ 7.3812 \end{bmatrix}$$

$$C_K = \begin{bmatrix} -9.314 & -0.727 & -3.298 & -5.418 & 3.877 \end{bmatrix}$$

$$D_K = 0$$

5.4 Performance results

The following steps were performed:

The synthesized supplementary damping controller (SDC) was implemented on the test system. A conventional H_∞ controller based on the same nominal OP without pole placement constraints is tested in the two-area system at the same time.

Perform small signal analysis using EPRI's MASS [50] software package. Table 5.1 shows the damping ratio of the system with the pole placement based SDC and with the conventional H_∞ SDC.

Table 5.1 DAMPING RATIO COMPARISON BETWEEN LMI-POLE PLACEMENT H_∞ SDC AND CONVENTIONAL H_∞ SDC

Ptie (MW)	Pole placement based H_∞ SDC		H_∞ SDC	
	Frequency (Hz)	Damping ratio (%)	Frequency (Hz)	Damping ratio(%)
100	0.4821	18.08	0.5225	8.04
200	0.4774	34.64	0.5443	10.45
300	0.8413	23.35	0.7318	9.69
400	0.8518	19.71	0.7393	9.73
500	0.8427	17.68	0.7346	9.53
600	0.8167	16.29	0.7151	9.04

The frequency jump of the poorly damped modes from Ptie=200MW to Ptie=300MW is due to the compensation level change of the TCSC device. From Table 5.1, it is obvious that the closed loop system with the LMI-based pole placement SDC has the largest damping ratio at all six operating points. The damping ratio at the nominal case of Ptie=400MW is 19.71%, which is smaller than the expected value in the design phase. This seems reasonable because the system considered at the design phase is different from the real system due to the linearization and model reduction.

Nonlinear time domain simulation was performed using the ETMSP [50] software. A three-phase short circuit fault was applied at bus 5 for 100 ms and the tie-line real power flow is monitored. The simulation results are shown in Fig. 5-3~5-8. Comparisons are made between the system with the LMI-based pole-placement SDC, with conventional SDC, and without SDC.

From Figures 5.3~5.8 it is very clear that the inter-area modes are well damped from Ptie=100MW to Ptie =600MW. The system takes a longer time to settle down to its equilibrium point at Ptie=100MW than at Ptie =600MW even though the result from the small signal analysis shows the damping ratio at Ptie=100MW is greater than the damping ratio at Ptie=600MW. This inconsistency between the small signal results and the transient results is due to the non-linearity being taken into account in the transient simulation. Another important point to mention is that the transient response looks better with the increase in the level of Ptie. That is to say, the controller is more effective when the power transfer level between areas is much higher. The TCSC device is a series-connected device that is installed between the tie-line, which makes it totally different from other FACTS devices in the way that it affects the controllability in this problem. Furthermore, the controllability increases with the increase in the power transfer level between the two areas. Consequently, the benefit of this controller is its increasing effect in an increasingly-stressed power network. In other words, as the inter-area power

transfer stress increases, the supplementary damping controller of TCSC will be more and more efficient.

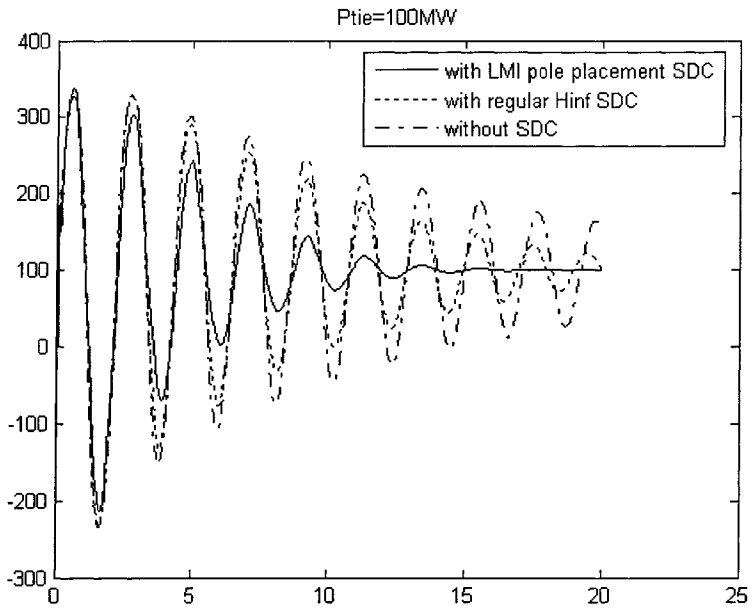

Figure 5.3. Three phase fault at Ptie=100MW

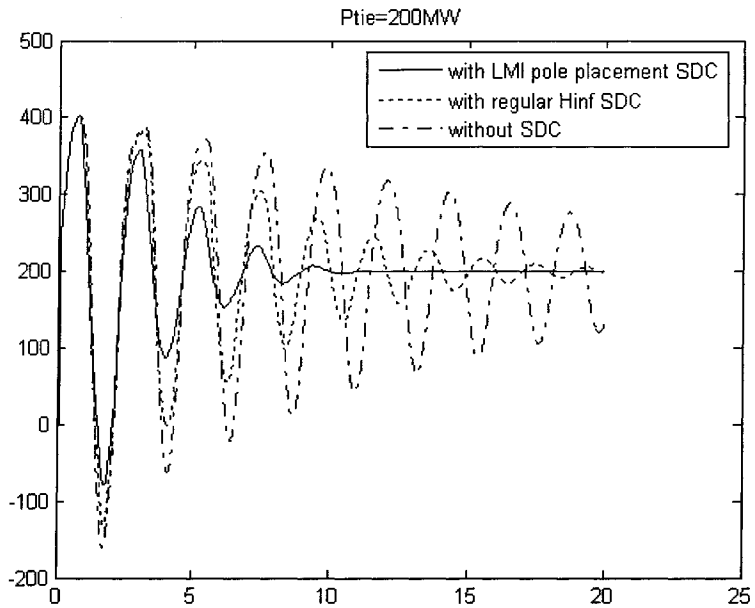

Figure 5.4. Three phase fault at Ptie=200MW

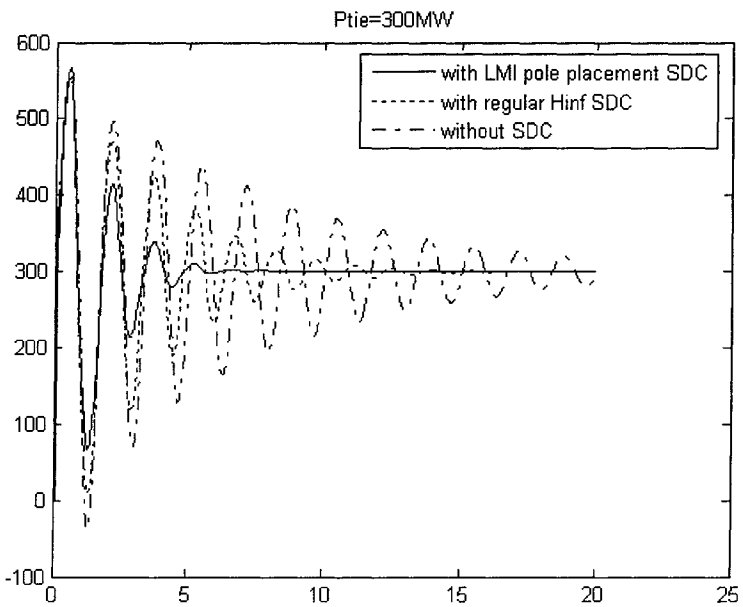

Figure 5.5. Three phase fault at Ptie=300MW

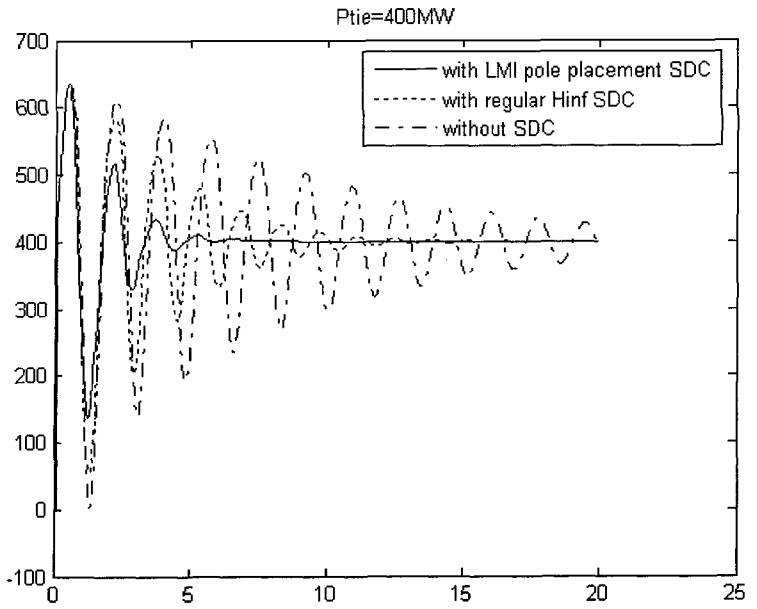

Figure 5.6 Three phase fault at Ptie=400MW

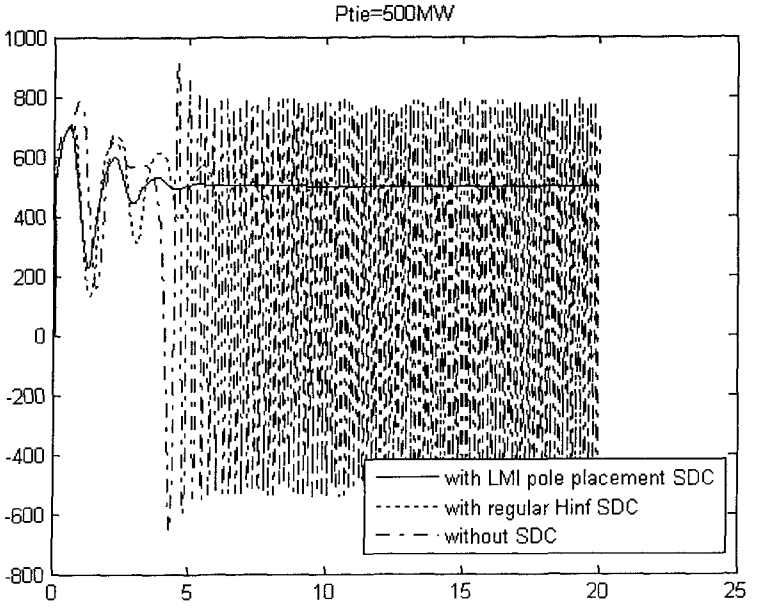

Figure 5.7. Three phase fault at Ptie=500MW

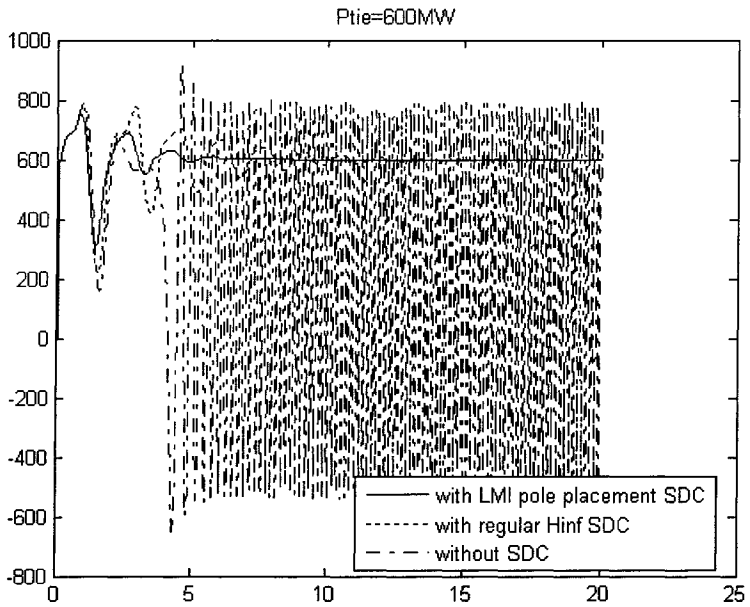

Figure 5.8. Three phase fault at Ptie=600MW

5.5 Summary

A fixed- parameter controller instead of an adaptive controller for TCSC is used to achieve better damping ratio at all of the six operating points. This controller is designed by imposing regional pole placement constraints. From its application to a two-area four-machine system, it is obvious that the benefit of this controller in enhancing the system damping is much greater than that of the conventional controller. This LMI-based pole placement SDC is easier to design than a more conventional controller because of the way the performance requirement is explicitly formed in terms of LMIs instead of being included in a complex weighting function selection. The approach is practical and provides a fixed-structure controller. The designed controller is robust and it can improve

the system damping over a very wide operating range. It is also shown that the controller becomes more and more effective with increase of power transfer level between the two areas.

6 INTERPOLATED LPV SVC CONTROLLER SYNTHESIS IN A 50-MACHINE SYSTEM

6.1 LPV method

6.1.1 LPV SQLF method

Definition 1 Given a compact set $P \subset R^s$, consider the open-loop LPV plant

$$\begin{bmatrix} \dot{x}(t) \\ e(t) \\ y(t) \end{bmatrix} = \begin{bmatrix} A(\rho(t)) & B_1(\rho(t)) & B_2(\rho(t)) \\ C_1(\rho(t)) & D_{11}(\rho(t)) & D_{12}(\rho(t)) \\ C_2(\rho(t)) & D_{21}(\rho(t)) & D_{22}(\rho(t)) \end{bmatrix} \begin{bmatrix} x(t) \\ d(t) \\ u(t) \end{bmatrix} \tag{6.1}$$

Where d is the disturbance, u is the control input, e is the error output, and y is the output feedback signal.

Definition 2 The function A is quadratically stable over P if there exists a $P \in R^{n \times n}, P = P^T > 0$, such that for all $\rho \in \mathcal{P}$, $A^T(\rho)P + PA(\rho) < 0$. An LPV system $\sum_{\mathcal{P}}$ is quadratically stable if A is quadratically stable.

Definition 3 Given a quadratically stable LPV system $\sum_P$, for zero initial conditions, the induced L_2 norm G_{F_P} is defined as

$$\left\| G_{F_P} \right\| := \sup_{\rho \in F_P} \sup_{\|d\|_2 \neq 0, d \in L_2} \frac{\|e\|_2}{\|d\|_2} \tag{6.2}$$

This quantity is finite.

Lemma *1 Given the LPV system,* $\sum(P,A,B,C,D)$ *and scalar* $\gamma > 0$. *If there exists an* $X \in R^{n\times n}$, $X = X^T > 0$ *such that for all* $\rho \in P$

$$\begin{bmatrix} A^T(\rho)X + XA(\rho) & XB(\rho) & \gamma^{-1}C^T(\rho) \\ B^T(\rho)X & -I & \gamma^{-1}D^T(\rho) \\ \gamma^{-1}C(\rho) & \gamma^{-1}D(\rho) & -I \end{bmatrix} < 0, \tag{6.3}$$

The function A is quadratically stable over P;

There exists a $\beta < \gamma$ *such that* $\left\|G_{F_P}\right\| \le \beta$.

From Lemma 1, a controller solving the quadratic LPV γ-performance problem guarantees that the closed-loop system is quadratically stable and the induced L_2-norm from *d* to *e* is less than γ. The following *Theorem I* says that there exists some controller to solve the γ-performance problem if and only if a set of affine matrix inequalities (AMIs) holds for all $\rho \in P$. The set of AMIs represents a convex constraint on two unknown positive definite matrices *X* and *Y*. Thus, the feasibility problem has become a convex optimization problem.

Theorem I: *Given P, the open loop system (3) and scalar* $\gamma > 0$*, the quadratic LPV* γ *-performance problem is solvable if and only if there exists matrix* $X_{11} \in R^{n \times n}$, $X_{11} = X_{11}^{\ T} > 0$, *and* $Y_{11} \in R^{n \times n}$, $Y_{11} = Y_{11}^{\ T} > 0$, *such that for all* $\rho \in P$:

$$\begin{Bmatrix} A_\rho(\rho)Y_{11} + Y_{11}A^T(\rho) & Y_{11}C_1^{\ T}(\rho) & \gamma^{-1}B_1(\rho) \\ -B_2(\rho)B_2(\rho) & & \\ C_1(\rho)Y_{11} & -I & 0 \\ \gamma^{-1}B_1^{\ T}(\rho) & 0 & -I \end{Bmatrix} < 0 \tag{6.4}$$

$$\begin{Bmatrix} A^T(\rho)X_{11} + X_{11}A(\rho) & C_2(\rho)X_{11}B_1(\rho) & \gamma^{-1}C_1^{\ T}(\rho) \\ -C_2^{\ T}(\rho) & & \\ B_1(\rho)^T X_{11} & -I & 0 \\ \gamma^{-1}C_1(\rho) & 0 & -I \end{Bmatrix} < 0 \tag{6.5}$$

$$\begin{Bmatrix} X_{11} & \gamma^{-1}I_n \\ \gamma^{-1}I_n & Y_{11} \end{Bmatrix} \geq 0 \tag{6.6}$$

Then the function A is quadratically stable over P, and there exists $\beta < \gamma$ *such that* $\|GF_P\| \leq \beta$. *Let:*

$$Z := (X_{11} - \gamma^{-1}Y_{11})^{-1}, \tag{6.7}$$

$$H(\rho) := -[Y_{11}A(\rho) + A(\rho)^T Y_{11}^{\ -1} - Y_{11}B_2(\rho)B_2(\rho)^T Y_{11}^{\ -1}$$

$$+ C_1(\rho)^T C_1(\rho) + \gamma^{-2}Y_{11}^{\ -1}B_1(\rho)^T Y_{11}^{\ -1}] \tag{6.8}$$

Then the LPV controller should be:

$$A_k(\rho) := A(\rho) + \gamma^{-2}B_1(\rho)B_1(\rho)^T Y_{11}^{\ -1} - B_2(\rho)B_2(\rho)^T \tag{6.9}$$

$$- Z[C_2(\rho)^T C_2(\rho) + \beta_{-2}H(\rho)];$$

$$B_k(\rho) := ZC_2(\rho)T; \tag{6.10}$$

$$C_k(\rho) := -B_2(\rho)^T Y_{11}^{-1}; \tag{6.11}$$

$$D_k(\rho) := 0. \tag{6.12}$$

From Theorem I, the linear matrix inequality has infinite dimension due to infinite ρ , causing difficulty in obtaining a solution. Alternatively a grid can be constructed on the parameter space and a finite problem can be solved based on this subset. Even though the solution obtained in this way may not satisfy requirements for all $\rho \in P$, since the open loop system is continuous in ρ, checking on a fine enough subset of P and looking at how the maximum eigenvalues of a matrix function change with respect to ρ, it is reasonable to expect that the LMIs hold for all $\rho \in P$.

6.1.2 LPV PDLF Method

Definition of parameter Dependent LPV system

The controller derived from the method in section 6.1.1 considers arbitrarily fast parameter changes. In other words, it uses a single-quadratic Lyapunov function (SQLF) for all cases, which leads to much conservatism. The conservatism can be reduced through a parameter-dependent Lyapunov function [58](PDLF) if the bounds on the parameter's rate of variation are known.

Definition 4 Given a compact subset $P \subset \Re^s$,finite non-negative numbers $\{v_i\}_{i=1}^s$ with $v := [v_1 ... v_s]^T$. Define the parameter v -variation set as

$F_P^v := \{\rho \in C^1(\Re, \Re^s) : \rho(t) \in P, |\dot{\rho}_i| \le v_i, i = 1,..., s\}$ where $C^1(\Re, \Re^s)$ stands for the class of piecewise continuously differentiable functions from $\Re$ to $\Re^s$.

The LPV systems studied in this section are slightly different because of their state space data dependence on parameters and their derivatives. The definition is as follows:

Definition 5 Given a compact subset $P \subset \Re^s$, and the continuous functions (A, B, C, D): $\Re^s \times \Re^s \to (\Re^{n \times n}, \Re^{n \times n_d}, \Re^{n_e \times n}, \Re^{n_e \times n_d})$. An $n-th$ order LPV system

with bounded parameter variation rates $\sum_P$ is given by

$$\begin{Bmatrix} \dot{X}(t) \\ e(t) \end{Bmatrix} = \begin{bmatrix} A(\rho(t), \dot{\rho}(t)) & B(\rho(t), \dot{\rho}(t)) \\ C(\rho(t), \dot{\rho}(t)) & D(\rho(t), \dot{\rho}(t)) \end{bmatrix} \begin{Bmatrix} X(t) \\ d(t) \end{Bmatrix}$$

where $\rho \in F_P^v, x(t) \in \Re^n, d(t) \in \Re^{n_d}$, and $e(t) \in \Re^{n_e}$.

Parameter dependent stability

Definition 6 Given a compact subset $P \subset \Re^s$, finite non-negative numbers $\{v_i\}_{i=1}^s$ and a function $A: \Re^s \times \Re^s \to \Re^{n \times n}$, the function A is parametrically-dependant stable over P if there exists a continuously differentiable function $P: \Re^s \to S^{n \times n}$, such that, $P(\rho) > 0$ and for all $\rho \in P$ and $|\beta_i| \le v_i, i = 1,2,...,s$

$$A^T(\rho, \beta)P(\rho) + P(\rho)A(\rho, \beta) + \sum_{i=1}^{s} (\beta_i \frac{\partial P}{\partial \rho_i}) < 0 \qquad (6.13)$$

If no bounds apply to parameter variation ($v_i \to \infty$ for $i = 1,2,...,s$), by restricting P to be a constant matrix, the notation for parameter-dependent stability goes to quadratic stability.

Definition 7 Given a parametrically-dependent stable LPV system, for zero initial conditions $X(0) = 0$, define induced L_2 norm to be:

$$\left\| G_{F_P} \right\|_{i,2} := \sup_{\rho \in F_P^v, \|d\|_2 \neq 0} \sup_{d \in L_2} \frac{\|e\|_2}{\|d\|_2} \qquad (6.14)$$

LPV γ-performance/v-Variation Problem

Definition 8 Given the open-loop LPV system $\sum_P$ in the above definition, and performance level $\gamma > 0$. The parameter-dependent γ-performance problem is solvable if there exists an integer $m \ge 0$, a function $W \in C^1(\Re_s, S^{(n+m)\times(n+m)})$, and continuous matrix functions $(A_K, B_K, C_K, D_K): \Re^s \times \Re^s \to (\Re^{m \times m}, \Re^{m \times n_y}, \Re^{n_u \times m}, \Re^{n_u \times n_y})$, such that $W(\rho) > 0$ and

$$\begin{bmatrix} A_{clp}^T(\rho,\beta)W(\rho)+W(\rho)A_{clp}^T(\rho,\beta)+\sum_{i=1}^{s}(\beta_i\frac{\partial W}{\partial \rho_i}) & W(\rho)B_{clp}(\rho,\beta) & \gamma^{-1}C_{clp}^T(\rho,\beta) \\ B_{clp}^T(\rho,\beta)W(\rho) & -I & \gamma^{-1}D_{clp}^T(\rho,\beta) \\ \gamma^{-1}C_{clp}(\rho,\beta) & \gamma^{-1}D_{clp}(\rho,\beta) & -I \end{bmatrix} < 0$$

(6.15)

for all $\rho \in P$ and $|\beta_i| \le v_i, i = 1,...,s$.

This is also a generalized sub-optimal H_∞ optimal control problem. It conceptually expands the applicability of the H_∞ control methodology.

Theorem II *Given a compact subset* $P \subset \Re^s$, *non-negative numbers* $\{v_i\}_{i=1}^s$, *performance level* $\gamma > 0$, *and the open-loop LPV system in (4.20), the LPV synthesis* γ *-performance/*v *-variation problem is solvable if and only if there exist continuously differentiable matrix functions* $X : \Re^s \to \varphi^{n\times n}$ *and* $Y : \Re^s \to \varphi^{n\times n}$, *such that for all* $\rho \in \mathsf{P}, X(\rho), Y(\rho) > 0$, *and*

$$\begin{Bmatrix} \hat{A}(\rho)Y(\rho) + Y(\rho)\hat{A}^T(\rho) - \gamma B_2(\rho)B_2^T(\rho) - \sum_{i=1}^{s} \pm (v_i \frac{\partial Y}{\partial \rho_i}) & Y(\rho)C_1^T(\rho) & \gamma^{-1}B_1(\rho) \\ C_1(\rho)Y(\rho) & -\gamma I_{n_{e1}} & 0 \\ B_1^T(\rho) & 0 & -I_{n_d} \end{Bmatrix} < 0 \tag{6.16}$$

$$\begin{Bmatrix} \overline{A}^T(\rho)X(\rho) + X(\rho)\overline{A}(\rho) - \gamma C_2^T(\rho)C_2(\rho) - \sum_{i=1}^{s} \pm (v_i \frac{\partial X}{\partial \rho_i}) & X(\rho)B_1(\rho) & C_1^T(\rho) \\ B_1^T(\rho)X(\rho) & -\gamma I_{n_{d1}} & 0 \\ C_1(\rho) & 0 & -I_{n_e} \end{Bmatrix} < 0 \tag{6.17}$$

$$\begin{Bmatrix} X(\rho) & I_n \\ I_n & Y(\rho) \end{Bmatrix} \geq 0 \tag{6.18}$$

where

$$\hat{A}(\rho) := A(\rho) - B_2(\rho)C_{12}(\rho), \tag{6.19}$$

$$\overline{A}(\rho) := A(\rho) - B_{12}(\rho)C_2(\rho)$$

(6.20)

Define the following:

$$Q(\rho) := X(\rho) - Y^{-1}(\rho),$$

(6.21)

$$F(\rho) := -[\gamma B_2^T(\rho) + C_{12}(\rho)],$$

(6.22)

$$L(\rho) := -[\gamma X^{-1}(\rho) C_2^T(\rho) + B_{12}(\rho)]$$

(6.23)

$$H(\rho, \dot{\rho}) := -[A_F^T(\rho) Y^{-1}(\rho) A_F(\rho) + \sum_{i=1}^{s} (\dot{\rho}_i \frac{\partial Y^{-1}}{\partial \rho_i}) + \gamma^{-1} C_F^T(\rho) C_F(\rho) \quad (6.24)$$

$$+ \gamma^{-1} Y^{-1}(\rho) B_1(\rho) B_1^T(\rho) Y^{-1}(\rho)]$$

$$A_F(\rho) := A(\rho) + B_2(\rho) F(\rho) \quad \textit{and} \quad C_F^T(\rho) := [C_{11}^T(\rho) C_{12}^T(\rho) + F^T(\rho)] \,.$$

(6.25)

Then the resulting LPV controller can be defined as:

$$A_k(\rho, \dot{\rho}) := A(\rho) + \gamma^{-1} [Q^{-1}(\rho) X(\rho) L(\rho) B_{12}^T(\rho) + B_1(\rho) B_1^T(\rho)] Y^{-1}(\rho)$$

(6.26)

$$+ B_2(\rho) F(\rho) + Q^{-1}(\rho) X(\rho) L(\rho) C_2(\rho) - Q^{-1}(\rho) H(\rho, \dot{\rho})];$$

$$B_k(\rho) := -Q^{-1}(\rho) X(\rho) L(\rho); \quad (6.27)$$

$$C_k(\rho) := F(\rho); \quad (6.28)$$

$$D_k(\rho) := 0. \quad (6.29)$$

To solve LMIs in (6.16)-(6.18), an ad hoc approach will be employed. Let $\{f_i\}_{i=1}^N$ and $\{g_i\}_{i=1}^N$ be user defined sets of continuously differentiable functions from $\Re^s$ to $\Re$.

$X(\rho) := \sum_{i=1}^{N} f_i(\rho) X_i$, $Y(\rho) := \sum_{i=1}^{N} g_i(\rho) Y_i$ are continuously differentiable on $\Re^s \to \varphi^{n \times n}$. So once the basis functions f_i and g_i are chosen, the original synthesis

LMIs are solvable by optimizing over the matrices $X_i, Y_i \in \varphi^{n \times n}$.

The rate-bounded LPV controllers are a function of the scheduling variables as well as their derivatives. The LPV controller can either be simulated by feeding in the scheduling derivative or eliminate them from the controllers. Eliminating the derivative usually has no effect on the controller performance.

6.2 Challenges in the LPV technique

For the given LPV system, it is clear that achievable performance relies on the choice of the Lyapunov function. In [41] an interpolated LPV technique with multiple parameter-dependent Lyapunov functions is proposed and applied to a detailed AMB (Active Magnetic Bearing) controller design. The interpolated LPV has the advantage of improving the obtained performance by finding the most appropriate Lyapunov functions in a local sense. Then a globally constructed Lyapunov function can be found to extend the local stability property to the entire parameter range. Since a power system is more complex and requires adequate damping under larger variation of system operating conditions, the interpolated LPV controller design using multiple Lyapunov functions (MLPV) is promising in the damping controller design in a large power system. In the following, an MLPV SDC for a SVC will be designed in an IEEE 50-machine test system with the interpolated LPV approach.

6.3 LPV interpolation analysis

Consider an LPV plant.

$$\begin{bmatrix} \dot{x}(t) \\ e(t) \\ y(t) \end{bmatrix} = \begin{bmatrix} A(\rho(t)) & B_1(\rho(t)) & B_2(\rho(t)) \\ C_1(\rho(t)) & D_{11}(\rho(t)) & D_{12}(\rho(t)) \\ C_2(\rho(t)) & D_{21}(\rho(t)) & D_{22}(\rho(t)) \end{bmatrix} \begin{bmatrix} x(t) \\ d(t) \\ u(t) \end{bmatrix} \tag{6.30}$$

where d is the disturbance, u is the control input, e is the error output, and y is the output

feedback signal. All the matrices have compatible dimensions. It is assumed that the vector-valued parameter ρ evolves continuously over time and its range is limited to a compact subset $P \subset R^S$. Its time derivative is bounded and satisfies the constant $-v_i \le \dot{\rho}_i \le v_i$, $i = 1,2,3,...,s$. Previous research on LPV control theory mainly focused on a single Lyapunov function (quadratic or parameter-dependent) over the entire set. The achieved performance heavily depends on the chosen Lyapunov function. With the restriction of using a single Lyapunov function in the entire parameter space, the achieved performance will be compromised in order to derive a uniform Lyapunov function in the overall parameter space. Therefore, it would be promising if different Lyapunov functions with a stability guarantee could be used over different parameter ranges to get improved performance. As a simple demonstration, suppose the parameter set has a dimension one. Suppose P^1, P^2 is an overlapped partition of the parameter set P. For each parameter subset, the design of a single LPV controller is sought. The overall interpolated LPV controller is then constructed by interpolating local LPV controllers. It is clear that the global controller is capable of achieving tighter performance due to the smaller parameter range. However, a critical issue associated with the proposed controller interpolation scheme is the stability of the global LPV controller. This will be guaranteed by constructing a globally continuous Lyapunov function over the entire parameter set.

Theorem III. *For a partition of parameter space* $P=[\underline{\rho},\bar{\rho}]$ *as subsets* $P^1=[\underline{\rho},b]$ *and* $P=[a,\bar{\rho}]$ $(a<b)$, *and given* $Q_R,Q_S\geq 0$ *matrix functions, if one of the following equivalent conditions are satisfied:*

there exist continuously differentiable matrix functions $R_i(\rho),S_i(\rho),i=1,2$ *such that for* $\rho\in P^i$

$$N_R^T\begin{bmatrix}\left\{\mp v\left(Q_R+\dfrac{\partial R_i}{\partial\rho}\right)+AR_i+R_iA^T\right\} & R_iC_1^T & B_1\\ C_1R_i & -\gamma_iI & 0\\ B_1^T & 0 & -\gamma_iI\end{bmatrix}N_R<0 \qquad (6.31)$$

$$N_S^T\begin{bmatrix}\left\{\mp v\left(Q_S+\dfrac{\partial S_i}{\partial\rho}\right)+A^TS_i+S_iA\right\} & S_iB_1 & C_1^T\\ B_1^TS_i & -\gamma_iI & 0\\ C_i & 0 & -\gamma_iI\end{bmatrix}N_S<0 \qquad (6.32)$$

$$\begin{bmatrix}R_i(\rho) & I\\ I & S_i(\rho)\end{bmatrix}\geq 0 \qquad (6.33)$$

with $N_R(\rho)=Ker[B_2^T(\rho)\quad D_{12}^T(\rho)\quad 0]$ (6.34)

$N_S(\rho)=Ker[C_2(\rho)\quad D_{21}(\rho)\quad 0]$

(6.35)

and for $\rho\in P^{12}(P^{12}=P^1\cap P^2)$

$R_2(\rho)-R_1(\rho)+(b-a)Q_R\geq 0$ (6.36)

$R_2(\rho)-R_1(\rho)-(b-a)Q_R\leq 0$ (6.37)

$S_2(\rho)-S_1(\rho)+(b-a)Q_S\geq 0$ (6.38)

$S_2(\rho)-S_1(\rho)+(b-a)Q_S\leq 0$ (6.39)

there exist continuously differentiable matrix functions $R_i(\rho), S_i(\rho) > 0$, $i = 1,2$ and continuous matrix functions $\hat{A}_k^{(i)}, \hat{B}_k^{(i)}, \hat{C}_k^{(i)}, i = 1,2$ such that for $\rho \in P^i$,

$$\begin{bmatrix} \left\{ \begin{matrix} \pm v\left(Q(s) + \dfrac{dS_i}{d\rho} \right) + S_i A \\ + \hat{B}_k^{(i)} C_2 + (*) \end{matrix} \right\} & \hat{A}_k^{(i)} & S_i B_1 + \hat{B}_k^{(i)} D_{21} & C_1^T \\ \hat{A}_k^{(i)T} & \left\{ \begin{matrix} \mp v\left(Q_R + \dfrac{dR_i}{d\rho} \right) + AR_i \\ + B_2 \hat{C}_k^{(i)} + (*) \end{matrix} \right\} & B_1 & R_i C_1^T + \hat{C}_k^{(i)T} D_{12}^T \\ B_1^T S_i + D_{21}^T \hat{B}_k^{(i)T} & B_1^T & -\gamma_i I & 0 \\ C_1 & C_1 R_i + D_{12} \hat{C}_k^{(i)} & 0 & -\gamma_i I \end{bmatrix} < 0 \tag{6.40}$$

$$\begin{bmatrix} R_i(\rho) & I \\ I & S_i(\rho) \end{bmatrix} \geq 0 \tag{6.41}$$

and for $\rho \in P^{12}$

$$R_2(\rho) - R_1(\rho) + (b-a)Q_R \geq 0 \tag{6.42}$$

$$R_2(\rho) - R_1(\rho) - (b-a)Q_R \leq 0 \tag{6.43}$$

$$S_2(\rho) - S_1(\rho) + (b-a)Q_S \geq 0 \tag{6.44}$$

$$S_2(\rho) - S_1(\rho) - (b-a)Q_S \leq 0 \tag{6.45}$$

then the closed-loop LPV system can be stabilized by a continuous LPV controller with induced L_2 performance less than $\bar{\gamma} = \max\{\gamma_1, \gamma_2\}$

(6.46)

Furthermore, let

$$\gamma(\rho) = \begin{cases} \gamma_1 & \rho \leq a \\ \left(\dfrac{b-\rho}{b-a} \right) \gamma_1 + \left(\dfrac{\rho - a}{b-a} \right) \gamma_2 & a < \rho < b \\ \gamma_2 & \rho \geq b \end{cases} \tag{6.47}$$

$$R(\rho),S(\rho)=\begin{cases} R_1(\rho),S_1(\rho) & \rho\le a \\ \left(\dfrac{b-\rho}{b-a}\right)\{R_1(\rho),S_1(\rho)\}+\left(\dfrac{\rho-a}{b-a}\right)\{R_2(\rho),S_2(\rho)\} & a<\rho<b \\ R_2(\rho),S_2(\rho) & \rho\ge b \end{cases}$$

(6.48)

and $$M(\rho)N^T(\rho) := I - R(\rho)S(\rho) \tag{6.49}$$

calculate

$$\begin{aligned} &\hat{A}_k(\rho,\dot{\rho}) = S(\rho)\frac{dR}{dt} + N(\rho)\frac{dM^T}{dt} - A^T(\rho) \\ &-\frac{1}{\gamma(\rho)}\left[S(\rho)B_1(\rho)+\hat{B}_k(\rho)D_{21}(\rho) \quad C_1^T(\rho)\right] \\ &\times\begin{bmatrix} B_1^T(\rho) \\ C_1(\rho)R(\rho)+D_{21}(\rho)\hat{C}_k(\rho)\end{bmatrix} \end{aligned} \tag{6.50}$$

$$\hat{B}_k(\rho) = -\left[\gamma(\rho)C_2^T(\rho)+S(\rho)B_1(\rho)D_{21}^T(\rho)\right]\times\left[D_{21}(\rho)D_{21}^T(\rho)\right]^{-1} \tag{6.51}$$

$$\hat{C}_k(\rho) = -\left[D_{12}^T(\rho)D_{12}(\rho)\right]^{-1}\times\left[\gamma(\rho)B_2^T(\rho)+D_{12}^T(\rho)C_1(\rho)R(\rho)\right] \tag{6.52}$$

$$\hat{D}_k(\rho) = 0 \tag{6.53}$$

Then the interpolated LPV controller K_P will be constructed as

$$\begin{aligned} A_k(\rho,\dot{\rho}) = N^{-1}(\rho)\{&\hat{A}_k(\rho,\dot{\rho}) - S(\rho)B_2(\rho)\hat{C}_k(\rho) \\ &-\hat{B}_k(\rho)C_2(\rho)R(\rho) - S(\rho)A(\rho)R(\rho)\}M^{-T}(\rho) \end{aligned} \tag{6.54}$$

$$B_k(\rho) = N^{-1}(\rho)\hat{B}_k(\rho) \tag{6.55}$$

$$C_k(\rho) = \hat{C}_k(\rho)M^{-T}(\rho) \tag{6.56}$$

$$D_k(\rho) = 0 \tag{6.57}$$

From Theorem III, a global stabilizing LPV controller with the potential to improve its local performance can be obtained with the proposed interpolation scheme. Also, the globally continuous Lyapunov function over the entire parameter set for the closed-loop LPV system is derived from the matrix functions $R_i(\rho)$ and $S_i(\rho)$. From equation (7)~(10), there are infinite-dimensional solvability conditions as well as its solution space.

To simplify, the search of parameter-dependent Lyapunov functions is restricted to a span of finite numbers of basis functions. That is, let

$$R_i(\rho) = \sum_{i=1}^{N_f} f_i^k(\rho) R_i^k \ , S_i(\rho) = \sum_{k=1}^{N_g} g_i^k(\rho) S_i^k \tag{6.58}$$

where $\{f_i^k(\rho)\}_{k=1}^{N_f}$ and $\{g_i^k(\rho)\}_{k=1}^{N_g}$ are user-specified scalar basis functions. With this parameterization, a gridding method over each parameter subset can be used to solve the LPV synthesis conditions.

6.4 LPV model of power system

The above linearization process is applied to every operating point (p). For each given set of operating conditions, specified in terms of real and reactive power load, real power generation schedules at generator buses, and voltage magnitude at certain buses, a power flow solution is obtained. With the voltage solution and the power injection at each generator bus, initial conditions for the state variables are calculated. The state equations and the network equatrions are then linearized, and a set of state-spce equations whose entries depend on the operating conditions (p) are obtained in the flowing form:

$$\dot{\mathrm{X}} = A(\rho)\mathrm{X} + B(\rho)u$$
$$\mathrm{Y} = C(\rho)\mathrm{X} + D(\rho)u$$

Where X is the vector of incremental state variables, u is the vector of incremental control variables, and $A(p)$, $B(p)$ are varying coefficient matrices with proper dimensions. P is a time-varying vector. It is bounded and its trajectory is unknown in advance, but can be measured in real time. At each specific p, A and B are constant

The linearization process is straightforward, but it is not feasible to achieve the complete LPV model in practice due to an infinite number of operating points (p) produced over the operating range. However, the complete form of the LPV model is not altogether necessary for the LPV synthesis. In practical design cases, in order to avoid the inifinite-dimensional LMIs, an alternative approximate problem is set up by gridding the parameter space and solving the set of LMIs that hold on the subset of P formed by

gridding points. If this approximate problem does not have a solution, neither does the original inifinite dimension problem. Even if the solution is found, it still does not guarantee that the solution satisfies the orginal constraints. However, since the matrix functions are continous with respect to p, after checking on a dense enough subset of P, the LMIs can be expected to hold for all p.

The power system is represented by a differential algebraic model which captures the differential dynamics of the various components and the algebraic relationship that governs the network.

$$\begin{aligned} \dot{X} &= F(X,Y) \\ 0 &= G(X,Y) \end{aligned} \tag{6.59}$$

Where X is the vector of state variables governed by the differential equations, and Y is the vector of the network variables.

To construct the LPV model for the power system, first some scheduling parameters should be chosen and then linearization performed at each scheduling point. For each scheduling point, specified in terms of real and reactive power load, real power generation schedules at generator buses, and voltage magnitude at certain buses, a power-flow solution is obtained. With this power flow solution, initial values of each state can be calculated and then the system can be linearized at this equilibrium point. Thus there is an LTI system dependent on its respective scheduling point at each operating point (OP). State-space equations dependent on different scheduling points (ρ) are obtained from the following form:

$$\begin{aligned} \dot{X} &= A(\rho)X + B(\rho)u \\ Y &= C(\rho)X + D(\rho)u \end{aligned} \tag{6.60}$$

where X is an incremental state variable from an equilibrium point, u is the controller input, Y is the output feedback, and ρ is the varying scheduling parameter vector.

6.5 Design objective

The design objective is to obtain an LPV controller for a SVC to provide sufficient damping at the inter-area oscillatory mode of the system at all operating conditions

characterized by a 1200-1800MW power generation range from Generator 93,110 with a compensation level range of 0-50%. The generating limit of the original system without an SVC and its controller for G93 and G110 is only 1400 MW.

6.6 Several issues in controller design

6.6.1 Constraints in controller design

There is both an upper and a lower limit in the SD2 block of the dynamic model for an SVC in ETMSP [50]. If the output of the damping controller is large enough to exceed any one of the limits of the SVC limiting block, the nonlinearity of the system will be excited and the assumption that the linearized system can represent the original system under a very small disturbance is violated. Thus the controller that is designed based on the linearized system cannot be expected to achieve the expected damping performance. Therefore, the control effort should be restricted so that such a violation of limits can be avoided.

6.6.2 Feedback signal selection

Furthermore, a different feedback signal corresponds to a different modal observability. Hence, a good choice of the feedback signal should provide good observability of the inter-area critical mode under the variation of operating conditions. The active power P_{tie} through Line 67-124 has a very large modal observability for the critical modes and can be easily measured on account of its proximity to Bus 66. Therefore, in the following section SDCs are designed at Bus 66 with the input of P_{tie} through Line 67-124 using different techniques.

6.6.3 System reduction in large power system

The obtained open-loop system is of 131st order, which is too complicated for an LPV calculation. Besides, most design techniques produce high-order controllers whose dimensions are related to the system size. It is impractical to realize the obtained controller with such a huge order. It is possible to get the controller of higher order first, and then reduce it to a practical lower order. However, since the controller will be achieved by the LPV technique, which can guarantee the smooth transition from one controller to another controller, the big reduction of the original controller of a higher order could cause system instability during the transition time. Therefore it is necessary to reduce the system to a smaller order at the same time preserving the critical dynamics of the system. Reference [8] suggested a good way of retaining the lightly damped modes and unstable modes while reducing the other modes. However, in the 50-machine system [9], there are more than 20 pairs of lightly damped modes which should be retained according to the method in [8]. Since our goal is to improve the critical mode around 0.28Hz, this pair of modes is retained and the rest of the system is reduced to 9th order by the balanced truncation method [21]. Thus the overall reduced system is of 11th order. Fig. 6.1 and Fig. 6.2 clearly show that the reduced LPV model accurately approximates the full-order model with the explicit parameter dependency at generation levels of 1200MW and 1500MW respectively. The same patterns exist at other generation levels.

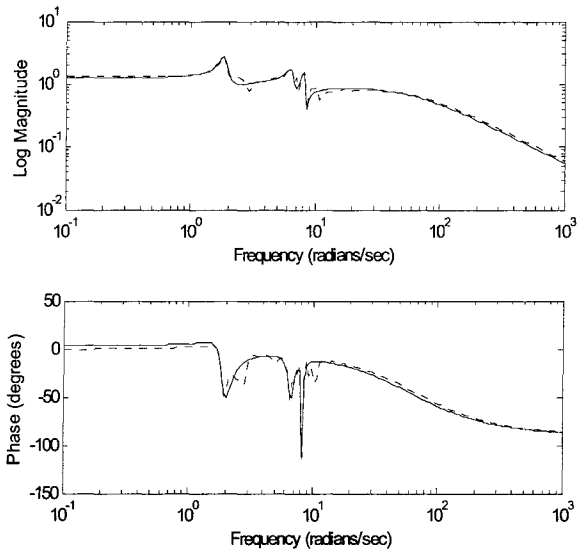

Figure 6.1 Frequency responses of the reduced system and the original system at 1200MW

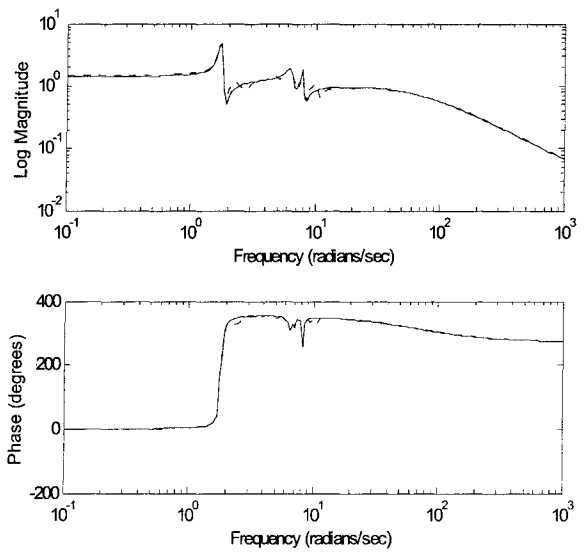

Figure 6.2 Frequency responses of the reduced system and the original system at 1500MW

6.6.4 LPV SDC setup

The setup of the controller design is shown in Fig. 6.3, where P represents the reduced

11th order system model of the 50-machine power system and the primary part of the SVC device. The K in this figure is the controller to be designed. The output of this controller is fed into the summing point of the SVC device as the damping modulating signal. An exact controller design is performed at each gridding point instead of only at one nominal point, and therefore there is no need to represent the uncertainty around the nominal point with a calculated weighting function of W_u. Thus W_u=0.1 to restrict the control effort imposed by the TCSC output limit. Hence:

$$W_{perf} = \frac{0.1s + 20}{s + 2} \tag{6.61}$$

which represents a low pass filter. Set $W_{noise} = 0.01$ to avoid singularity problems.

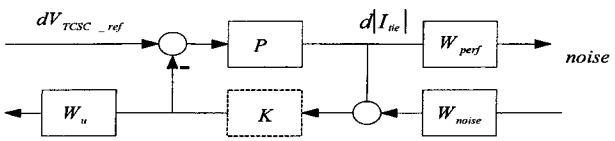

Figure 6.3 SDC design setup

6.7 SLPV SDC design

An LPV solution can be obtained using either a single fixed or a single parameter-dependent quadratic Lyapunov function over all gridding points in a one-dimensional parameter [58]. An LPV controller with a single fixed Lyapunov function (SF-LPV) can be obtained in the scheduling parameter space of [2× 1200– 2× 1400] MW. No feasible solution can be obtained in the parameter range higher than 2× 1400 MW. Therefore, the feasible scheduling parameter space for the SF-LPV is [2× 1200– 2× 1400] MW. The SF-LPV sacrifices the possibly larger operational parameter range to guarantee closed-loop stability under arbitrarily-varying parameters. In the real case, the load change rate always has some bounds. Motivated by the available bound information, an LPV controller using a single parameter-dependent Lyapunov function (SLPV) can be employed to reduce conservatism and extend the operating range. Assume that the real power generation changes at a rate between

$[-50MW/\sec, 50MW/\sec]$. The basis functions used to parameterize the functional space are:

$$f^1(\rho)=1,\ f^2(\rho)=\rho \tag{6.62}$$

The resulting operating range is [2× 1200– 2× 1600] MW, larger than that of the system with the SF-LPV. Still, no solution can be obtained that covers the whole operating range of [2× 1200– 2× 1800] MW. The results for the SLPV SDC of reduced 3rd order are shown in Table 6.1 at five frozen operating points.

Table 6.1 SLPV CONTROLLER FOR THE SVC AT DIFFERENT FROZEN OPERATING POINTS.

OP	Interpolated LPV SVC
1200	$0.108\frac{1-1.6685s+0.0391s^2-0.0333s^3}{1-0.0755s+0.0338s^2+0.0015s^3}$
1300	$0.318\frac{1-0.7941s+0.033s^2-0.0154s^3}{1+0.1106s+0.0349s^2+0.0022s^3}$
1400	$0.364\frac{1-0.9440s+0.0405s^2-0.0195s^3}{1+0.1428s+0.0407s^2+0.0034s^3}$
1500	$0.327\frac{1-1.219s+0.061s^2-0.0273s^3}{1+0.189s+0.0506s^2+0.0043s^3}$
1600	$0.295\frac{1-1.3068s+0.0605s^2-0.0293s^3}{1+0.1182s+0.05084s^2+0.0041s^3}$

6.8 MLPV SDC design

Concurrently, based on the Theorem III, an interpolated LPV controller synthesis using multiple parameter-dependent Lyapunov functions (MLPV) may be conducted with the whole parameter space divided into two subsets $([2\times1200-2\times1520]\cup[2\times1500-2\times1700])$ MW. Then four points are used to grid each parameter subspace uniformly. In the case of each partitioned parameter space, two sets of

identical basis functions are used to parameterize the functional space,

$$f_i^1(\rho) = 1,\ f_i^2(\rho) = \rho \tag{6.63}$$

$$g_i^1(\rho) = 1,\ g_i^2(\rho) = \rho. \tag{6.64}$$

With the basis functions

$$R_i(\rho) = R_i^1 + \rho R_i^2,\ S_i(\rho) = S_i^1 + \rho S_i^2. \tag{6.65}$$

Which become functions of scheduling parameters after the interpolation. The interpolated LPV controller gain will depend on both the parameter and its derivative. The same rate bound as in the SLPV synthesis is used here. Two Lyapunov functions are sought in the two subregions satisfying conditions (6.42) through (6.45), which can guarantee the existence of a globally continuous Lyapunov function over the entire parameter set. Thus the interpolated LPV controller is capable of achieving a tighter performance due to divided small parameter ranges.

Finally the obtained controller is reduced to third order for simplicity of application. Its parameters at seven gridding frozen points are shown in Table 6.2.

Table 6.2 INTERPOLATED MLPV CONTROLLER FOR THE SVC AT DIFFERENT FROZEN OPERATING POINTS.

OP	Interpolated LPV SVC
1200	$0.0629\frac{1-2.720s+0.0315s^2-0.0532s^3}{1+0.0698s+0.0334s^2+0.0013s^3}$
1300	$0.324\frac{1-1.0201s+0.0315s^2-0.0214s^3}{1+0.2440s+0.0402s^2+0.0049s^3}$
1400	$0.480\frac{1-1.0446s+0.0561s^2-0.0232s^3}{1+0.3507s+0.0456s^2+0.0081s^3}$
1500	$0.120\frac{1-4.971s+0.1109s^2-0.1305s^3}{1+0.271s+0.0681s^2+0.0069s^3}$
1600	$0.087\frac{1-0.306s+0.2360s^2-0.1978s^3}{1+0.325s+0.0567s^2+0.0084s^3}$
1700	$0.651\frac{1-2.212s+0.0688s^2-0.0522s^3}{1+0.3763s+0.0760s_2+0.0125s^3}$

6.9 SLPV and MLPV realization

The state space data of the LPV controller depends on the parameter vector $\rho(t)$ as in (6.50) through (6.57). If the dependence could be expressed by polynomiasl and/or rational functions, then the parameter dependent controller could be realized in LFT form in Fig. 6.4.

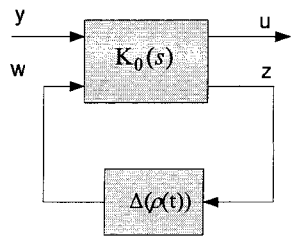

Figure 6.4 LFT realization of the LPV controller

$\Delta(\rho(t)) = diag(\rho_1(t)I_{r1}, \rho_2(t)I_{r2}, ..., \rho_f(t)I_{rf}) \in \mathbb{R}^{r\times r}, r = r_1 + r_2 + ... + r_f$.

For $i = 1,2,...,f$, the varying parameter ρ_i is repeated r_i times in the LFT. $K_0(s)$ is an LTI plant. At each time instant, the LPV controller is obtained by $K = F_l(K_0(s), \Delta(\rho(t)))$.

For our problem, ρ represents the power generation level from Generator #93 and #110, and the LPV controller has the following dynamics:

$$\begin{bmatrix} \dot{x}_k(t) \\ u(t) \end{bmatrix} = \begin{bmatrix} A_k(\rho(t)) & B_k(\rho(t)) \\ C_k(\rho(t)) & D_k(\rho(t)) \end{bmatrix} \begin{bmatrix} x_k(t) \\ y(t) \end{bmatrix} \tag{6.66}$$

At the five gridding points, each component of the state space matrices of the SLPV controller could be closely approximated by a first order polynomial in ρ. Using least-squares estimation, the state-space matrices of the SLPV controller are approximated as:

$$\begin{bmatrix} A_k(\rho(t)) & B_k(\rho(t)) \\ C_k(\rho(t)) & D_k(\rho(t)) \end{bmatrix} \doteq \left\{ \begin{bmatrix} A_0 & B_0 \\ C_0 & D_0 \end{bmatrix} + \rho(t) \begin{bmatrix} A_1 & B_1 \\ C_1 & D_1 \end{bmatrix} \right. \tag{6.67}$$

At the first three gridding points (1200MW, 1300MW, 1400MW), each component of the state space matrices of the MLPV controller could be closely approximated by a first-order polynomial in ρ. Then at the gridding points 1400MW and 1500MW, each component of the state-space matrices of the LPV controller can be approximated by another first order polynomial in ρ. Finally, at the gridding points 1500MW, 1600MW, and 1700MW, another first order polynomial in ρ can be obtained to approximate each component of the state space matrices of the LPV controller. The whole expression of the MLPV controller thus becomes:

$$\begin{bmatrix} A_k(\rho(t)) & B_k(\rho(t)) \\ C_k(\rho(t)) & D_k(\rho(t)) \end{bmatrix} \doteq \begin{cases} \begin{bmatrix} A_{01} & B_{01} \\ C_{01} & D_{01} \end{bmatrix} + \rho(t) \begin{bmatrix} A_{11} & B_{11} \\ C_{11} & D_{11} \end{bmatrix}, 1200 \le \rho(t) \le 1400 \\ \begin{bmatrix} A_{02} & B_{02} \\ C_{02} & D_{02} \end{bmatrix} + \rho(t) \begin{bmatrix} A_{12} & B_{12} \\ C_{12} & D_{12} \end{bmatrix}, 1400 < \rho(t) < 1500 \\ \begin{bmatrix} A_{03} & B_{03} \\ C_{03} & D_{03} \end{bmatrix} + \rho(t) \begin{bmatrix} A_{13} & B_{13} \\ C_{13} & D_{13} \end{bmatrix}, 1500 \le \rho(t) \le 1700 \end{cases} \tag{6.68}$$

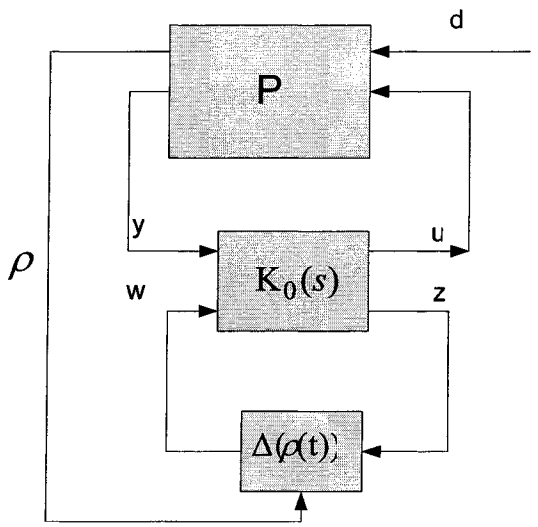

Figure 6.5 Closed-loop configuration of the LPV system. Parameter dependent controller is realized in LFT form

The closed loop system is shown in Fig. 6.5 with the MLPV or SLPV controller realized in LFT form.

6.10 Simulation results

6.10.1 Small- signal stability

Small-signal analysis is performed using EPRI's MASS [50] software package. An RL SDC [1] is designed with root-locus methods at the generation level of 2×1200MW

from Generators #93 and #110. The parameters of the RL SDC are $-0.1\times(\frac{0.35s+1}{0.1s+1})^2$. Comparisons of the system without SDC, the system with an MLPV SDC, the system with an SLPV SDC, and the system with an RL SDC are shown in Table 6.3.

Table 6.3 COMPARISON OF DAMPING RATIO

Power (MW)	Open loop	RL SDC	SLPV SDC	MLPV SDC
1200	4.74% @0.297Hz	7.08% @0.297Hz	12.3% @0.284Hz	11.31% @0.287Hz
1300	3.17% @0.291Hz	6.08% @0.292Hz	15.91% @0.305Hz	16.19% @0.300Hz
1400	1.09% @0.285Hz	4.67% @0.285Hz	19.49% @0.309Hz	13.50% @0.311Hz
1500	-1.62% @0.277Hz	2.70% @0.277Hz	18.50% @0.301Hz	13.79% @0.308Hz
1600	-5.10% @0.267Hz	-0.10% @0.267Hz	6.79% @0.194Hz	13.27% @0.300Hz
1700	-9.71% @0.255Hz	-4.14% @0.255Hz	0.8% @0.193Hz	12.51% @0.304Hz
1800	-16.58% @0.238Hz	-10.61% @0.238Hz	-7.43% @0.188Hz	12.96% @0.307Hz

As expected, both the SLPV SDC and the MLPV SDC can achieve better damping than the conventional RL SDC because of the robust control design method. There is litttle difference between the SLPV SDC and the MLPV SDC with regard to damping performance in the range of [2× 1200– 2× 1500] MW as seen from Fig 6.6. Unfortunately

after the generation level of #93, #110 exceeds 2× 1500MW, the damping effect of the SLPV SDC drops steeply with insufficient damping for the system operation. Therefore, the upper limit of generation at G93 and G110 in the original system without a SVC and its controller is expanded from 1400 MW to 1600MW with the SLPV SVC SDC. Conversely, with the MLPV SVC SDC, the system still has adequate damping even when the generation level reaches 1800MW. Obviously the MLPV SDC can extend the system's operating range to a much higher level with sustaining damping.

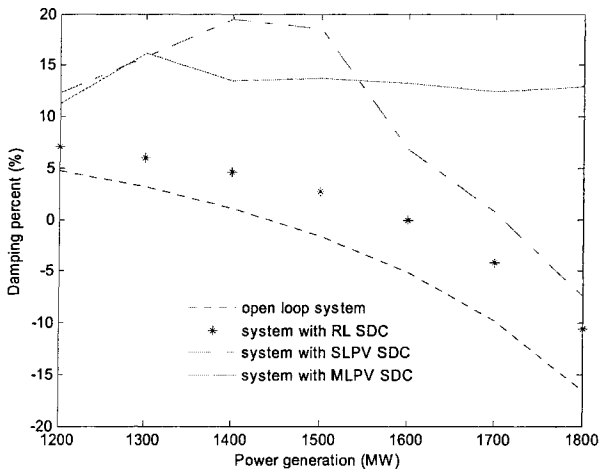

Figure 6.6 Damping comparison under different system operating points

Nonlinear time-domain simulation was performed using ETMSP [50]. The AVR reference of Generator 93 drops 0.1pu for one cycle. The real power from generator 137 is monitored to show the effect of the damping controller due to its large participation in the critical mode. The simulation results are shown in Fig. 6.7~6.9. Comparisons are made among cases with RL SDC, with SLPV SDC and the MLPV SDC at three different operating points.

The results are consistent with the results from the small signal analysis by MASS. In the power production range of [2×1200-2×1500] MW from generator 93,110, the damping improvement introduced by the MLPV SDC looks almost the same as that of the SLPV SDC and much better than that of the RL SDC. However, if power production

from Generators 93,110 is larger than 2×1500MW, there are apparent advantages from the MLPV SDC in terms of improving the damping compared to the SLPV SDC and the RL SDC. Therefore the MLPV SDC works well in a larger operational range than the SLPV SDC designed using a single parameter-dependent Lyapunov function.

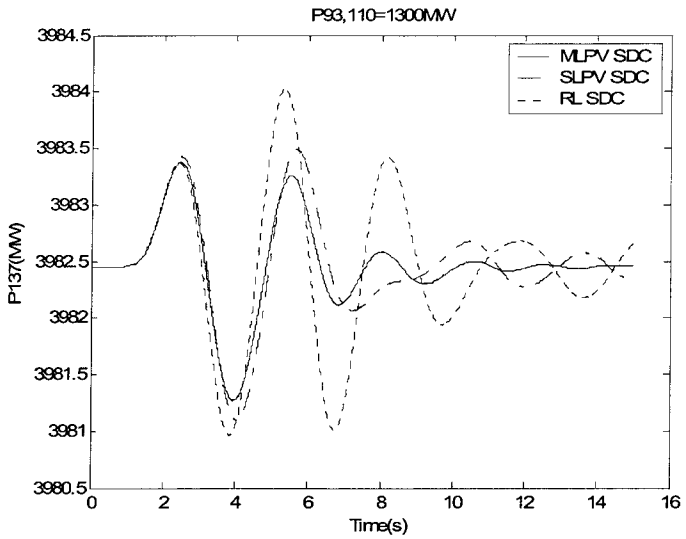

Figure 6.7 Active power of the Generator 137: AVR reference drop 0.1 for 1 cycle at Bus 93 (at 1300MW)

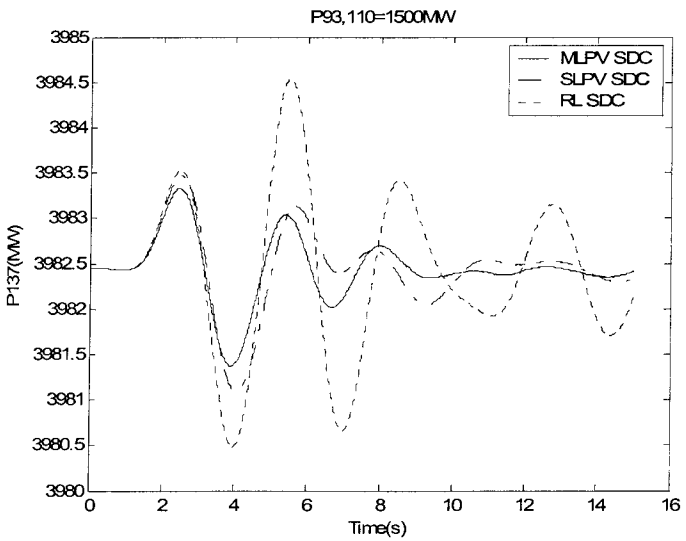

Figure 6.8 Active power of the Generator 137: AVR reference drop 0.1 for 1 cycle at Bus 93 (at 1500MW)

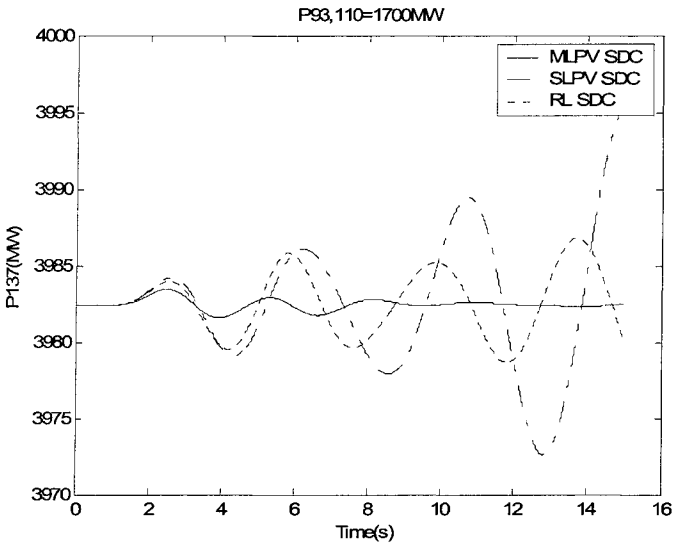

Figure 6.9 Active power of the Generator 137: AVR reference drop 0.1 for 1 cycle at Bus 93 (at 1700MW)

A three-phase fault at Bus 6 for 100ms is applied to the system at the generation level of 2×1500MW. The real power from generator 137 is monitored in Fig. 6.10.

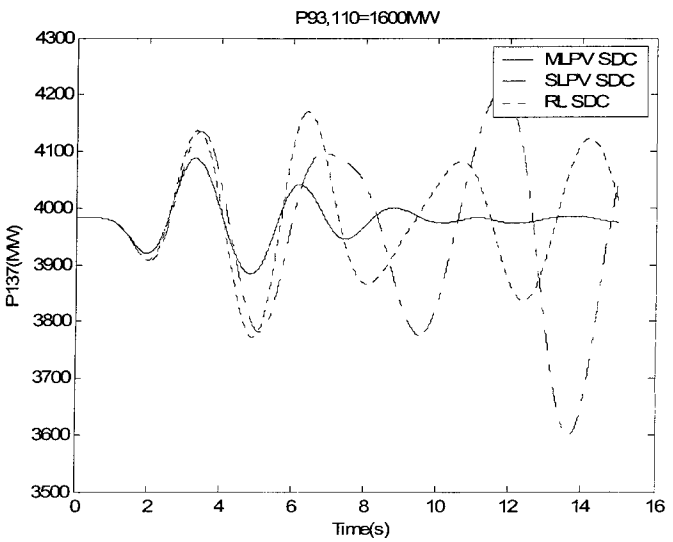

Figure 6.10 Active power of the Generator 137: 2cycles 3-phase fault at Bus 33 and clear the fault by opening the line33-50 at 1600MW

Additionally, a three-phase fault at Bus 33 for 2 cycles was applied and the fault then cleared by opening Line 33-50 at the generation level of 2×1600MW. The real power from generator 137 was monitored to show the effect of the damping controller in Fig. 6.11. It is apparent that the MLPV SDC is more effective and robust with regard to damping improvement than the SLPV SDC and the RL SDC.

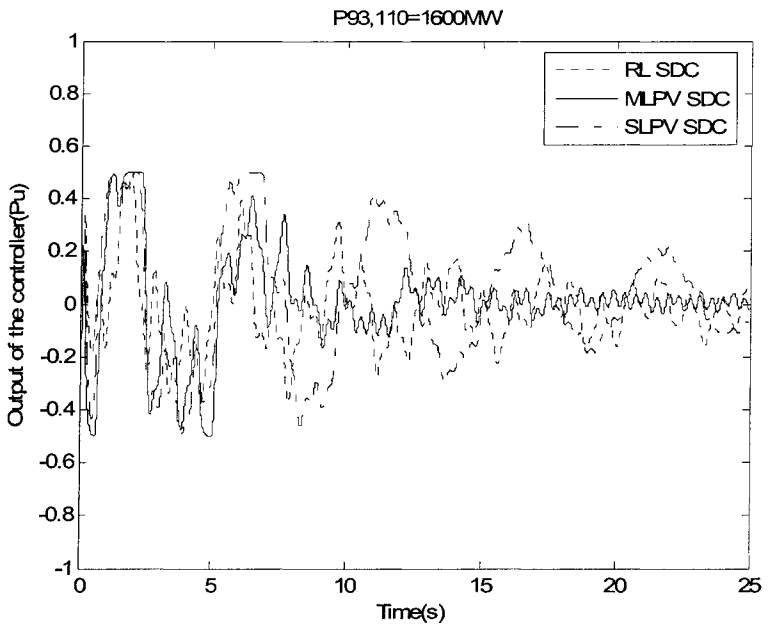

Figure 6.11 Output of the controller: 2cycles 3-phase fault at Bus 33 and clear the fault by opening the line33-50 at 1600MW

6.10.2 Transient stability

The effect of the LPV SVC SDC in enhancing transient stability performance may be verified by evaluating the critical clearing time (CCT) at three different operating points for a three-phase fault at Bus #1. The results given in Table 6.4 further illustrate the advantages of the MLPV SVC SDC in comparison with the SLPV SDC. The CCT difference among the system with different SDCs becomes larger when the stress level of

the system is higher than 2×1500 MW.

Table 6.4 COMPARISON OF CRITICAL CLEARING TIME

	MLPV SDC	SLPV SDC	RL SDC
2×1800 MW	2 cycles	0 cycle	0 cycle
2×1700 MW	5 cycles	3 cycles	3 cycles
2×1500 MW	9 cycles	9 cycles	7 cycles
2×1300 MW	12 cycles	12 cycles	11cycles

A three-phase fault with a fixed clearing time of four cycles is applied to verify the performance of the MLPV SDC under transient conditions. The results are shown in Table 6.5. With the MLPV SDC for the SVC at Bus66, the system transient stability is enhanced in terms of the maximal power generation at both Bus #93 and Bus #110 to keep the system stable after the fault.

Table 6.5 COMPARISON OF CRITICAL POWER GENERATION

Fault location	MLPV SDC	SLPV SDC	RL SDC
Bus7	2×1800 MW	2×1700 MW	2×1600 MW
Bus1	2×1800 MW	2×1700 MW	2×1700 MW
Bus33	2×1800 MW	2×1750 MW	2×1650 MW

While the damping controller for FACTS device is primarily designed to deal with the damping issue, the transient stability results show that an appropriate designed MLPV SDC can have an additional unanticipated benefit of slightly improving the transient stability.

6.11 Weighting function selection and damping performance

In this dissertation, the LPV technique is based on the mixed sensitivity setup, where weighting functions need to be carefully chosen. So far there is no theory showing any direct relation between the selection of weighting functions and the structure of the LPV controller obtained. Thus it is difficult to incorporate constraints on the controller structure into the weighting function selection. In some systems, by using different weighting functions, RHP zeros in the LPV controller may be avoided. However, in other complicated systems like the 50-machine system, even after an extensive weighting function selection, there are still some RHP zeros in the LPV controller. If the bigger concern in the controller design is the controller structure, other controller design methods should be considered to deal with these constraints.

The damping performance achieved also has an indirect dependence on the chosen weighting functions. To obtain a good LPV solution, a time-consuming selection of the appropriate weighting functions should be conducted. This is a drawback of the LPV technique, which is based on the mixed-sensitivity formulation and consequently the result relies on the chosen weighing functions. In this particular 50-machine case, no minimum damping constraints can be set due to the existence of a number of uncontrollable poles near the imaginary axis.

6.12 Computational level and the dimension of the parameter space

In this dissertation, a LPV solution is successfully obtained within a one-dimensional parameter space. There is usually more than one scheduling parameter in real systems in order to handle more complicated uncertainties, which will consequently increase the dimension of the parameter space. In fact, the same procedure in the MLPV technique can be followed with an increasing computational level in a multi-dimensional parameter case.

6.13 Summary

The MLPV controller design using multiple Lyapunov functions in different subsets facilitates the feasibility of the LPV solutions over a much larger scheduling parameter space. With certain conditions satisfied the interpolated MLPV controller can guarantee the continuity of the overall Lyapunov function as well as the global system stability in the entire parameter set. Furthermore, it can improve the local damping performance in each divided smaller subset. The more subsets the parameter space is divided into, the better the local performance achieved. However, more continuity conditions have to be satisfied with increasing computational burden. In addition, problems will arise in field implementation. After balancing its benefits and disadvantages, the interpolated LPV technique is still cost-effective in extending the system operating range if the parameter space is divided into a moderate number of subsets. The results from small signal analysis and transient stability analysis consistently show that the MLPV SVC SDC can enhance the system stability in a 50-machine system without any PSS. In general, its application in power systems has significant potential to extend the operational level with guaranteed stability especially when large variation of the operating conditions challenges the conventional robust controller design methods.

7 IMPROVEMENT OF TCSC CONTROLLER DESIGN IN A 50-MACHINE SYSTEM USING AN ADDITIONAL FEEDBACK SIGNAL

7.1 Background

With regard to improving damping, there are many possible choices to consider in designing a damping controller. Different methods may yield different controllers with varying damping performance. In the previous chapters, one SVC controller was designed for the 50-machine system. Results from small-signal stability analysis as well as the transient time-domain simulation show that the single damping controller obtained worked well in achieving the desired critical-mode damping ratio. In the 50-machine system, significant improvement has been obtained with the application of a SVC controller designed by an advanced interpolated LPV method. The advanced LPV method is beneficial in that it can easily manage the uncertainty and thus extend the system operational level. However, more computational effort is required to obtain the solution from several LMIs. This raises the question: is it possible to design a controller with simple structure and fixed parameters to achieve satisfactory damping performance without the complexity of LPV calculation?

Up to now, TCSC controller design has not been investigated for the 50-machine. As discussed in Chapter 4, the TCSC SDC is not a favorable choice for this large case. Not only is the controllability from the TCSC SDC smaller than that from the SVC SDC at Bus 66, but the zero-pole interaction limits the damping enhancement as well. Also, because of physical attributes such as plant/controller structure in applications in power industry, a

single TCSC SDC with a feedback signal is not adequate to achieve desired damping effects in such large and complex systems even after a careful selection of locations and feedback signals. Thus, combining a secondary controller in a different location to enhance the overall damping at the critical mode [57] is a natural option. However, a large computational effort must be taken to carefully develop the coordination scheme between two controllers due to their possible interactions. Furthermore, the coordination scheme is challenged when the system is subjected to a large change of operating conditions.

Instead of adding another controller, results were obtained for a variety of applications where limitations imposed by severe constraints on closed-loop performance could be avoided by feeding back an additional measurement. Ref. [12] gives an example of the inverted pendulum where it was shown that stability margins and performance were significantly improved when both the cart position and the rod angle were fed back. Furthermore, reference [59] gives a theoretical proof about how tradeoffs encountered in single-loop systems can be avoided when using a second plant output for feedback. In this chapter the damping improvement of the TCSC controller by adding an additional measurement, which overcomes the performance limitation in a single-input single-output (SISO) controller design and therefore results in a better damping at the critical mode will be considered.

7.2 Objective

The following will show that the challenges of achieving satisfactory damping performance in designing a SISO TCSC SDC can be overcome by designing a two-input one-output (TISO) TCSC SDC through use of an additional feedback signal.

7.3 Challenges in the SISO TCSC controller design in 50-machine system

Based on the result of Chapter 4, Line 63-66 and Line 67-124 are two lines with largest controllability for the installation of TCSC controllers besides Line 128-129.

Considering that they are two of the lines between two areas oscillating against each other, the effectiveness of a TCSC controller at these two locations will be investigated.

7.3.1 TCSC SDC setup

The setup of the controller design is shown in Fig. 7.1, where P represents the reduced 11^{th}-order system model of the 50-machine power system and the primary part of the TCSC device. The K in this figure is the desired supplementary controller. The output of this controller is fed into the summing point of the TCSC device as the damping modulating signal. Set $W_u = 0.1\frac{4.23s}{s+1.05}$ in order to reduce the control effort and to ensure robustness against the multiplicative uncertainties in the system model around the nominal operating point. Here $W_{perf} = \frac{0.1}{s+1.12}$, which represents a low pass filter. Set $W_{noise} = 0.01$ to avoid singularity problems.

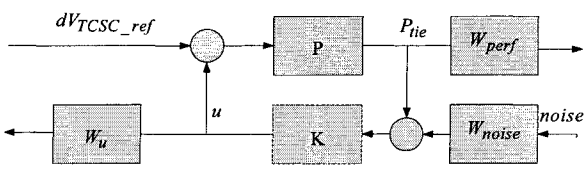

Figure 7.1 SDC design setup

7.3.2 SISO controller design and its damping performance

With P66-63 as a single feedback signal

A SISO H_∞ controller is designed at the generation level of 1500MW from Buses#93 and #110. The same reduction method as the previous chapter is used here. The obtained controller is of 11th order, and reduced to 7th order for the convenience of application in the simulation software. Its parameters are shown as follows:

Controller parameter of the SISO SDC

$$A=\begin{bmatrix} -1.9420 & 32.7785 & -31.1304 & 50.9687 & -22.6792 & -8.4617 & -0.3759 \\ 0 & -2.5769 & 7.6353 & -4.2612 & 3.8745 & 1.5769 & -0.7096 \\ 0 & -5.2096 & 1.3674 & -2.5807 & -1.6253 & -0.8185 & 1.0855 \\ 0 & 0 & 0 & 1.1658 & -6.9310 & 1.3532 & -1.5929 \\ 0 & 0 & 0 & 9.8412 & -1.3442 & -1.0414 & 0.5460 \\ 0 & 0 & 0 & 0 & 0 & -0.2069 & -1.8479 \\ 0 & 0 & 0 & 0 & 0 & 1.9382 & 0.0822 \end{bmatrix}$$

$$B=\begin{bmatrix} 8.8040 \\ -0.8363 \\ 0.2087 \\ -0.0466 \\ 0.1750 \\ 0.0884 \\ -0.0770 \end{bmatrix}$$

$$C=\begin{bmatrix} 0.9168 & -0.0213 & 3.2638 & -5.4404 & 4.5678 & 80.4092 & -64.0749 \end{bmatrix}$$

$$D=0;$$

Fig. 7.2 shows the root-locus plot associated with the single feedback signal of Ptie through Line 66-63 at the nominal operating point. There is a pair of poles in the right half plane that are the critical modes to damp. Also, there is a pair of zeros at the left side of the poles. The location of these zeros determines the movement direction of the poles associated with instability. Thus, if the feedback gain increases toward infinity, the poles will eventually moved to the zeros' position, at which a maximum 3.01% damping can be achieved. In this case, it can be predicted that there is a limitation on the achieved damping ratio for this pair of critical modes, which is set by their nearby zeros.

Small signal analysis was performed using EPRI's MASS [50] software package. A damping ratio of 3.0% is achieved at the nominal operating point in the closed loop system with the SISO controller obtained, consistent with the prediction of the possible achieved damping from its root-locus plot. Therefore, the nearby zeros do indeed set the limitation of the damping improvement in the SISO system with the single feedback signal of

P66-63.

With P67-124 as a single feedback signal

At the same time, P_{tie} through Line 67-124 is found to have large observability of the critical modeas well, so it is used as a single feedback signal in the SISO controller design. With the same weighting functions, no solution can be obtained in the H_∞ controller design. The damping improvement by the controller will cause instability at other modes. Fig. 7.3 shows the root-locus plot when P67-124 is used as the only feedback signal. There is a pair of zeros in the right half plane introduced by this remote feedback signal.

The existence of the RHP zeros sets limitations of the applicable feedback gain. The more interesting observation is that critical poles can be moved to their nearby zeros with much better damping ratio on the condition that infinite gain is provided. The larger the feedback gain, the better the damping ratio that can be achieved for the critical modes. However, the existence of the RHP zeros near j7 makes the poles move to the right half plane and then causes system instability when the feedback gain increases sufficiently. Therefore, the interaction between these modes hinders damping improvement at the critical modes.

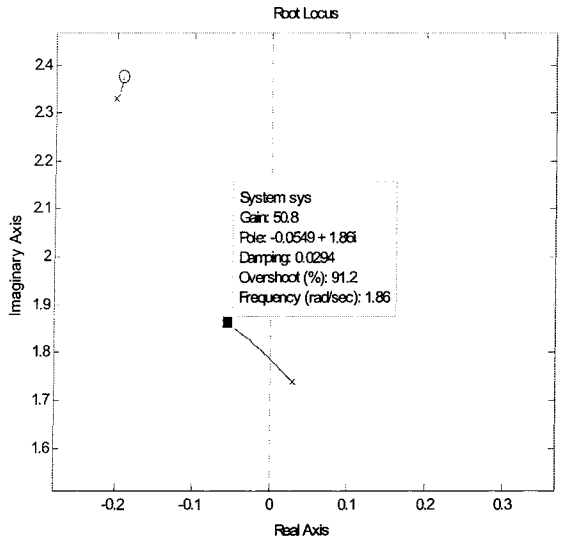

Figure 7.2 Root-locus plot for the system with P66-63 as the single output

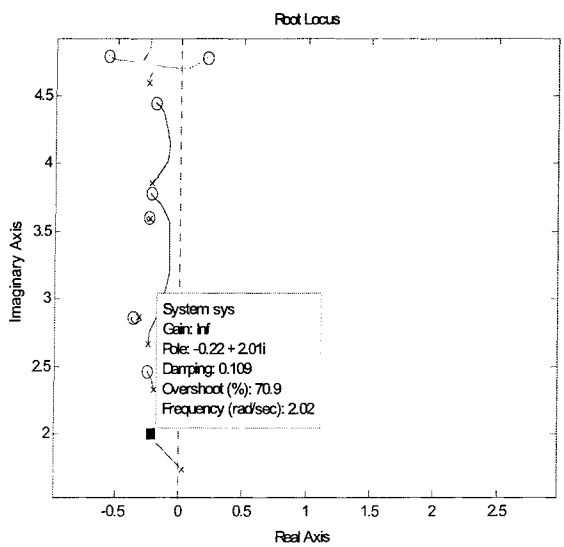

Figure 7.3 Root-locus plot for the system with P67-124 as the single output

7.4 Two-input one-output (TISO) TCSC controller design

7.4.1 Feedback signal selection

As discussed in the previous section, neither the SISO controller with a single feedback signal of P66-63 nor with a single feedback signal of P67-124 can have satisfactory damping performance in the 50-machine system. The difficulties are intrinsic in the SISO structure because of the interaction of pole-zero pairs. Based on the theoretical details in section II, if both feedback signals are used to form a SITO system and then design of a TISO controller, the limitations set on the system structure can possibly be alleviated. The pole-zero map in the SITO system is shown in Figure 7.4. With two output feedback signals in the system, there are no zeros in the SITO system, which consequently eliminate the orginal zero-pole interaction in the SISO case. With an additional parameter to manipulate, the damping performance is expected to increase. Therefore a TISO controller was designed at the generation level of 2×1500MW from Generators #93 and #110 using the same setup as in the previous section. It was also reduced to 7th order and the parameters are shown in the following.

$$A=\begin{bmatrix} -37.857 & 60.155 & 21.323 & 28.494 & 9.805 & -54.596 & -3.853 \\ 0 & 2.814 & 3.626 & 0.159 & -0.254 & -0.269 & 0.357 \\ 0 & -8.879 & -5.199 & -6.403 & 3.687 & 3.725 & 2.177 \\ 0 & 0 & 0 & -0.320 & 2.615 & 1.327 & 0.905 \\ 0 & 0 & 0 & -0.876 & -0.905 & 0.668 & -0.173 \\ 0 & 0 & 0 & 0 & 0 & -0.407 & 6.980 \\ 0 & 0 & 0 & 0 & 0 & -7.672 & 0.025 \end{bmatrix}$$

$$B = \begin{bmatrix} 3.117 & -8.533 \\ 0.317 & 1.044 \\ -1.927 & -1.739 \\ -0.777 & -0.166 \\ 0.591 & -0.029 \\ 0.223 & -0.137 \\ 0.031 & 0.204 \end{bmatrix}$$

$$C = \begin{bmatrix} -3.051 & 4.748 & 1.006 & 1.441 & -1.687 & -4.433 & -0.429 \end{bmatrix}$$

$$D = 0;$$

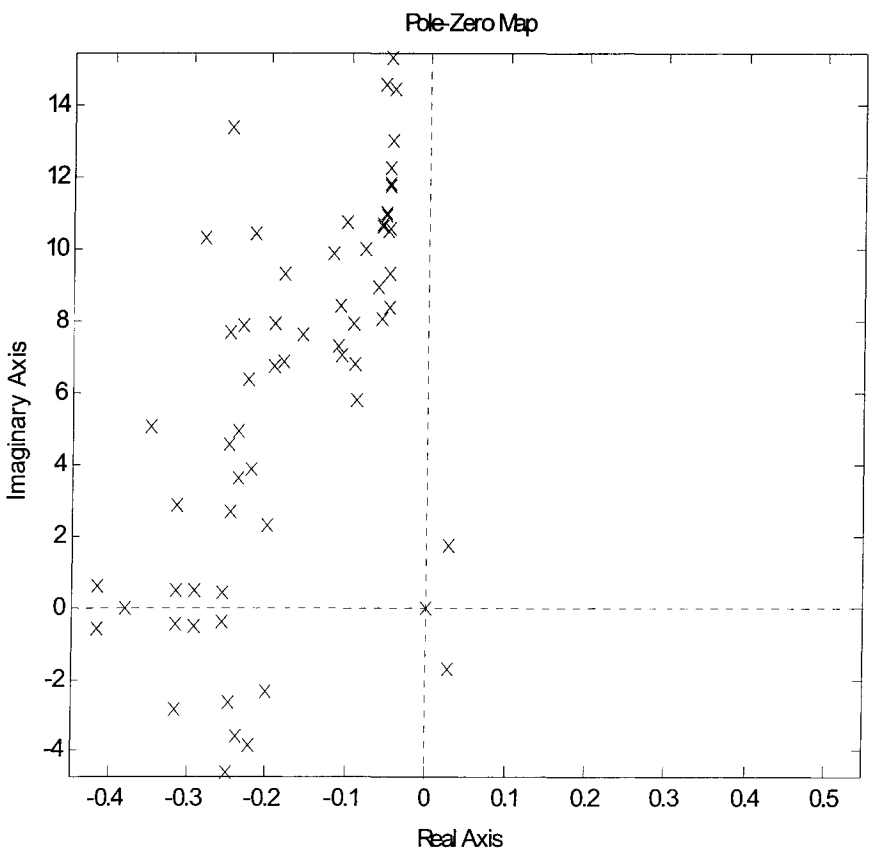

Figure 7.4 Pole-zero map in the SITO system

7.5 Theoretical explanations of the performance improvement by the TISO controller

7.5.1 Theoretical explanations with coprime factorization

Mixed sensitivity setup in the damping problem

The primary function of damping controllers is to minimize the impact of disturbances on the system that are triggered by sudden variations in the system due to faults etc.. Usually it can be formulated in the disturbance rejection problem setup in Fig. 7.5, where d is the disturbance, $G(s)$ represents the plant, and $K(s)$ is the controller to be designed. With carefully selected weighting functions, the closed-loop system can have desired performance of disturbance rejection and robustness by achieving the objective of

$\left\| \begin{bmatrix} W_{perf}(s)G(s)S(s) \\ W_u T(s) \end{bmatrix} \right\|_\infty < 1$, where $S(s)$ is the sensitivity transfer function satisfying $S = \frac{1}{1+GK}$ and $T(s)$ is the complementary sensitivity transfer function satisfying $T(s) = 1 - S(s)$.

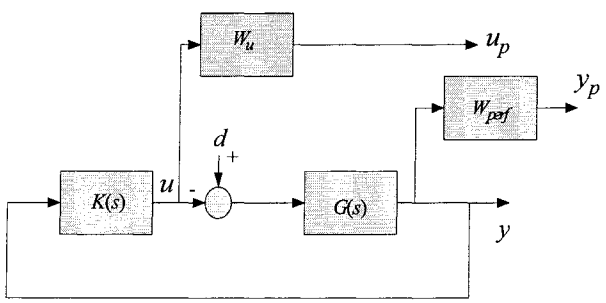

Figure 7.5 Damping control problem setup

A secondary feedback loop is added as shown in Fig.7.6, where $[G_1 \quad G_2]$ represent the SITO system, and $[K_1 \quad K_2]$ is the TISO controller to be designed. Also, z, y are

the two outputs of the system while d is the disturbance. By minimizing the H_∞ norm of the transfer function from d to z, denoted by T_{zd}, a good disturbance attenuation performance is dealt with. Furthermore, it is required that the closed-loop system be robust with respect to uncertainties such as modeling and measurement errors. Thus, the H_∞ norm of the complementary sensitivity transfer function in the output y loop can be used to quantify the stability robustness to multiplicative uncertainty in G_2. In Fig.7.6, the complementary sensitivity function is equal to the transfer function from d to u_2, denoted by $T_{u2,d}$.

Thus, to obtain both the desired beneficial disturbance attenuation and system robustness, weighting functions like W_{perf} and W_u can be used to shape the characteristics of the closed-loop plant. Therefore the mixed sensitivity (GS/T) design objective in the SITO case is represented as

$$\left\| \begin{bmatrix} W_{perf}(s)T_{z,d}(s) \\ W_u T_{u2,d}(s) \end{bmatrix} \right\|_\infty < 1$$

In a SISO system which used for comparison, only one output of the system, y, is used as the feedback signal with $K_1 = 0$. In the following section, based on the coprime factorization [59], it is shown that the tradeoff between achievable performance and stability robustness can be improved with the additional measurement z.

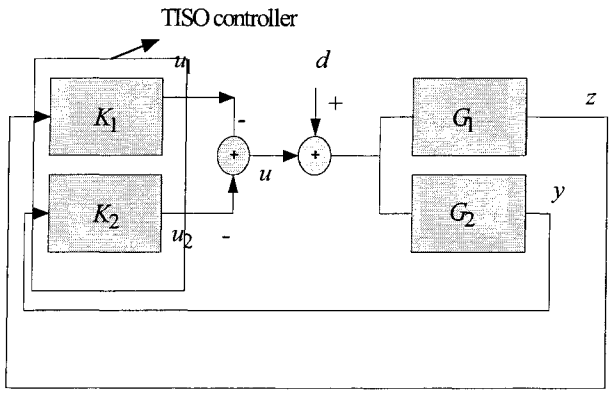

Figure 7.6 Problem setup in a SITO system

Performance and robustness tradeoff improvement in SITO system

By using coprime factorization, the following descriptions for the controller and closed loop systems are calculated; details can be seen in [59]:

$$\text{SISO: } K2 = \frac{r}{1 - rG_2} \quad r \in RH_\infty$$

$$\text{SITO: } \begin{matrix} K1 = \dfrac{q}{(1 - rG_2)(1 - qG_1)} \\ K2 = \dfrac{r}{1 - rG_2} \end{matrix} \quad r, q \in RH_\infty$$

The relationships in the SITO case are:

$$\begin{cases} z = (d + u)G1 \\ y = (d + u)G2 \\ u = -u1 - u2 = -zK1 - yK2 \end{cases}$$

The calculated transfer functions are shown in Table 7.1.

Table 7.1 COMPARISON OF TRANSFER FUNCTIONS IN SISO AND SITO CASE

Transfer function	SISO	SITO
$T_{z,d}$	$G1(1 - rG2)$	$G1(1 - rG2)(1 - qG1)$
$T_{u2,d}$	$rG2$	$rG2(1 - qG1)$

It is observed that SITO becomes SISO when $q = 0$. The strong disturbance attenuation is translated into the minimization of $\|T_{z,d}\|$. Therefore, by comparing $\|T_{z,d}\|$ in the SISO case and the SITO case, it is observed that in the SITO case the additional parameter q can be used to manipulate $\|T_{z,d}\|$. Comparing $\|T_{u2,d}\|$ in both cases, the additional parameter q helps to minimize its H_∞ norm in the SITO case.

Suppose a strong disturbance attenuation and stability robustness to multiplicative uncertainty in G2 is desired. This translates to simultaneously minimizing $\|T_{z,d}\|_\infty$ and $\|T_{u2,d}\|_\infty$. In the SISO case, the decrease of $\|G1(1 - rG2)\|_\infty$ will cause the increase of

$\|rG2\|_\infty$. In another words, there is an obvious tradeoff between performance and robustness. However, by introducing another manipulative parameter q, the tradeoff is less pronounced.

Furthermore, the introduction of q adds a second dimension to the shaping of the closed-loop system. Thus the desired shape at a specific frequency can be obtained by adjusting q when the one-dimensional SISO system faces difficulties in achieving certain goals at the specific frequency. In all, the increased dimension gives the system more flexibility in handling loop-shaping so as to achieve certain damping performance

7.5.2 Performance improvement

Fig. 7.7 shows the frequency response magnitude comparison of the $T_{z,d}$ with the SISO controller and with the TISO controller. Since the critical mode is around 0.3Hz, observe that $|T_{z,d}(j2\pi 0.3)|$ is reduced from 2.3724 to 0.828. Fig. 7.8 shows the frequency response magnitude comparison of the $T_{u2,d}$ with the SISO controller and with the TISO controller. Observe that $|T_{u2,d}(j2\pi 0.3)|$ is reduced from 2.3501 to 0.295. As mentioned in section II.B, the additional feedback signal of the TISO controller introduces an additional parameter q, which helps to minimize the H_∞ norm as well as add flexibility to shape the closed-loop system at some particular frequency. Also the additional q relaxes constraints on achievable robustness in the original SISO system with only one-dimension manageability. Also the tradeoff between the achieved damping performance and system robustness is expected to decrease in the TISO SDC case. In other words, the system with the TISO SDC should have better damping and still maintain robustness in a larger operating range than the system with the SISO controller.

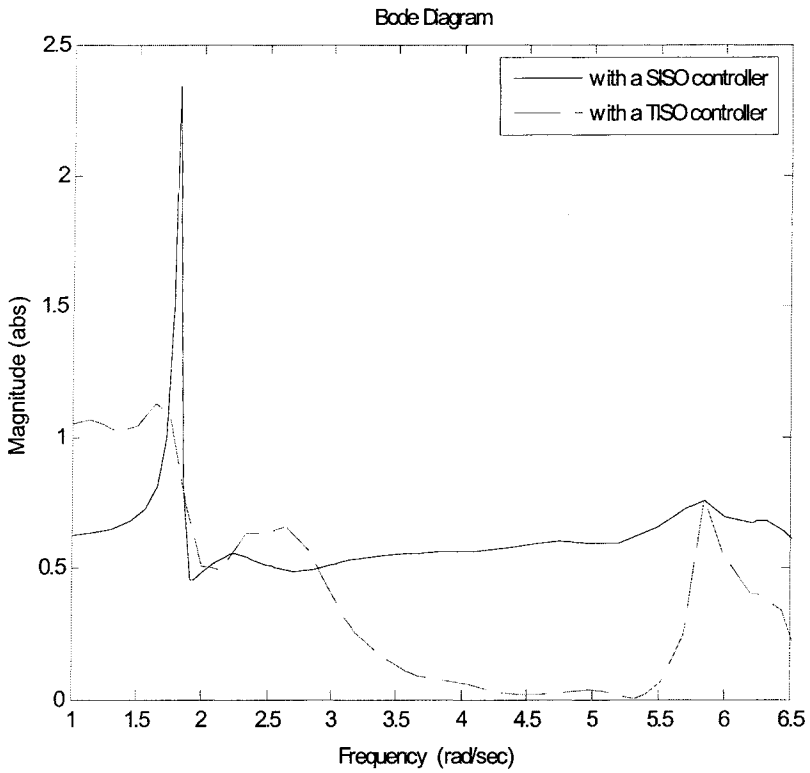

Figure 7.7 comparison of damping performance sensitivity $|T_{z,d}|$

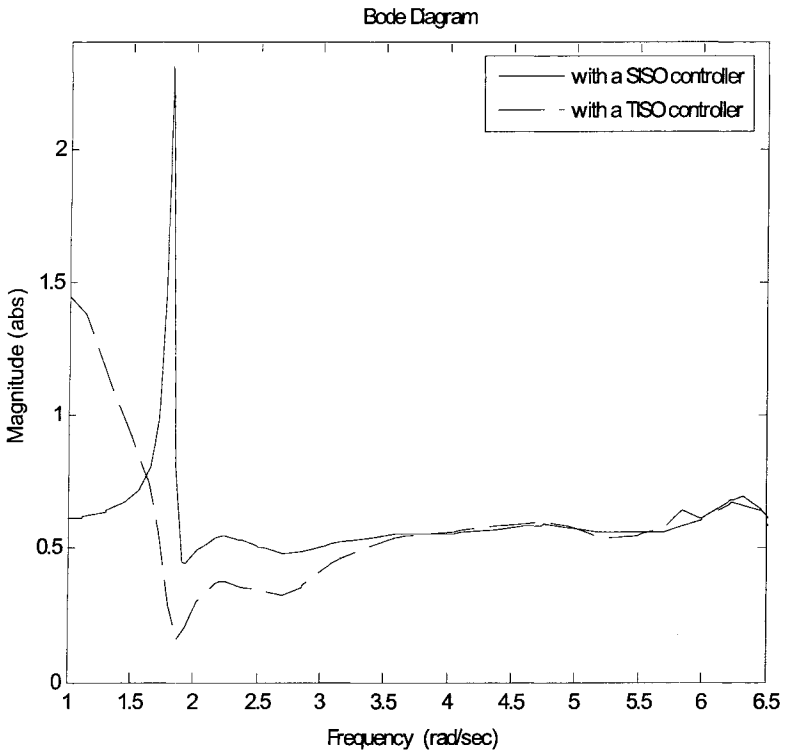

Figure 7.8 comparison of output complementary sensitivity $|T_{u2,d}|$

7.6 Simulation results

7.6.1 Small-signal analysis

Small-signal analysis was performed using EPRI's MASS [50] software package. Comparisons among the system without SDC, the system with the SISO SDC, and the system with the TISO SDC are shown in Table 7.2. As expected, the TISO SDC can achieve much better damping in the range of [2× 1200– 2× 1700] MW than the SISO SDC because of the additional feedback signal. The system with the SISO SDC will become unstable when the power generation level exceeds 1600 MW while the system with the TISO controller will still remain sufficiently damped even when the generation level reaches 1700MW. More interestingly, it is observed that the damping at the critical mode

increases with the increase of system stress if the TISO SDC is applied. Conversely, neither the open-loop system nor the system with the SISO SDC will have an increasing damping ratio at the critical modes. Obviously the TISO SDC can extend the system's operating range to a much higher level while sustaining a sufficient damping ratio.

Table 7.2 COMPARISON OF DAMPING RATIO

Power (MW)	Open loop	SISO SDC	TISO SDC
1200	4.74%	7.52%	9.38%
1300	3.17%	6.53%	9.36%
1400	1.09%	5.10%	9.50%
1500	-1.62%	3.0%	10.01%
1600	-5.10%	0.04%	11.36%
1700	-9.71%	-4.38%	11.57%

Nonlinear time domain simulation was performed using ETMSP [50]. The AVR reference of Generator 93 drops 0.1pu for one cycle. The real power from generator 139 is monitored to show the effect of the damping controller due to its large participation in the critical mode. The simulation results are shown in Fig. 7.9, 7.10. Comparisons are made among cases with the SISO SDC and with the TISO SDC at two different operating points.

The results are consistent with the results from the small-signal analysis by MASS. At the power generation of 2×1300 MW from generator 93,110, the damping ratio achieved by the TISO SDC is less than 3% larger than that by the SLPV SDC and hence in Fig. 7.9 the curve with the TISO controller shows slightly better damping improvement than that produced by the SISO SDC. However, if the power production from Generators 93,110 is larger than 2×1400MW, there are apparent advantages from the TISO SDC in

terms of improved damping compared to the SISO SDC. Fig. 7.10 shows that the damping improvement introduced by TISO SDC at the generation level of 1600MW is much better than that by the SISO SDC. Therefore the simple additional feedback signal does help increase the system damping while maintaining the system stability in a larger operational range.

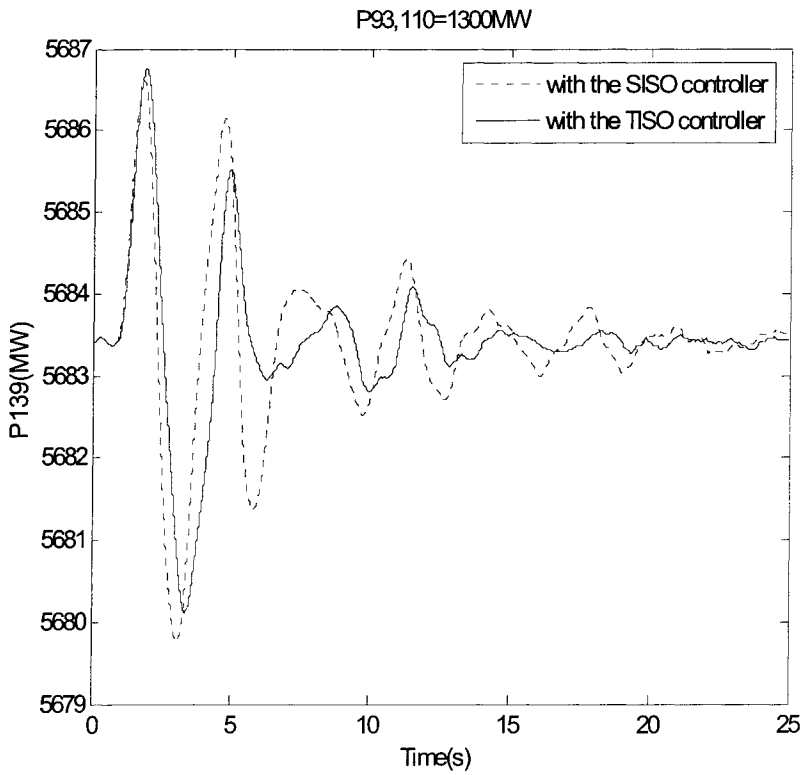

Figure 7.9 Active power of the Generator 139: AVR reference drop 0.1 for 1 cycle at Bus 93 (at 1300MW)

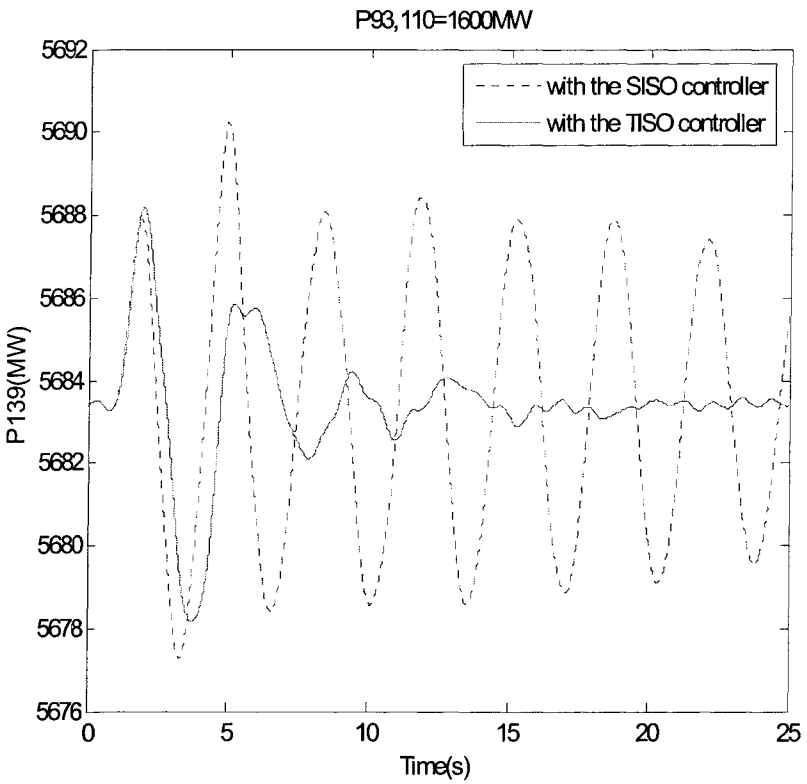

Figure 7.10 Active power of the Generator 139: AVR reference drop 0.1 for 1 cycle at Bus 93 (at 1600MW)

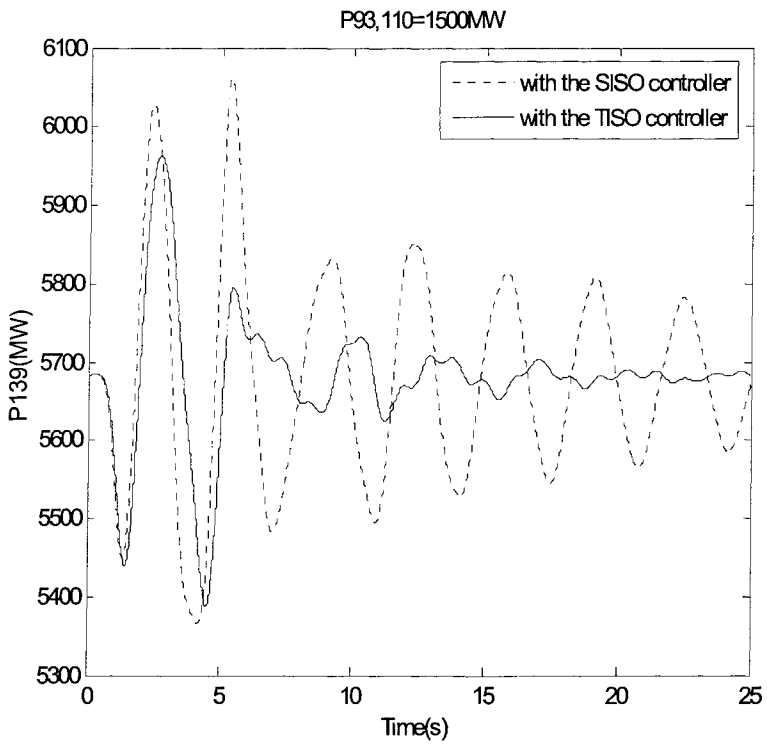

Figure 7.11 Active power of the Generator 139: 2cycles 3-phase fault at Bus 33 and clear the fault by opening the line33-50 at 1500MW

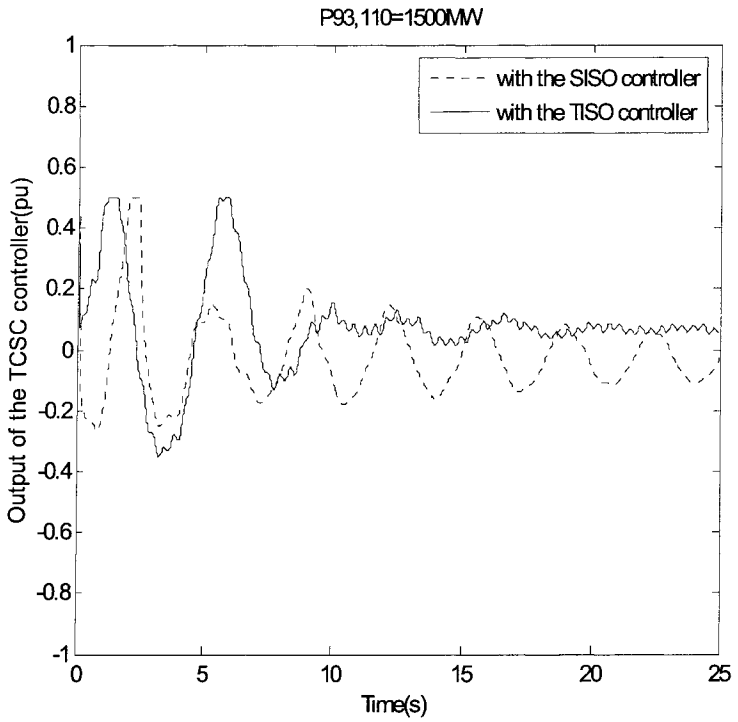

Figure 7.12 Output of the controller: 2cycles 3-phase fault at Bus 33 and clear the fault by opening the line33-50 at 1500MW

A three-phase fault at Bus 33 for 2 cycles was applied and the fault was then cleared by opening Line 33-50 at the generation level of 2×1600MW. The real power from generator 139 was monitored to show the effect of the damping controller in Fig. 7.11. It is apparent that the TISO SDC is more effective and robust with regard to damping improvement than the SISO SDC. The outputs of controllers are also shown in Fig. 7.12.

The control effort from the TISO SDC is slightly larger than that from the SISO SDC. This seems reasonable since the TISO output is the sum of the two SISO outputs. Also, the TISO SDC has the better overall performance considering its better damping performance and its moderate control performance.

7.7 Summary

There are limitations in achieving desired damping performance in some systems using a single-input single-output feedback controller. Besides, tradeoffs between the achievable damping performance and the system robustness exist in a SISO system as explained in Section II. Without the effort of designing a second controller and developing complex coordination between these two controllers, the system can achieve better damping simply by introducing a secondary feedback signal still with the simple H_∞ technique. With the additional parameter, the TISO controller has more flexibility in shaping the closed-loop system at the critical mode as well as reducing the tradeoffs. Then a TISO supplementary damping controller for a TCSC is designed in the IEEE 50-machine system. From the simulation results, it is found that not only the damping performance can be increased, but also the closed loop system can provide desired damping in a larger operating range. Furthermore, with the increase of the generation level at generator 93 and 110, the TISO controller has an increasing damping effect at the critical mode while the damping effect from the SISO SDC is becoming weaker. The TISO controller, therefore, can extend the system operation range to a larger level while maintaining adequate damping in the system under varying operating conditions. Furthermore, its simple structure and fixed parameters due to the simple design method facilitate its applications in the real field. Due to the remote second feedback signal, it does need some advanced telecommunication tools. In general, the TISO controller design is promising in damping control because of its flexibility and easy manageability with regard to the damping performance improvement and system robustness especially when a SISO controller design cannot manage to overcome limitations set by the system structure.

8 CONCLUSION AND FUTURE WORK

8.1 Conclusions

In this dissertation, three different control techniques have been developed and adapted for improved application to a 4-machine test system and an IEEE 50-machine system. Based on each different system, a different control design technique which considers the complexity of the modal interaction in the system, the computational effort taken in the controller calculation and the desired damping performance was carefully chosen. The effectiveness of TCSC controllers and SVC controllers in improving the damping ratio is investigated in Chapter 4. It is found that the preferred TCSC controller location is in a tie line that tightly connects two oscillating areas. Thus, in Chapter 5, a LMI-based robust pole-placement TCSC controller was found to be best for the small and tightly-connected 4-machine system with regard to damping control. However, the obscure appearance of tie lines in the IEEE 50-machine system makes a TCSC controller not a favorable first choice. Thus, in Chapter 6, the choice was made to design an SVC controller using an advanced interpolated LPV technique for the IEEE 50-machine system. In Chapter 7, the TCSC controller is tested on the 50-machine system and its limitation in achieving certain damping improvement is investigated. Then in Chapter 7 it was shown that improved system damping can be achieved simply by adding an additional feedback signal. The main goal in this dissertation was to find the best control design method for different systems in order to obtain a cost-effective controller. A summary of some significant contributions is as follows:

1. Investigation of the changing effectiveness of damping improvement from different types of FACTS controllers with change of system operating conditions. The in-depth

investigation is based on detailed derivation of equations and hence it provides guidelines for selecting an appropriate FACTS device according to a specific system profile.

2. Location selection for damping controller of FACTS devices is addressed in detail using analysis of mode shape and controllability calculation.
3. Proposal of an LMI-based robust pole placement method to directly impose the minimum damping ratio requirement, to produce a simple and robust controller under system changes with respect to the achieved minimal damping ratio.
4. Exploration of difficulties in applying an LMI-based robust pole placement method to controller design in an IEEE 50-machine. The large uncertainty in such a large system challenges the traditional uncertainty representation, and the LPV technique is more suitable when the large uncertainty cannot be easily represented around a nominal case.
5. Investigation of limitations in application of the traditional LPV technique to large systems, where local performance is sacrificed in order to obtain a feasible solution over the entire system space with a single Lyapunov function. An advanced interpolated LPV controller design using multiple Lyapunov functions in different subregions is proposed to facilitate the feasibility of LPV solutions over a much larger scheduling-parameter space. With certain conditions satisfied the interpolated MLPV controller can guarantee the continuity of the overall Lyapunov function as well as global system stability in the whole parameter space. Furthermore, it can improve the local damping performance in each subregion because of the divided smaller region.
6. Investigation of the limitations of achieving certain damping performance in some systems using a single-input single-output feedback controller as well as its tradeoffs between the achievable damping performance and system robustness. The addition of a secondary measurement instead of a second controller is proposed to relax the limitations and develop complex coordination between these two controllers. The

simulation results show that the system with the obtained controller can achieve better damping simply by introducing a secondary feedback signal still with the simple H_∞ technique.

7. Comparison of advantages and disadvantages of different controller design methods. Different methods were applied to different systems based on the mode shape, system structure and required computational level.

8.2 Future work

In future work, the following issues should be addressed:

1. In this dissertation, all the discussed LPV controllers have the same performance requirement for all operating points. This is not necessary for all cases. LPV synthesis offers an ability to emphasize different performance objectives depending on different operating conditions. By adjusting weighting functions according to different operating conditions, more flexibility can be achieved. This could be used to further reduce conservatism.
2. For a large system, the LMI-based robust pole placement has constraints in application due to the existence of too many uncontrollable poles, and the LPV is thus useful in this case. However, the LPV solution does not guarantee no occurrence of RHP zeros in the controller obtained. Although the existence of these RH zeros does not impact the function of the damping controller in the IEEE 50-machine system, future study is worthy to conduct to investigate the impacts of RHP zeros in other systems and to attempt to set constraints in the design phase.
3. In the advanced LPV technique, a one-dimensional parameter is used to parameterize the system operating range. It is worthwhile to investigate situations where the uncertainty should be represented by higher-dimensional parameters, as usually happens in real systems. With the increase of dimension, the computational effort

will be increased, and then new techniques should be applied in solving LPV problems.

4. Controller coordination between PSSs and FACTS devices will be researched in future work.

8.3 Contribution

For modern power systems, lack of damping can cause system instability and potential loss to the economy and society. By comparing advantages and disadvantages in damping controller design methods, different control strategies have been chosen to be applied in different systems in this dissertation. The most significant contributions may be summarized as follows:

1. A systematic and comprehensive comparison: Different approaches in damping controller design in the literature have been investigated and compared; different FACTS devices have been analyzed with regard to their effectiveness in damping improvement at varying operating points.
2. Robust regional pole-placement approach: this approach makes it possible to directly impose the damping constraints in controller design phase. The consequent benefits are: 1) achieve a simple structure in the damping controller obtained 2) avoid time-consuming selection of weighting functions, which only has a vague relationship with the achieved damping objective.
3. LPV method has been widely used in different applications. However, this is the first time it has been improved to increase feasible solution range by using multiple Lyapunov functions in power systems. This may be of great interest to the power industry after increasing stress in power grids due to some economical issues in the United States and Canada because the proposed method provides a sufficient damping in a wider operating range in power systems.

4. A study has been conducted to investigate the benefit of additional feedback signal in damping controller design. It has been shown that with a secondary feedback signal, a TISO controller has more flexibility in shaping the closed-loop system at the critical mode as well as reducing the tradeoffs, which set limitations in damping performance in a SISO case. In addition, with the secondary feedback signal, satisfactory results can be achieved by a traditional controller design method.

In all, three major approaches proposed in this dissertation have different emphasises in damping control improvement. They are customizd for different needs under particular system structure.

APPENDIX

Details of system linearization

The linearization of (3.45) and (3.46) is derived as follows

$$\dot{X} = f(X, Y, u)$$

$$0 = g(X, Y)$$

to form the state space representation of the system, as shown in (3.49)
for function f_{1i} from (3.38)

$$f_{1i} = \dot{E}'_{qi}$$

$$= \frac{1}{\tau'_{d0i}}[E_{FDi} - E'_{qi} + (x_{di} - x'_{di})I_{di}] \qquad i = 1,\ldots,m \qquad \text{(A-1)}$$

The partial derivatives of f_{1i} with respect to state variables and non-state variables are:

$$\frac{\partial f_{1i}}{\partial E'_{qj}} = \frac{1}{\tau'_{d0i}}[(x_{di} - x'_{di})\frac{\partial I_{di}}{\partial E'_{qj}} - \frac{\partial E'_{qi}}{\partial E'_{qj}}] \qquad \text{(A-2)}$$

$$\frac{\partial f_{1i}}{\partial E'_{dj}} = \frac{1}{\tau'_{d0i}}(x_{di} - x'_{di})\frac{\partial I_{di}}{\partial E'_{dj}} \qquad \text{(A-3)}$$

$$\frac{\partial f_{1i}}{\partial \delta_{k1}} = \frac{1}{\tau'_{d0i}}(x_{di} - x'_{di})\frac{\partial I_{di}}{\partial \delta_{k1}} \qquad \text{(A-4)}$$

$$\frac{\partial f_{1i}}{\partial E_{FDi}} = \frac{1}{\tau'_{d0i}} \qquad \text{(A-5)}$$

$$\frac{\partial f_{1i}}{\partial V_{n+1}} = \frac{1}{\tau'_{d0i}}(x_{di} - x'_{di})\frac{\partial I_{di}}{\partial V_{n+1}} \qquad \text{(A-6)}$$

$$\frac{\partial f_{1i}}{\partial \theta_{n+1}} = \frac{1}{\tau'_{d0i}}(x_{di} - x'_{di})\frac{\partial I_{di}}{\partial \theta_{n+1}} \qquad \text{(A-7)}$$

$$\frac{\partial f_{1i}}{\partial V_{n+2}} = \frac{1}{\tau'_{d0i}}(x_{di} - x'_{di})\frac{\partial I_{di}}{\partial V_{n+2}} \qquad \text{(A-8)}$$

$$\frac{\partial f_{1i}}{\partial \theta_{n+2}} = \frac{1}{\tau'_{d0i}}(x_{di} - x'_{di})\frac{\partial I_{di}}{\partial \theta_{n+2}} \tag{A-9}$$

$$i, j = 1,..., m \qquad k = 2,..., n$$

where

$$\frac{\partial E'_{qi}}{\partial E'_{qj}} = \begin{cases} 1 & for i = j \\ 0 & otherwise \end{cases} \tag{A-10}$$

for function f_{2i} from

$$\begin{aligned} f_{2i} &= \dot{E}'_{di} \\ &= \frac{1}{\tau'_{q0i}}[-E'_{di} - (x_{qi} - x'_{qi})I_{qi}] \end{aligned} \qquad i = 1,..., m \tag{A-11}$$

The partial derivatives are:

$$\frac{\partial f_{2i}}{\partial E'_{qj}} = \frac{-1}{\tau'_{q0i}}(x_{qi} - x'_{qi})\frac{\partial I_{qi}}{\partial E'_{qj}} \tag{A-12}$$

$$\frac{\partial f_{2i}}{\partial E'_{dj}} = \frac{-1}{\tau'_{q0i}}(x_{qi} - x'_{qi})\frac{\partial I_{qi}}{\partial E'_{dj}} + \frac{\partial E'_{di}}{\partial E'_{dj}} \tag{A-13}$$

$$\frac{\partial f_{2i}}{\partial \delta_{k1}} = \frac{-1}{\tau'_{q0i}}(x_{qi} - x'_{qi})\frac{\partial I_{qi}}{\partial \delta_{k1}} \tag{A-14}$$

$$\frac{\partial f_{2i}}{\partial V_{n+1}} = \frac{-1}{\tau'_{q0i}}(x_{qi} - x'_{qi})\frac{\partial I_{qi}}{\partial V_{n+1}} \tag{A-15}$$

$$\frac{\partial f_{2i}}{\partial \theta_{n+1}} = \frac{-1}{\tau'_{q0i}}(x_{qi} - x'_{qi})\frac{\partial I_{qi}}{\partial \theta_{n+1}} \tag{A-16}$$

$$\frac{\partial f_{2i}}{\partial V_{n+2}} = \frac{-1}{\tau'_{q0i}}(x_{qi} - x'_{qi})\frac{\partial I_{qi}}{\partial V_{n+2}} \tag{A-17}$$

$$\frac{\partial f_{2i}}{\partial \theta_{n+2}} = \frac{-1}{\tau'_{q0i}}(x_{qi} - x'_{qi})\frac{\partial I_{qi}}{\partial \theta_{n+2}} \tag{A-18}$$

$$i, j = 1,..., m \qquad k = 2,..., n$$

where

$$\frac{\partial E'_{di}}{\partial E'_{dj}} = \begin{cases} 1 & for i = j \\ 0 & otherwise \end{cases} \tag{A-19}$$

for function f_{3i} from

$$f_{3i} = \dot{\omega}_i$$
$$= \frac{1}{M_i}[P_{mi} - (I_{di}E'_{di} + I_{qi}E'_{qi}) + (x'_{qi} - x'_{di})I_{qi}I_{di} - D_i(\omega_i - \omega_S)] \tag{A-20}$$

The partial derivatives are:

$$\frac{\partial f_{3i}}{\partial E'_{qj}} = -\frac{1}{M_i}(\frac{\partial I_{di}}{\partial E'_{qj}}E'_{di} + \frac{\partial I_{qi}}{\partial E'_{qj}}E'_{qi} + \frac{\partial E'_{qi}}{\partial E'_{qj}}I_{qi})$$
$$+ \frac{1}{M_i}(\frac{\partial I_{di}}{\partial E'_{qj}}I_{qi} + \frac{\partial I_{qi}}{\partial E'_{qj}}I_{di})(x'_{qi} - x'_{di}) \tag{A-21}$$

$$\frac{\partial f_{3i}}{\partial E'_{dj}} = -\frac{1}{M_i}(\frac{\partial I_{di}}{\partial E'_{dj}}E'_{di} + \frac{\partial I_{qi}}{\partial E'_{dj}}E'_{qi} + \frac{\partial E'_{qi}}{\partial E'_{dj}}I_{qi})$$
$$+ \frac{1}{M_i}(\frac{\partial I_{di}}{\partial E'_{dj}}I_{qi} + \frac{\partial I_{qi}}{\partial E'_{dj}}I_{di})(x'_{qi} - x'_{di}) \tag{A-22}$$

$$\frac{\partial f_{3i}}{\omega_i} = -\frac{D_i}{M_i} \tag{A-23}$$

$$\frac{\partial f_{3i}}{\partial V_{n+1}} = -\frac{1}{M_i}(\frac{\partial I_{di}}{\partial V_{n+1}}E'_{di} + \frac{\partial I_{qi}}{\partial V_{n+1}}E'_{qi})$$
$$+ \frac{1}{M_i}(\frac{\partial I_{di}}{\partial V_{n+1}}I_{qi} + \frac{\partial I_{qi}}{\partial V_{n+1}}I_{di})(x'_{qi} - x'_{di}) \tag{A-24}$$

$$\frac{\partial f_{3i}}{\partial \theta_{n+1}} = -\frac{1}{M_i}(\frac{\partial I_{di}}{\partial \theta_{n+1}}E'_{di} + \frac{\partial I_{qi}}{\partial \theta_{n+1}}E'_{qi})$$
$$+ \frac{1}{M_i}(\frac{\partial I_{di}}{\partial \theta_{n+1}}I_{qi} + \frac{\partial I_{qi}}{\partial \theta_{n+1}}I_{di})(x'_{qi} - x'_{di}) \tag{A-25}$$

$$\frac{\partial f_{3i}}{\partial V_{n+2}} = -\frac{1}{M_i}(\frac{\partial I_{di}}{\partial V_{n+2}}E'_{di} + \frac{\partial I_{qi}}{\partial V_{n+2}}E'_{qi})$$
$$+ \frac{1}{M_i}(\frac{\partial I_{di}}{\partial V_{n+2}}I_{qi} + \frac{\partial I_{qi}}{\partial V_{n+2}}I_{di})(x'_{qi} - x'_{di}) \tag{A-26}$$

$$\frac{\partial f_{3i}}{\partial \theta_{n+2}} = -\frac{1}{M_i}\left(\frac{\partial I_{di}}{\partial \theta_{n+2}} E'_{di} + \frac{\partial I_{qi}}{\partial \theta_{n+2}} E'_{qi}\right) + \frac{1}{M_i}\left(\frac{\partial I_{di}}{\partial \theta_{n+2}} I_{qi} + \frac{\partial I_{qi}}{\partial \theta_{n+2}} I_{di}\right)(x'_{qi} - x'_{di}) \tag{A-27}$$

$$i, j = 1,\ldots, m \qquad k = 2,\ldots, n$$

For function f_{4i} from

$$f_{4i} = \dot{\delta}_{i1} = \omega_i - \omega_1 \qquad i = 2,\ldots, n \tag{A-28}$$

The partial derivatives are:

$$\frac{\partial f_{4i}}{\partial \omega_j} = \begin{cases} -1 & for \quad j = 1 \\ 1 & for \quad j = i, j \neq 1 \\ 0 & otherwise \end{cases} \tag{A-29}$$

$$i = 2,\ldots, n \quad j = 1,\ldots, n$$

For function f_{5i} from

$$f_{5i} = \dot{E}_{FDi} = \frac{K_{Ai}}{T_{Ai}} X_{E2i} - \frac{1}{T_{Ai}} E_{FDi} + \frac{aK_{Ai}}{T_{Ai}}(V_{REFi} - X_{E1i}) \qquad i = 1,\ldots, m \tag{A-30}$$

The partial derivatives are:

$$\frac{\partial f_{5i}}{\partial E_{FDi}} = -\frac{1}{T_{Ai}} \tag{A-31}$$

$$\frac{\partial f_{5i}}{\partial X_{E1i}} = -\frac{aK_{Ai}}{T_{Ai}} \tag{A-32}$$

$$\frac{\partial f_{5i}}{\partial X_{E2i}} = \frac{K_{Ai}}{T_{Ai}} \tag{A-33}$$

for function f_{6i} from

$$f_{6i} = \dot{X}_{E1i} = -\frac{1}{T_{Ri}} X_{E1i} + \frac{1}{T_{Ri}} V_{Ti} \qquad i = 1,\ldots, m \tag{A-34}$$

the partial derivatives are:

$$\frac{\partial f_{6i}}{\partial E'_{qj}} = \frac{1}{T_{Ri}} \frac{\partial V_{Ti}}{\partial E'_{qj}} \tag{A-35}$$

$$\frac{\partial f_{6i}}{\partial E'_{dj}} = \frac{1}{T_{Ri}} \frac{\partial V_{Ti}}{\partial E'_{dj}} \tag{A-36}$$

$$\frac{\partial f_{6i}}{\partial \delta_{k1}} = \frac{1}{T_{Ri}} \frac{\partial V_{Ti}}{\partial \delta_{k1}} \tag{A-37}$$

$$\frac{\partial f_{6i}}{\partial X_{E1i}} = -\frac{1}{T_{Ri}} \tag{A-38}$$

$$\frac{\partial f_{6i}}{\partial V_{n+1}} = -\frac{1}{T_{Ri}} \frac{\partial V_{Ti}}{\partial V_{n+1}} \tag{A-39}$$

$$\frac{\partial f_{6i}}{\partial \theta_{n+1}} = -\frac{1}{T_{Ri}} \frac{\partial V_{Ti}}{\partial \theta_{n+1}} \tag{A-40}$$

$$\frac{\partial f_{6i}}{\partial V_{n+2}} = -\frac{1}{T_{Ri}} \frac{\partial V_{Ti}}{\partial V_{n+2}} \tag{A-41}$$

$$\frac{\partial f_{6i}}{\partial \theta_{n+2}} = -\frac{1}{T_{Ri}} \frac{\partial V_{Ti}}{\partial \theta_{n+2}} \tag{A-42}$$

$$i, j = 1,..., m \qquad k = 2,..., n$$

for function f_{7i} from

$$f_{7i} = \dot{X}_{E2i}$$

$$= -\frac{1}{T_{Bi}} X_{E2i} + \frac{1-a}{T_{Bi}} (V_{REFi} - X_{E1i}) \qquad i = 1,..., m \tag{A-43}$$

The partial derivatives are:

$$\frac{\partial f_{7i}}{\partial X_{E1i}} = \frac{a-1}{T_{Bi}} \tag{A-44}$$

$$\frac{\partial f_{7i}}{\partial X_{E2i}} = -\frac{1}{T_{Bi}} \tag{A-45}$$

$$\frac{\partial f_{7i}}{\partial V_{REFi}} = \frac{1-a}{T_{Bi}} \tag{A-46}$$

$$i = 1,...,m$$

for function f_8 from

$$f_8 = \dot{X}_{FACTS} = -\frac{1}{T_{FACTS}} X_{FACTS} - \frac{1}{T_{FACTS}} V_{REF} \tag{A-47}$$

The partial derivatives are:

$$\frac{\partial f_8}{\partial X_{FACTS}} = -\frac{1}{T_{FACTS}}$$

$$\frac{\partial f_8}{\partial V_{REF}} = -\frac{1}{T_{FACTS}}$$

Some derivatives on the right sides of (A-2)-(A-42) are still unknown. From (3.27) and (3.28),

$$I_{qi} = \sum_{j=1}^{m} [F_{G+B}(\delta_{ij}) E'_{qj} - F_{B-G}(\delta_{ij}) E'_{dj}] + \sum_{k=m+1}^{n} F_{G+B}(\delta_{ik}) E_k + F_{G+B}(\delta_{i,n+1}) V_{n+1} + F_{G+B}(\delta_{i,n+2}) V_{n+2}$$

(A-48)

$$I_{di} = \sum_{j=1}^{m} [F_{B-G}(\delta_{ij}) E'_{qj} + F_{G+B}(\delta_{ij}) E'_{dj}] + \sum_{k=m+1}^{n} F_{B-G}(\delta_{ik}) E_k + F_{B-G}(\delta_{i,n+1}) V_{n+1} + F_{B-G}(\delta_{i,n+2}) V_{n+2}$$

(A-49)

$$I_k = \sum_{j=1}^{m} [F_{G+B}(\delta_{kj}) E'_{qj} - F_{B-G}(\delta_{kj}) E'_{dj}] + \sum_{l=m+1}^{n} F_{G+B}(\delta_{kl}) E_l + F_{G+B}(\delta_{k,n+1}) V_{n+1} + F_{G+B}(\delta_{k,n+2}) V_{n+2}$$

$$i = 1,2,...,m \quad k,l = m+1,...,n \tag{A-50}$$

Therefore

$$\frac{\partial I_{qi}}{\partial E'_{qj}} = F_{G+B}(\delta_{ij}) \quad i = 1,...,n \quad j = 1,...,m \tag{A-51}$$

$$\frac{\partial I_{qi}}{\partial E'_{dj}} = -F_{B-G}(\delta_{ij}) \quad i = 1,...,n \quad j = 1,...,m \tag{A-52}$$

$$\frac{\partial I_{qi}}{\partial \delta_{k1}} = \sum_{j=1}^{n} \frac{\partial \delta_{ij}}{\partial \delta_{k1}} [F_{B-G}(\delta_{ij}) E'_{qj} + F_{G+B}(\delta_{ij}) E'_{dj}] \quad \text{(A-53)}$$

$i, j = 1,\ldots, n \quad k = 2,\ldots, n$

$$\frac{\partial I_{qi}}{\partial V_{n+1}} = F_{G+B}(\delta_{i,n+1}) \quad i = 1,\ldots, n \quad \text{(A-54)}$$

$$\frac{\partial I_{qi}}{\partial \theta_{n+1}} = -F_{B-G}(\delta_{i,n+1}) V_{n+1} \quad i = 1,\ldots, n \quad \text{(A-55)}$$

$$\frac{\partial I_{qi}}{\partial V_{n+2}} = F_{G+B}(\delta_{i,n+2}) \quad i = 1,\ldots, n \quad \text{(A-56)}$$

$$\frac{\partial I_{qi}}{\partial \theta_{n+2}} = -F_{B-G}(\delta_{i,n+2}) V_{n+2} \quad i = 1,\ldots, n \quad \text{(A-57)}$$

$$\frac{\partial I_{di}}{\partial E'_{qj}} = F_{B-G}(\delta_{ij}) \quad i, j = 1,\ldots, m \quad \text{(A-58)}$$

$$\frac{\partial I_{di}}{\partial E'_{dj}} = F_{G+B}(\delta_{ij}) \quad i, j = 1,\ldots, m \quad \text{(A-59)}$$

$$\frac{\partial I_{di}}{\partial \delta_{k1}} = \sum_{j=1}^{n} \frac{\partial \delta_{ij}}{\partial \delta_{k1}} [-F_{G+B}(\delta_{ij}) E'_{qj} + F_{B-G}(\delta_{ij}) E'_{dj}] \quad \text{(A-60)}$$

$i, j = 1,\ldots, m \quad k = 2,\ldots, n$

$$\frac{\partial I_{di}}{\partial V_{n+1}} = F_{B-G}(\delta_{i,n+1}) \quad i = 1,\ldots, m \quad \text{(A-61)}$$

$$\frac{\partial I_{di}}{\partial \theta_{n+1}} = F_{G+B}(\delta_{i,n+1}) V_{n+1} \quad i = 1,\ldots, m \quad \text{(A-62)}$$

$$\frac{\partial I_{di}}{\partial V_{n+2}} = F_{B-G}(\delta_{i,n+2}) \quad i = 1,\ldots, m \quad \text{(A-63)}$$

$$\frac{\partial I_{di}}{\partial \theta_{n+2}} = F_{G+B}(\delta_{i,n+2}) V_{n+2} \quad i = 1,\ldots, m \quad \text{(A-64)}$$

where

$$\frac{\partial \delta_{ij}}{\partial \delta_{k1}} = \begin{cases} 1 & for \quad i = k, i \neq j \\ -1 & for \quad j = k, j \neq i \\ 0 & otherwise \end{cases} \tag{A-65}$$

For the exciter input voltage V_T:

$$\begin{aligned} V_T{}^2 &= V_{Tq}{}^2 + V_{Td}{}^2 \\ &= (E'_q + x'_d I_d)^2 + (E'_d - x'_q I_q)^2 \end{aligned} \tag{A-66}$$

Therefore,

$$\frac{\partial V_{Ti}}{\partial E'_{qj}} = \frac{1}{V_{Ti}}[V_{qi}(\frac{\partial E'_{qi}}{\partial E'_{qj}} + x'_{di}\frac{\partial I_{di}}{\partial E'_{qj}}) - V_{di}x'_{qi}\frac{\partial I_{qi}}{\partial E'_{qj}}] \tag{A-67}$$

$$\frac{\partial V_{Ti}}{\partial E'_{dj}} = \frac{1}{V_{Ti}}[V_{di}(\frac{\partial E'_{di}}{\partial E'_{dj}} + x'_{qi}\frac{\partial I_{qi}}{\partial E'_{dj}}) + V_{qi}x'_{qi}\frac{\partial I_{di}}{\partial E'_{dj}}] \tag{A-68}$$

$$\frac{\partial V_{Ti}}{\partial V_{n+1}} = \frac{V_{qi}}{V_{Ti}}\frac{\partial I_{di}}{\partial V_{n+1}}x'_{di} - \frac{V_{di}}{V_{Ti}}\frac{\partial I_{qi}}{\partial V_{n+1}}x'_{qi} \tag{A-69}$$

$$\frac{\partial V_{Ti}}{\partial \theta_{n+1}} = \frac{V_{qi}}{V_{Ti}}\frac{\partial I_{di}}{\partial \theta_{n+1}}x'_{di} - \frac{V_{di}}{V_{Ti}}\frac{\partial I_{qi}}{\partial \theta_{n+1}}x'_{qi} \tag{A-70}$$

$$i, j = 1, \ldots, m$$

Substituting (A-51)-(A-70) into (3.45), the linearized equation of (3.45) can be written as follows:

$$\begin{bmatrix} \Delta\dot{E}'_{qj} \\ \Delta\dot{E}'_{dj} \\ \Delta\dot{\omega}_i \\ \Delta\dot{\delta}_{k1} \\ \Delta\dot{E}_{FDi} \\ \Delta\dot{X}_{E1i} \\ \Delta\dot{X}_{E2i} \\ \Delta\dot{X}_{FACTS} \end{bmatrix} = \begin{bmatrix} \frac{\partial f_{1i}}{\partial V_{n+1}} & \frac{\partial f_{1i}}{\partial \theta_{n+1}} & \frac{\partial f_{1i}}{\partial V_{n+2}} & \frac{\partial f_{1i}}{\partial \theta_{n+2}} \\ \frac{\partial f_{2i}}{\partial V_{n+1}} & \frac{\partial f_{2i}}{\partial \theta_{n+1}} & \frac{\partial f_{2i}}{\partial V_{n+2}} & \frac{\partial f_{2i}}{\partial \theta_{n+2}} \\ \frac{\partial f_{3i}}{\partial V_{n+1}} & \frac{\partial f_{3i}}{\partial \theta_{n+1}} & \frac{\partial f_{3i}}{\partial V_{n+2}} & \frac{\partial f_{3i}}{\partial \theta_{n+2}} \\ 0 & 0 & 0 & 0 \\ 0 & 0 & 0 & 0 \\ \frac{\partial f_{6i}}{\partial V_{n+1}} & \frac{\partial f_{6i}}{\partial \theta_{n+1}} & \frac{\partial f_{6i}}{\partial V_{n+2}} & \frac{\partial f_{6i}}{\partial \theta_{n+2}} \\ 0 & 0 & 0 & 0 \\ 0 & 0 & 0 & 0 \end{bmatrix} \begin{bmatrix} V_{n+1} \\ \theta_{n+1} \\ V_{n+2} \\ \theta_{n+2} \end{bmatrix} + \begin{bmatrix} 0 \\ 0 \\ 0 \\ 0 \\ 0 \\ 0 \\ 0 \\ \frac{\partial f_8}{\partial V_{REF}} \end{bmatrix} \Delta V_{REF}$$

$$+ \begin{bmatrix} \frac{\partial f_{1i}}{\partial E'_{qj}} & \frac{\partial f_{1i}}{\partial E'_{dj}} & 0 & \frac{\partial f_{1i}}{\partial \delta_{k1}} & \frac{\partial f_{1i}}{\partial E_{FDi}} & 0 & 0 & 0 \\ \frac{\partial f_{2i}}{\partial E'_{qj}} & \frac{\partial f_{2i}}{\partial E'_{dj}} & 0 & \frac{\partial f_{2i}}{\partial \delta_{k1}} & 0 & 0 & 0 & 0 \\ \frac{\partial f_{3i}}{\partial E'_{qj}} & \frac{\partial f_{3i}}{\partial E'_{dj}} & \frac{\partial f_{3i}}{\partial \omega_i} & \frac{\partial f_{3i}}{\partial \delta_{k1}} & 0 & 0 & 0 & 0 \\ 0 & 0 & \frac{\partial f_{4i}}{\partial \omega_i} & 0 & 0 & 0 & 0 & 0 \\ 0 & 0 & 0 & 0 & \frac{\partial f_{5i}}{\partial E_{FDi}} & \frac{\partial f_{5i}}{\partial X_{E1i}} & \frac{\partial f_{5i}}{\partial X_{E2i}} & 0 \\ \frac{\partial f_{6i}}{\partial E'_{qj}} & \frac{\partial f_{6i}}{\partial E'_{dj}} & 0 & \frac{\partial f_{6i}}{\partial \delta_{k1}} & 0 & \frac{\partial f_{6i}}{\partial X_{E1i}} & 0 & 0 \\ 0 & 0 & 0 & 0 & 0 & \frac{\partial f_{7i}}{\partial X_{E1i}} & \frac{\partial f_{7i}}{\partial X_{E2i}} & 0 \\ 0 & 0 & 0 & 0 & 0 & 0 & 0 & \frac{\partial f_8}{\partial X_{FACTS}} \end{bmatrix} \begin{bmatrix} \Delta E'_{qj} \\ \Delta E'_{dj} \\ \Delta\omega_i \\ \Delta\delta_{k1} \\ \Delta E_{FDi} \\ \Delta X_{E1i} \\ \Delta X_{E2i} \\ \Delta X_{TCSC} \end{bmatrix} \tag{A-71}$$

The above equation corresponds to (3.45)

For the algebraic equations (3.27)-(3.28)

$$0 = \sum_{j=1}^{m} \left[F_{G+B}\left(\delta_{n+1,j}\right) E'_{qj} - F_{B-G}\left(\delta_{n+1,j}\right) E'_{dj} \right] + \sum_{j=m+1}^{n} \left[F_{G+B}\left(\delta_{n+1,j}\right) E_j \right] + F_{G+B}\left(\delta_{n+1,n+1}\right) V_{n+1} + F_{G+B}\left(\delta_{n+1,n+2}\right) V_{n+2} = g_1 \tag{A-72}$$

$$0 = \sum_{j=1}^{m}\left[F_{B-G}\left(\delta_{n+1,j}\right)E'_{qj} + F_{G+B}\left(\delta_{n+1,j}\right)E'_{dj}\right] + \sum_{j=m+1}^{n}\left[F_{B-G}\left(\delta_{n+1,j}\right)E_j\right] + F_{B-G}\left(\delta_{n+1,n+1}\right)V_{n+1} + F_{B-G}\left(\delta_{n+1,n+2}\right)V_{n+2} = g_2 \quad \text{(A-73)}$$

$$0 = \sum_{j=1}^{m}\left[F_{G+B}\left(\delta_{n+2,j}\right)E'_{qj} - F_{B-G}\left(\delta_{n+2,j}\right)E'_{dj}\right] + \sum_{j=m+1}^{n}\left[F_{G+B}\left(\delta_{n+2,j}\right)E_j\right] + F_{G+B}\left(\delta_{n+2,n+1}\right)V_{n+1} + F_{G+B}\left(\delta_{n+2,n+2}\right)V_{n+2} = g_3 \quad \text{(A-74)}$$

$$0 = \sum_{j=1}^{m}\left[F_{B-G}\left(\delta_{n+2,j}\right)E'_{qj} + F_{G+B}\left(\delta_{n+2,j}\right)E'_{dj}\right] + \sum_{j=m+1}^{n}\left[F_{B-G}\left(\delta_{n+2,j}\right)E_j\right] + F_{B-G}\left(\delta_{n+2,n+1}\right)V_{n+1} + F_{B-G}\left(\delta_{n+2,n+2}\right)V_{n+2} = g_4 \quad \text{(A-75)}$$

The partial derivatives of g_1, g_2, g_3, g_4 with respect to state variables (X) and non-state variables (Y) are obtained as follows:

$$\frac{\partial g_1}{\partial E'_{qi}} = F_{G+B}(\delta_{n+1,i}) \quad i = 1,\ldots,m \quad \text{(A-76)}$$

$$\frac{\partial g_1}{\partial E'_{di}} = -F_{B-G}(\delta_{n+1,i}) \quad i = 1,\ldots,m \quad \text{(A-77)}$$

$$\frac{\partial g_1}{\partial \delta_{k1}} = \sum_{i=1}^{m}\frac{\partial \delta_{n+1,i}}{\partial \delta_{k1}}[F_{B-G}(\delta_{n+1,i})E'_{qi} + F_{G+B}(\delta_{n+1,i})E'_{di}] + \sum_{i=m+1}^{n}\frac{\partial \delta_{n+1,i}}{\partial \delta_{k1}}[F_{B-G}(\delta_{n+1,i})E_i]$$

$$k = 2,\ldots,n \quad \text{(A-78)}$$

$$\frac{\partial g_1}{\partial V_{n+1}} = G_{n+1,n+1} \quad \text{(A-79)}$$

$$\frac{\partial g_1}{\partial \theta_{n+1}} = \sum_{i=1}^{m}[F_{B-G}(\delta_{n+1,i})E'_{qi} + F_{G+B}(\delta_{n+1,i})E'_{di}] + \sum_{i=m+1}^{n}[F_{B-G}(\delta_{n+1,i})E_i] + F_{B-G}(\delta_{n+1,n+2})V_{n+2}$$

(A-80)

$$\frac{\partial g_1}{\partial V_{n+2}} = F_{G+B}(\delta_{n+1,n+2}) \quad \text{(A-81)}$$

$$\frac{\partial g_1}{\partial \theta_{n+2}} = F_{B-G}(\delta_{n+1,n+2})V_{n+2} \quad \text{(A-82)}$$

$$\frac{\partial g_1}{\partial X_{FACTS}} = \frac{\partial F_{G+B}\left(\delta_{n+1,n+1}\right)}{\partial X_{FACTS}} V_{n+1} + \frac{\partial F_{G+B}\left(\delta_{n+1,n+2}\right)}{\partial X_{FACTS}} V_{n+2} \tag{A-83}$$

where

$$\frac{\partial \delta_{n+1,i}}{\partial \delta_{k1}} = \begin{cases} -1 & i = k, k = 2,\ldots,n \\ 0 & otherwise \end{cases}$$

(A-84)

And

$$\frac{\partial g_2}{\partial E'_{qi}} = F_{B-G}(\delta_{n+1,i}) \quad i = 1,\ldots,m \tag{A-85}$$

$$\frac{\partial g_2}{\partial E'_{di}} = F_{G+B}(\delta_{n+1,i}) \quad i = 1,\ldots,m \tag{A-86}$$

$$\frac{\partial g_2}{\partial \delta_{k1}} = \sum_{i=1}^{m} \frac{\partial \delta_{n+1,i}}{\partial \delta_{k1}} [F_{B-G}(\delta_{n+1,i}) E'_{di} - F_{G+B}(\delta_{n+1,i}) E'_{qi}] - \sum_{i=m+1}^{n} \frac{\partial \delta_{n+1,i}}{\partial \delta_{k1}} [F_{G+B}(\delta_{n+1,i}) E_i]$$

(A-87)

$$k = 2,\ldots,n$$

$$\frac{\partial g_2}{\partial V_{n+1}} = B_{n+1,n+1} \tag{A-88}$$

$$\frac{\partial g_2}{\partial \theta_{n+1}} = \sum_{i=1}^{m} [F_{B-G}(\delta_{n+1,i}) E'_{di} - F_{G+B}(\delta_{n+1,i}) E'_{qi}] - \sum_{i=m+1}^{n} [F_{B-G}(\delta_{n+1,i}) E_i] - F_{B-G}(\delta_{n+1,n+2}) V_{n+2}$$

(A-89)

$$\frac{\partial g_2}{\partial V_{n+2}} = F_{B-G}(\delta_{n+1,n+2})$$

(A-90)

$$\frac{\partial g_2}{\partial \theta_{n+2}} = -F_{G+B}(\delta_{n+1,n+2}) V_{n+2}$$

(A-91)

$$\frac{\partial g_2}{\partial X_{FACTS}} = \frac{\partial F_{B-G}\left(\delta_{n+1,n+1}\right)}{\partial X_{FACTS}} V_{n+1} + \frac{\partial F_{B-G}\left(\delta_{n+1,n+2}\right)}{\partial X_{FACTS}} V_{n+2}$$

(A-92)

where

$$\frac{\partial \delta_{n+1,i}}{\partial \delta_{k1}} = \begin{cases} -1 & i = k, k = 2,..., n \\ 0 & otherwise \end{cases}$$

(A-93)

and

$$\frac{\partial g_3}{\partial E'_{qi}} = F_{G+B}(\delta_{n+2,i}) \qquad i = 1,..., m$$

(A-94)

$$\frac{\partial g_3}{\partial E'_{di}} = -F_{B-G}(\delta_{n+2,i}) \qquad i = 1,..., m$$

(A-95)

$$\frac{\partial g_3}{\partial \delta_{k1}} = \sum_{i=1}^{m} \frac{\partial \delta_{n+2,i}}{\partial \delta_{k1}} [F_{B-G}(\delta_{n+2,i}) E'_{qi} + F_{G+B}(\delta_{n+2,i}) E'_{di}] + \sum_{i=m+1}^{n} \frac{\partial \delta_{n+2,i}}{\partial \delta_{k1}} [F_{B-G}(\delta_{n+2,i}) E_i]$$

(A-96)

$$k = 2,..., n$$

$$\frac{\partial g_3}{\partial V_{n+2}} = G_{n+2,n+2} \qquad \text{(A-97)}$$

$$\frac{\partial g_3}{\partial \theta_{n+2}} = \sum_{i=1}^{m} [F_{B-G}(\delta_{n+2,i}) E'_{qi} + F_{G+B}(\delta_{n+2,i}) E'_{di}] + \sum_{i=m+1}^{n} [F_{B-G}(\delta_{n+2,i}) E_i] + F_{B-G}(\delta_{n+2,n+1}) V_{n+1}$$

(A-98)

$$\frac{\partial g_3}{\partial V_{n+1}} = F_{G+B}(\delta_{n+2,n+1}) \qquad \text{(A-99)}$$

$$\frac{\partial g_3}{\partial \theta_{n+1}} = F_{B-G}(\delta_{n+2,n+1}) V_{n+1}$$

(A-100)

$$\frac{\partial g_3}{\partial X_{FACTS}} = \frac{\partial F_{G+B}(\delta_{n+2,n+2})}{\partial X_{FACTS}} V_{n+2} + \frac{\partial F_{G+B}(\delta_{n+2,n+1})}{\partial X_{FACTS}} V_{n+1}$$

(A-101)

where

$$\frac{\partial \delta_{n+2,i}}{\partial \delta_{k1}} = \begin{cases} -1 & i = k, k = 2,...,n \\ 0 & otherwise \end{cases}$$

(A-102)

And

$$\frac{\partial g_4}{\partial E'_{qi}} = F_{B-G}(\delta_{n+2,i}) \qquad i = 1,...,m$$

(A-103)

$$\frac{\partial g_4}{\partial E'_{di}} = F_{G+B}(\delta_{n+2,i}) \qquad i = 1,...,m$$

(A-104)

$$\frac{\partial g_4}{\partial \delta_{k1}} = \sum_{i=1}^{m} \frac{\partial \delta_{n+2,i}}{\partial \delta_{k1}} [F_{B-G}(\delta_{n+2,i}) E'_{di} - F_{G+B}(\delta_{n+2,i}) E'_{qi}] - \sum_{i=m+1}^{n} \frac{\partial \delta_{n+2,i}}{\partial \delta_{k1}} [F_{G+B}(\delta_{n+2,i}) E_i]$$

(A-105)

$$k = 2,...,n$$

$$\frac{\partial g_4}{\partial V_{n+2}} = B_{n+2,n+2} \qquad \text{(A-106)}$$

$$\frac{\partial g_4}{\partial \theta_{n+2}} = \sum_{i=1}^{m} [F_{B-G}(\delta_{n+2,i}) E'_{di} - F_{G+B}(\delta_{n+2,i}) E'_{qi}] - \sum_{i=m+1}^{n} [F_{B-G}(\delta_{n+2,i}) E_i] - F_{B-G}(\delta_{n+2,n+1}) V_{n+1}$$

(A-107)

$$\frac{\partial g_4}{\partial V_{n+1}} = F_{B-G}(\delta_{n+2,n+1})$$

(A-108)

$$\frac{\partial g_4}{\partial \theta_{n+1}} = -F_{G+B}(\delta_{n+2,n+1}) V_{n+1}$$

(A-109)

$$\frac{\partial g_4}{\partial X_{FACTS}} = \frac{\partial F_{B-G}(\delta_{n+2,n+2})}{\partial X_{FACTS}} V_{n+2} + \frac{\partial F_{B-G}(\delta_{n+2,n+1})}{\partial X_{FACTS}} V_{n+1}$$

(A-110)

where

$$\frac{\partial \delta_{n+2,i}}{\partial \delta_{k1}} = \begin{cases} -1 & i = k, k = 2,\ldots,n \\ 0 & otherwise \end{cases}$$

(A-111)

therefore, the matrices of the partial derivatives $\frac{\partial g}{\partial X}$ and $\frac{\partial g}{\partial Y}$ in (3.48) are obtained. Hence the A and B matrices in (3.50) and (3.51) can be calculated directly.

REFERENCES

[1] P. Kundur, Power System Stability and Control, McGraw-Hill, Companies, Inc, 1994. ISBN 0-07-030958-X

[2] S.E.M. De Oliveira, "Synchronizing and damping torque coefficients and power system steady-state stability as affected by Static Var Compensators", IEEE Trans. Power Systems, vol. 9, pp.109-119, Feb. 1994

[3] Taranto G.N., Chow, J.H., "A robust frequency domain optimization technique for tuning series compensation damping controllers", Power Systems, IEEE Trans. On Power Systems,Vol. 10, pp. 1219-1225, Aug. 1995

[4] H.F. Wang, F. J. Swift, "A Unifed Model for the Analysis of FACTS Devices in Damping Power System Oscillations Part I:Single-machine Infinite-bus Power System", IEEE Trans. on Power Delivery, Vol. 12, No.2, April 1997

[5] H.F. Wang, F. J. Swift, "A Unifed Model for the Analysis of FACTS devices in Damping Power System Oscillations Part II: Multi-machine Power systems", IEEE Trans. on Power Delivery, Vol. 12, No. 4, Oct. 1998

[6] Juan J. Sanchez-Gasca(M), Joe H. Chow, "Power System Reduction to Simplify the Design of Damping Controllers for Interarea Oscillations", IEEE Trans. on Power Systems, Vol. 11, No. 3, Aug 1996

[7] Wenzheng Qiu, M. Khammash, V. Vittal, "Power System Stabilizer Design Using LPV Approach", Proceedings of the 34th North American Power Symposium, pp. 67-74,2002

[8] J.S. Freudenberg, D.P Looze, "Right half plane poles and zeros and design tradeoffs in feedback systems", IEEE Trans. on Automatic Control, vol. 40, pp. 853-864, MayAC-30(6) 1985

[9] V. Toochinda, C.V. Hollot, Y. Chait, "On selecting sensor and actuator locations for ANC in Ducts", IEEE Conference on Decision and Control., Orlando, FL, 2001

[10] V. Toochinda, T. Klawitter, C.V. Hollot, Y. Chait, "A single-input two-output feedback formulation for ANC problems", Proceedings of the American Control Conference, Arlington, VA, 2001.

[11] V. Toochinda, "Fundamental limitations of ANC in one-dimensional ducts using 2 sensors and 1 actuator," Ph.D. dissertation, University of Massachusetts, Amherst, 2001

[12] S. K. Tso, J.Liang, "Coordination of TCSC and SVC for stability improvement of power systems", Proceedings of the 4th international conference on advances in power system control, operation and management, APSCOM-97, Hong Kong, Nov. 1997

[13] M. Klien, L.X. Le, G.J. Rogers, and S. Farrokhpay, "H_∞ damping controller design in large power systems", IEEE Trans. on power systems, vol. 10, pp158-166, Feb. 1995

[14] G. N. Taranto, J. K. Shiau, "Robust Decentralized Control Design for damping Power System Oscillations", Proceeding of the 33rd Conference on Desition and Control Lake Buena Vista, FL, December 1994

[15] Qihua Zhao, Jin Jiang, "Robust SVC controller design for improving power system damping", IEEE Trans on Power Systems, Vol.10, No.4, November 1995

[16] Gahinet, P., and P. Apkarian, "A linear Matrix Inequality Approach to H_∞ Control", Int. J. Robust and Nonlinear Contr., 4 (1994), pp. 421-448.

[17] J.S. Shamma, M. Athans, "Guaranteed properties of gain scheduled control for linear parameter varying plants", Automatica, vol. 27, pp. 559-564, 1991

[18] J.S. Shamma, M. Athans, "Gain scheduling: potential hazards and possible remedies", IEEE Control Systems Magazine, vol. 12, pp.101-107, 1992

[19] P. Apkarian, R.J. Adams, "Advanced gain-scheduling techniques for uncertain systems", IEEE Trans. on Control Systems Technology, vol. 6, pp.21-32, Jan. 1998.

[20] P. Apkarian, P. Gahinet, "A convex characterization of gain-scheduled H_∞ controllers," IEEE Trans. on Automatic Control, vol. 40, pp. 853-864, May 1995

[21] F. Wu, S.W. Kim, "LPV controller interpolation for improved gain-scheduling control performance", American Institute of Aeronautics and Astronautics,2002, pp.4759

[22] M. Klein, G. J. Rogers, ad P. Kundur, " A fundamental study of inter-area oscillations in power systems," IEEE Trans on Power systems, vol. 6, no. 3, pp. 914-921, Aug. 1991

[23] M. Noroozian and G. Andersson, "Power Flow Control by Use of Controllable Series Components", IEEE Trans. on Power Delivery, Vol. 8, No. 3, July 1993, pp.12-28

[24] M. Noroozian, et al, "Use of UPFC for Optimal Power Flow Control", Proceedinds of Stockholm Power Tech, Stockholm, June 1995.

[25] E. W. Kimbark, "Improvement of System Stability by Switched Series Capacitors," IEEE Trans on Power Apparatus and Systems, PAS-85(2), Feb. 1966, pp.180-188.

[26] M. Noroozian and G. Andersson, "Damping of Power System Oscillations by Controllable Components", IEEE Trans. on Power Delivery, vol 9, No. 4, Oct. 1994, pp.2046-2054

[27] E.V Larsen, J. J. Sanchez-Gasca, J. H. Chow, "Concepts for Design of FACTS Controllers to Damp Power Swings", IEEE Trans. on Power Systems, Vol. 10, No.2, May 1995, pp. 948-956

[28] F. P. de Mello, "Exploratory Concepts on Control of Variable Series Compensation in the Transmission Systems to Improve Damping of Intermachine/system Oscillations" IEEE Trans. on Power System, vol. 9, No.1, Feb. 1994

[29] C. Gamma, R. Tenorio, et. Al, "Brazilan North-South Interconnection-Application of Thyristor Controlled Series Compensation (TCSC) to Damp Inter-area Oscillation Mode", Cigre 37 Session, Paris, 1998

[30] J. Urbanek, et al., "Thyristor Controlled Series Compensation Prototype Installation at the Slatt 500 KV Substation", IEEE Trans. on Power Delivery, vol. 8, no. 3, July 1993, pp. 1460-1469

[31] J. J. Sanchez-Gasca, "Coordinated Control of Two FACTS Devices for Damping Interarea Oscillation", IEEE Trans. on Power Systems, vol. 13,no. 2, May 1998, pp.428-434

[32] Pouyan Pourbeik, "Simultaneous Coordination of Power System Stabilizers and FACTS Device Stabilizers in a Multimachine Power System for Enhancing Dynamic Performance", IEEE Trans. on Power Systems, Vol. 13, No.2, May 1998;

[33] Bikash C. Pal and Alun H. Coonick. "A Linear Matrix Inequality Approach to Robust Damping Control Design in Power Systems with Superconducting Magnetic Energy Storage Device", IEEE Trans. on Power Systems, Vol.15, No.1, February 2000.

[34] Hiyama, T.; Tsutsumi, Y., "Neural network based adaptive fuzzy logic excitation controller", Power System Technology, 2000. Proceedings. PowerCon 2000. International Conference,Vol. 1, 4-7 Dec. 2000 Page(s):235 - 240

[35] P. Gahinet, A.Nemivovskil, A. Laub, and M. Chilali, "LMI Control Toolbox", Mathworks Inc, Naha, MA 1995

[36] G. Becker, A. Packard, "Robust performance of linear parametrically varying systems using parametrically-dependent linear feedback," Systems & Control Letters, vol. 23, pp.205-215, 1994

[37] G. Becker, "Additional Results on Parameter Dependent Controllers for LPV Systems," Proceeding of 13th IFAC World Congress, 1996, pp. 351-356

[38] A.K. Packard, "Gain scheduling via linear fractional transformations," Syst. Contr. Lett., 22(2): 1994, pp. 77-92.

[39] P. Apkarian, P. Gahinet, "A Convex Characterization of Gain Scheduled H_∞ controllers," IEEE Trans. on Automatic Control., AC-40(5), 1995, pp.853-864.

[40] F. Wu, X.H. Yong, A.K Packard, and G. Becker. "Induced L_2 norm control for LPV systems with Bounded Parameter Variation Rates," Int. J. Robust Non. Contr., 6(9/10), 1996, pp.983-1996

[41] J.S. Shamma and M. Athans. "Analysis of Gain Scheduled Control for Nonlinear Plants," IEEE Trans. On Automat. Contr., AC-35 1990, pp.898-907.

[42] G. Becker, "Quadratic stability and performance of linear parameter dependent systems", Ph.D. dissertation, Department of Mechanical Engineering, University of California at Berkeley, 1993

[43] Z. Lin, M. Khammash, "Robust gain-scheduled aircraft longitudinal controller design using an H_∞ approach," Proceedings of the American Control Conference, June, 2001, Volume: 5 pp.2724-2729

[44] G.J. Balas, I. Fialho, A. Packard, J. Renfrow, and C. Mullaney, "On the design of LPV controllers for the F-14 aircraft lateral-directional axis during powered approach," Proceedings of the American Control Conference, 1997, Volume:1 pp.123-127

[45] F. Wu, A. Packard, and G. Balas, "LPV Control Design for Pitch-axis Missile Autopilots," Proceedings of the 34th IEEE Conference on Decision and Control, vol. 1, 1995, pp. 188-193

[46] F. Wu, "Switching LPV control Design for Magnetic Bearing Systems," Proceedings of the 2001 IEEE International Confereence on Control Applications, 2001, pp. 41-46.

[47] W. Qiu, V. Vittal, M.H. Khammash, "Decentralized power system stabilizer design using linear parameter varying approach," IEEE Trans. on Power Systems, vol. 4, pp. 1951-1960, Nov. 2004

[48] John Reeve, "Gain Scheduling Adaptive Control Strategies for HVDC Systems to Accommodate Large Disturbances", IEEE Trans. on Power Systems, Vol. 9, No.1, Feb 1994

[49] P.M.Anderson and A.A.Fouad, "Power System Control and Stability," IEEE Press, 1994.

[50] P.Kundur, G. J. Rogers, and D. Y. Wong, Extended Transient-midterm Stability Program Package: Version 2.0, User's Manuals, EPRI EL-6648,December 1989

[51] IEEE committee Report, "Excitation System Models for Power System Stability Studies," IEEE Trans. on Power Apparatus and Systems, vol. PAS-100, pp. 494-509, Feburary 1981.

[52] J.J. Paserba, N. W. Miller, E. V. Larsen, R. J. Piwko, "A thyristor controlled series compensation model for power system stability analysis", IEEE Trans. on Power Delivery, vol. 10, pp. 1471-1478, July 1995

[53] V. Vittal, "Transient stability test systems for direct stability methods", IEEE Trans. on Power Systems, vol. 7, pp. 37–44, Feb. 1992.

[54] J. Ackermann, Robust Control: Systems with uncertain Physical Parameters., London Springer_Verlag, 1993.

[55] M. Chilaili and P. Gahinet, "H_∞ design with pole placement constraints: an LMI approach," IEEE Trans. on Automatic Control, vol. 41, o. 3, pp. 358-367, Mar. 1996

[56] S. Skogestad and I. Postlethwaite, Multivariable Feedback Control Analysis and Design, John Wiley and Sons, 1996.

[57] P. Gahinet, "Explicit Controller Formulas for LMI-based Hinfinity Sythesis," to appear in Automatica, 1996

[58] F.Wu, X.H.Yong, A.K.Packard, and G.Becker, "Induced L_2 Norm Control for LPV Systems with Bounded Parameter Variation Rates," Int. J. Robust Non. Contr., 6(9/10), 1996, pp. 983-1996

[59]V. Toochinda, C.V. Hollot, Y. Chait, "Disturbance attenuation in a SITO feedback control system", Proceedings of the American Control Conference, Anchorage, AK, 2002.